CAIT-UTC-NC33

Installation of Thermocouples, and Analysis of Temperature Data from the 21st South Bridge

FINAL REPORT
August, 2018

Submitted by:

Gilbert A. Nichols
Graduate Student, USU

Marvin W. Halling
Professor, USU

Paul J. Barr
Professor, USU

Utah State University
4110 Old Main Hill
Logan, Utah 84332

External Project Manager
Tom Hales
Project Manager
Utah Department of Transportation

In cooperation with

Rutgers, The State University of New Jersey
and
Bridge Diagnostic Instruments
and
U.S. Department of Transportation
Federal Highway Administration

Disclaimer Statement

The contents of this report reflect the views of the authors, who are responsible for the facts and the accuracy of the information presented herein. This document is disseminated under the sponsorship of the Department of Transportation, University Transportation Centers Program, in the interest of information exchange. The U.S. Government assumes no liability for the contents or use thereof.

The Center for Advanced Infrastructure and Transportation (CAIT) is a National UTC Consortium led by Rutgers, The State University of New Jersey. Members of the consortium are the University of Delaware, Utah State University, Columbia University, New Jersey Institute of Technology, Princeton University, University of Texas at El Paso, Virginia Polytechnic Institute and the University of South Florida. The Center is funded by the U.S. Department of Transportation.

1. Report No.	2. Government Accession No.	3. Recipient's Catalog No.
CAIT-UTC-NC33		

4. Title and Subtitle	5. Report Date
Installation of Thermocouples, and Analysis of Temperature Data from the 21st South Bridge	August, 2018
	6. Performing Organization Code CAIT/Utah State University
7. Author(s) Gilbert A. Nichols, Marvin W. Halling, Paul J. Barr	8. Performing Organization Report No. CAIT-UTC-NC33
9. Performing Organization Name and Address Utah State University 4110 Old Main Hill	10. Work Unit No.
	11. Contract or Grant No. DTRT13-G-UTC28
12. Sponsoring Agency Name and Address Center for Advanced Infrastructure and Transportation Rutgers, The State University of New Jersey 100 Brett Road Piscataway, NJ 08854	13. Type of Report and Period Covered Final Report 04/01/16 to 08/31/17
	14. Sponsoring Agency Code

15. Supplementary Notes
U.S. Department of Transportation/Research and Innovative Technology Administration
1200 New Jersey Avenue, SE
Washington, DC 20590-0001

16. Abstract

Structural Health monitoring is to determine the condition of a bridge based on instrument measurements. The C-846 Bridge in Salt Lake City has such instrumentation. The bridge is located in Salt Lake City at about 2100 South and Interstate 15. This bridge has two kinds of instruments on it: accelerometers and thermocouples. The accelerometers measure the vibrations of the bridge. The accelerometers have been recording data on the bridge since 2001. The thermocouples, which measure temperature, were added as part of this installation in April 2016.

In light of recent research, damage may be detected from measuring the change in the natural frequency of a bridge, which can be obtained by manipulating the accelerometer data. However, the natural frequencies of a bridge change due to environmental effects, especially temperature. Temperature effects must be accounted for in order to better understand the damage.

The purpose of this research is not to detect damage. The bridge that is being monitored does not have any damage. The purpose of this study is to show how the dynamic properties of the C-846 Bridge in South Salt Lake City correlate with temperature. Additionally, several frequencies including the fundamental frequency of the bridge are identified.

It was found that the natural frequencies of the bridge increase with a decrease in temperature, and that the fundamental frequency of the bridge is 1.15 Hz.

17. Key Words	18. Distribution Statement
Structural Health Monitoring, modal analysis, bridge instrumentation, damage detection, temperature, ambient vibration, bridge field testing	

19. Security Classification (of this report)	20. Security Classification (of this page)	21. No. of Pages	22. Price
Unclassified	Unclassified	109	

Table of Contents

Chapter 1: Introduction

Problem Statement

When a bridge is damaged, its natural frequencies change. Temperature changes on the bridge also cause changes in the natural frequency. According to one source, "changes in the vibrational properties of a bridge could be more significant than those caused by a medium degree of structural damage under normal operation loads" (Xia 2012). The changes in the natural frequencies of the bridge due to temperature can "mask the changes that are caused by damage, especially in the bridge structure that are always exposed to environmental elements" (Nandan and Singh 2014). This makes studying the correlation between the natural frequencies of a bridge and the temperature important. It can provide insight into the condition of the bridge, whether or not there is damage, and even help predict damage. According to Zhou (2014), research on the relationship of the temperature to the natural frequency has three approaches: theoretical derivations, trend analysis, and quantitative monitoring. Theoretical derivations use the classical structural dynamics equations and the heat transfer equations to develop a model. Trend analysis uses the change in the vibration properties of the bridge with numerically generated, lab collected, or field collected data. The quantitative analysis uses linear, nonlinear, or learning models on bridges that have a long history of data (Zhou and Yi 2014). In this literature review, the quantitative analysis is divided up into the different statistical models of temperature effects on modal frequencies (Xia 2012).

Objective

The purpose of this paper is to find the fundamental frequency of the C-846 bridge and several other natural frequencies that correlate well between the accelerometers. Then, these

frequencies are correlated with temperature. The temperature across the cross section of the bridge is also studied, and the change in the temperature throughout the day is discussed. Since two different data loggers are being used, comparing the data from each is also an objective.

The reason that correlating the natural frequencies and temperature is important is because it may help detect damage on the bridge. This process of detecting damage is called structural health monitoring. Housner (1997) defines structural health monitoring as "the use of in-situ, nondestructive sensing and analysis of structural characteristics, including the structural response, for the purpose of detecting changes that may indicate damage or degradation." This report is primarily concerned with damage indication based on the removal of the temperature effects to the natural frequency on the bridge. To remove temperature effects, I-15 Bridge C-846 has a temperature and vibration data history that is continuously recorded. The temperature data filters out the environmental effects due to temperature, allowing other effects, such as damage, to show in the data. For example, if there is a shift in the natural frequency that does not match the change in temperature, then it may be an indication of damage. The papers cited should be used only as a starting point for further research; they certainly are not a comprehensive list of papers on the topic.

Chapter 2: Literature Review

Theoretical Derivations

Vibration

Bridges are very complex systems; therefore, it is difficult to develop a closed form solution to relate vibrational properties of a bridge with environmental effects, including temperature. However, there are several closed form equations to describe the behavior of the bridge. The following equations taken from Zhou and Yi (2014) approximate the vibration properties for a single span beam of isotropic material. The undamped flexural vibration frequency of order n is:

$$f_n = \frac{n^2 \pi h}{2l^2} \sqrt{\frac{E}{12\rho}} \tag{1}$$

Where f_n is the nth frequency, h and l are the height and length of the beam, E is the Young's modulus, and ρ is the density of the material. The same equation using the following variation is:

$$\frac{\delta f_n}{f_n} = \frac{\delta h}{h} - \frac{2\delta l}{l} + \frac{1}{2}\frac{\delta E}{E} - \frac{1}{2}\frac{\delta \rho}{\rho} \tag{2}$$

Where δ is the increment of its corresponding parameter. The above expression is the same as the following:

$$\frac{\delta h}{h} = \theta_t \delta t, \frac{\delta l}{l} = \theta_t \delta t, \frac{\delta \rho}{\rho} = -3\theta_t \delta t, \frac{\delta E}{E} = \theta_E \delta t, \tag{3}$$

Where θ_t is the coefficient of linear expansion of the material, θ_E is the temperature coefficient of the Young's modulus, and t is the temperature of the beam. The next step assumes that the Young's modulus is linear for small changes. With that assumption, and substituting Equation 3 into Equation 2 gives:

$$\frac{\delta f_n}{f_n} = \frac{1}{2}(\theta_t + \theta_E)\delta t \tag{4}$$

Natural frequencies of prismatic beams are similar to those of a simply supported beam. The equation for a prismatic beam, therefore, is similar to that of a simply supported beam as shown in Equation 5:

$$f_n = \frac{\lambda_n^2 \pi h}{2l^2}\sqrt{\frac{E}{12\rho}} \tag{5}$$

Where λ_n is a dimensionless parameter that is a function of the boundary conditions, allowing Equations 2-4 to still be applicable for multi-span beam structures.

Brecolotti et al. (2004) also proposed a closed form analysis in his paper, "Sensitivity of Dynamic Methods for Damage Detection in Structural Concrete Bridges." His model is based on the parameters of the modal shape, the Young's Modulus, the section moment of inertia, and the mass per unit length. The same equations for a simply supported beam or a cantilever beam were applied to a reinforced concrete bridge over the Tiber River in Rieti, Italy. Below are the equations for a simply supported beam's corresponding variation of pulsation:

$$\Delta\omega_r = \frac{r^2\pi^2\Delta J}{L^3}\sqrt{\frac{E}{Jm}}\left(\frac{b}{2} - \frac{L}{2\pi r}\sin\frac{r\pi b}{L}\cos\frac{2r\pi\alpha}{L}\right) \tag{6}$$

$$\frac{\Delta\omega_r}{\omega_r} = \frac{1}{2\pi r}\frac{\Delta J}{J}(\beta - \sin\beta\cos\alpha) \tag{7}$$

Where $\alpha = 2r\pi a/L$ and $\beta = r\pi b/L$, ΔJ is modeled as a constant decrement, E is the Young's modulus, L is the length of the beam, and r is one of the parameters for the Kronecker delta function. The calculations only relied on the modal shapes and frequencies in order to monitor the bridge. They concluded that other methods might be more efficient and reliable.

Temperature

Temperature distribution is complicated also, but there have been some closed form equations used to describe temperature distribution in a bridge. Below is the Fourier partial differential equation, which shows that the rate of heat transfer is equal to the temperature gradient in a solid (Oh et al. 2006):

$$\frac{\partial}{\partial x}\left(k_x\frac{\partial T}{\partial x}\right)+\frac{\partial}{\partial y}\left(k_y\frac{\partial T}{\partial y}\right)+\frac{\partial}{\partial z}\left(k_z\frac{\partial T}{\partial z}\right)+Q=c\rho\frac{\partial T}{\partial t} \quad (8)$$

Where $x, y,$ and z are Cartesian coordinates which are horizontal, vertical, and longitudinal axes of the bridge; $k_x, k_y,$ and k_z are defined as the thermal conductivities to their respective Cartesian coordinates; t represents time; and T represents temperature. On the right hand side of the equation, c is the coefficient of specific heat of the solid and ρ is the density of the solid.

For a bridge that is exposed to solar radiation, it may be assumed that the material is continuous, isotropic, and homogeneous. According to thermocouples that were placed on a bridge by McClure (1983), there was no significant longitudinal temperature variation. From these results, the thermal flow along the direction of the longitudinal axis can normally be neglected. Therefore, Equation 7 is simplified into the following equation:

$$k\left(\frac{\partial^2 T}{\partial x^2}+\frac{\partial^2 T}{\partial y^2}\right)=c\rho\frac{\partial T}{\partial t} \quad (9)$$

Considering only the vertical component of the temperature gradient, Equation 9 simplifies further to Equation 10.

$$k\left(\frac{\partial^2 T}{\partial y^2}\right)=c\rho\frac{\partial T}{\partial t} \quad (10)$$

Considering the boundary conditions of Equation 9, Equation 10 becomes:

$$k\left(\frac{\partial T}{\partial x}n_x + \frac{\partial T}{\partial y}n_y\right) + q = 0 \quad (11)$$

Where n_x and n_y are the direction cosines of the unit outward vector normal to the boundary surfaces and q is the rate of energy transferred between the boundary and the environment per unit area. The following equation models the heat exchange between the boundary of the bridge and the environment.

$$q = q_s + q_c + q_r \quad (12)$$

Where q_s is solar radiation, q_c is convection, and q_r is the irradiation from the surface to the surrounding air. Each of these parameters are position and time dependent. The rate of heat due to solar radiation is the product of α, the absorptivity of the surface of the bridge, and I, the solar radiation on a tilted surface, shown in Equation 13.

$$q_s = \alpha I \quad (13)$$

The solar radiation can be formulated using variables related to the orientation and location of the bridge, or can be formulated using the beam/direct radiation, diffuse radiation, and ground-reflected radiation and using sinusoidal functions as expressed in the following equation by Duffie & Beckman (2013) and Orgill & Hollands (1977).

$$I = I_b \frac{cos\theta}{cos\theta_z} + I_d \frac{(1 + cos\beta)}{2} + (I_b + I_d)\eta \frac{(1 - cos\beta)}{2} \quad (14)$$

Newton's law of cooling, as shown below, gives the heat lost or gained from the surrounding air by convection.

$$q_c = h_c(T_s - T_a) \quad (15)$$

Then the Stefan-Boltzmann radiation law yields the heat transfer between the bridge surface and the surrounding atmosphere due to thermal irradiation, as shown below.

$$q_r = C_s e[(T_s + T^*) - (T_a + T^*)] \quad (16)$$

This summarizes how to obtain each of the terms in (12).

Trend Analysis

Theoretical derivations provide a simplified model, but in order to get more accurate results and model the complexity of what the bridge is doing, trend analysis provides an alternative. Numerically simulated, lab collected, or field-collected data provide a basis for understanding the relationship between the vibration properties of a bridge and the temperature.

Numerically Simulated Trend Analysis

Nandan & Singh (2014) developed a finite element model and then used laboratory data to validate it. Then they performed the finite element analysis using measured accelerometer and temperature data for a box-girder and a T-beam girder. They created a hole in the deck to simulate bridge damage. They also used the Monte Carlo method to incorporate the effect of response measurement errors on the frequency time series calculated by the finite element analysis. They found that environmentally induced frequency variations could be large enough to mask the changes in modal frequencies induced by potential damage of the structure.

Changqing (2011) studied the effects of temperature on the Taizhou Yangtze River Bridge using finite element modeling. They used ANSYS software. They treated the stiffness of the bridge pavement as negligible. They determined that the relationship between temperature and the elevation of the main beam is negative. They also determined that the relationship between temperature and frequency is negative. They also determined that the effects of temperature could not be neglected when dynamically analyzing a suspension bridge.

Fu & DeWolf (2001) developed a finite element model for a bridge with partially restrained bearings. They verified that the natural frequencies of the bridge changed in cold

weather and that it was because of the restraints in the end bearings. They developed a nonlinear dynamic finite-element analysis to assess the changes in the bridge from the partially restrained bearings. The finite-element model (FEM) was based on use of beam elements for the girders and diaphragms and shell elements for the slab. They collected field data and used it to calibrate the model. The FEM was then modified with eccentrically applied forces that developed during cold weather. They concluded that the variations of boundary conditions due to changes in temperature did cause a change in natural frequencies. Liu & DeWolf (2007) also used a FEM to model the behavior of a curved posttensioned bridge. They used Four-node shell elements with six degrees of freedom per node to model the superstructure of the bridge. Nine hundred-twenty-one elements for the top deck were used, 763 for the bottom deck, 607 for the web, and 157 for the diaphragms for 2448 elements with 2529 nodes. The analysis yielded eight vibration modes.

Macdonald & Daniell (2005) used a FEM for the Second Severn crossing bridge. They used 4 shell elements across the width of the bridge and 130 elements along the length. Beam elements represented each girder with their individual properties varying according to their properties from girder to girder. Vertical rigid links between the nodes of the shells and beam elements modeled the composite behavior. Beam elements, connected by rigid links to the shell elements of the slab represented the transverse elements. Cable anchorage elements were modeled by beam elements and each cable was modelled as a single truss element. The bearings were modeled as fixed in all translational directions, whilst being free to rotate. Twenty-three measured mode shapes from data obtained on the bridge were matched with modes from the FEM. The modal analyses were conducted for two different temperature conditions; a uniform temperature of 5°C to the whole structure, and a temperature differential of +10°C for the top of the deck compared to the rest of the structure. For both conditions, the natural frequencies of

about one third of the modes shifted by ± 0.2%, while there was no noticeable change in the others.

Xu & Wu (2007) carried out a FEM of a cable-stayed bridge also. Their FEM used beam elements, link elements, contact elements, spring elements, and mass elements. They concluded that the variation due to temperature will approach 2% from -20°C to +40°C, changes of mode shape curvature from temperature vary from 1 to 8%, the change in the sequence of mode shapes in unaffected by change in temperature, and frequency changes from damage are smaller than frequency changes from temperature.

Balmés et al. (2008) developed a FEM of a bridge deck using 28 supports and a deck, which is 3 m high 6.6-10 m wide and 100 m long. They used the program Structural Dynamics Toolbox. The whole bridge span is modeled with 9600 standard 8-node isoperimetric volume elements and 13,668 nodes. Motion is blocked in the y and z directions at the ends while the supports in the bridge direction x are modeled as 28 scalar springs. They modeled temperature variations using either a uniform temperature elevation or a linear variation with z from 25°C on the deck to 15°C at the bottom. They simulated damage as the reduction of stiffness in some of the elements. They simulated undamaged and damaged scenarios at multiple temperatures and repeated each scenario 50 times. The output data was simulated under white noise excitations. In the damaged and the undamaged scenarios, the frequency increased as expected, but the frequencies were different. The frequency of the damaged case could be matched by modifying the temperature of the undamaged case though.

Laboratory Tests

Unlike the theoretical derivation approach and the numerical collected data approach, laboratory tests can provide conclusions that are more rational because it can reveal the

variations of structural vibration properties given different environmental effects (Zhou and Yi 2014).

A laboratory test of a reinforced concrete (RC) slab was conducted by Xia et al. (2006). The slab was 6.4 m x 8 m x 1 m with 3 m spans and a 2 m overhang on each end. The sampling rate for the 12 attached accelerometers was 500 Hz. An impact hammer excited the slab. The data was recorded on the slab from June 2003 to March 2005, developing 136 valid data sets. The first four modes were extracted. The results from the study indicate that the first two modal frequencies decrease by 0.23% when temperature increases by one degree. Additionally, all four frequencies decreased with the temperature increase, and there was a linear relation between frequencies and temperature. They concluded that the temperature affects the Young's modulus as well as the geometry. The results show that damping has a positive correlation with temperature. The damping increases slightly with an increase in temperature.

Balmés et al. (2008) performed a laboratory test-case of a clamped aluminum beam within a climatic chamber. A vertical beam was clamped at both ends on a workbench made of four steel columns and two horizontal deck. Four accelerometers were placed on the nodes of the 5^{th} flexural mode in order to avoid modes 1 through 4. Aluminum strain gauges measured the actual axial prestress without any temperature measurement for the beam. The climate-controlled room slowly cooled the beam at -1°C per hour and a loudspeaker with white noise input acoustically excited the beam. The results show that prestress and frequencies increase as temperature decreases with time. The beam was modeled with undamaged and damaged cases as well. A horizontal spring was used to model local nondestructive damage. The results showed that the deviations of prestress for modes 1 to 4 were +0.8, +0.4, -0.1, and -0.2% respectively.

Kim et al. (2006) conducted experimental tests for a single span, stainless steel plate girder bridge model. The bridge was 2 m long and had simply supported connections modeled by a set of pin supports at the left edge and a set of roller supports at the other edge. The deck consists of a 5 mm thick, 50 cm wide stainless steel plate. The deck was supported by 3 mm thick, 30 mm deep floor beams that are slender, rectangular shaped, and are framed into the girders with welds. Eighteen accelerometers measured the bridge. The bridge was excited using an excitation-inducing shaker. A series of forced vibration tests were conducted for about 7 months. The temperatures varied from -3°C to a high of 23°C. In all of the modes, the natural frequencies went down as the temperature increased. Bending modes were found to be more sensitive than torsional modes. The lower the mode, the greater the effect temperature has on the natural frequency. Next, damage was made to the girder and a series of forced vibration tests were performed at the temperature of 23°C. Except for local variations, the mode shapes of the damaged structures looked identical to those of the undamaged structure.

Laboratory tests verify the FEMs frequently (Nandan and Singh 2014, Xia et al. 2011). Xia et al. (2011) conducted laboratory tests of a simply supported RC slab. The slab measured 3.2 m long, 0.8 m wide, and 0.12 m thick with a 0.1 mm overhang at each end. Grade C30 concrete was used with 12 mm diameter reinforcing bars at 150 mm intervals. Seven thermocouples embedded every 20 mm along the thickness of the slab measured the temperature. The method with embedded thermocouples is similar to the process used in this paper's project; the thermocouples were put in a plastic tube with holes and embedded into the concrete. Seven accelerometers measured the vibration responses. An instrumented hammer created the excitations. Modal testing was conducted during one day from 8:00 am to 10:00 pm on February 11, 2009. The results verify that the temperature gradient exists along through the thickness of

the beam, the temperature gradient in the thickness of the beam is non-uniform and non-linear during the day when the temperatures vary, and when the temperature is stable the gradient becomes more linear. Furthermore, it was verified that the frequency of the structure decreases when temperature goes up before noon while the frequency increases as temperature drops down in the afternoon. The variation of temperature was not significant, so the change in the damping ratio was mostly masked by measurement noise. A similar test to that performed by Xia and his colleagues was later used by Nandan to verify his FEM model.

Xia performed another study with an RC slab, a steel beam, and an aluminum beam. The RC slab was simply supported and the steel and aluminum beams were cantilevers. Each of the beams were outside and exposed to solar irradiation. The beams were excited with an instrumented hammer. The first four frequencies of the two metallic beams and the first two frequencies of the RC slab were collected. All the natural frequencies decreased with an increase in surface temperature before 11:30 am and then increased slowly from then on. The frequency shows a good inverse relationship with the temperature.

Trend Analysis with Field Monitoring

According to Zhou, "Field measurement that monitored the temperatures and vibration responses of a bridge by sensors installed on it can give the most objective data subjected to real service circumstance" (Zhou and Yi 2014). Wei-Hua Hu studied temperature effects on the "Pedro e Inês" footbridge in Coimbra. The study included using six accelerometers and five temperature sensors to measure the data. Their results show that the frequency and temperature are negatively related (Hu et al. 2009).

Sohn et al. (1999) monitored the Alamosa Canyon Bridge. The bridge has seven independent spans. Each span has a deck that is supported by W30x116 steel girders. The top

flanges of the girders are embedded into the concrete slab. The roadway in a span is approximately 7.3 m wide and 15.2 m long. They tested the bridge for several months. Thirty-one accelerometers were placed on the concrete deck and on the girders below the bridge. Five accelerometers were spaced along the length of each girder. An impact hammer was used to excite the bridge. Nine meaningful modes were identified. Temperature measurements were made on nine different locations across the center of the span. Three assumptions were made during the testing. First, the changes in the modal parameters are linearly proportional to changes in temperature. Second, the mass of the bridge forced the change in modal parameters to lag behind the temperature because the bridge takes time to heat up and cool off. Third, the geographical orientation of the structure (north and south) with respect to the sun suggests that the temperature of the west end of the bridge will have a time lag behind the temperature of the east end. The results reveal that the first three natural frequencies of the bridge varied about 4.7%, 6.6%, and 5.0% during a 24 hour period as the temperature of the bridge deck changed by approximately 22°C. The temperature gradient largely influences the variation of the fundamental frequency (Zhou 2013).

Peeters et al. (2001) monitored the Z24 Bridge in Switzerland for almost a year before artificially damaging it. The bridge was a classical post-tensioned concrete box girder bridge with a main span of 30 m and two side spans of 14 m. Sensors obtained both temperature and accelerometer data for the bridge. The bridge was excited using two shakers and a drop weight. They found that the temperature of the asphalt greatly effects the frequency below 0°C, causing a bilinear behavior between frequency and temperature. The results found by Gonzales et al. (2013) support the conclusion of the bilinear behavior and suggest that the change in natural frequencies is due to changes in the stiffness parameters of some materials with the onset of frost

because the stiffness parameters did not change until the structure was below 0°C for several days.

Ni et al. (2005) studied the modal properties of the Ting Kau cable stayed bridge with temperature. The bridge has two main spans of 448 m and 475 m respectively, and two side spans of 127 m each. The bridge is equipped with 45 accelerometers and 83 temperature sensors permanently installed on the bridge. Each hour the first ten modes and temperatures at different locations on the bridge are obtained. They report that for the first ten modes the natural frequencies lie in the range of 0.1-0.4 Hz. The normal environmental change (2.83 to 53.46°C) yields variance from 0.20% to 1.52% for the first ten modes. For all ten modes, as the temperature increases, the modal frequency decreases. They remark that the environmental effects may mask any damage that occurs.

Liu & DeWolf (2007) studied the changes in temperature and modal properties for a curved posttensioned bridge. A long-term remote-controlled continuous monitoring system was installed on the bridge, which was comprised of 12 temperature sensors, 16 accelerometers and 6 tilt meters. The bridge data shows an inverse relationship between frequency and temperature; the normalized frequency decreases as the temperature increases. In the test, the natural frequencies varied by a maximum of 6% in a peak to peak temperature range of 21°C during 1 full year. The first and second modes were found to be more sensitive to temperature than the higher modes. They suggest that the higher mode parameters may be a better for damage diagnostic prediction, but could be problematic because of the large scatter and nonlinear phenomena that they exhibit. They contend that the use of natural frequencies alone is not enough for damage detection because of the sensitivity to temperature. They also suggest that the influence of temperature on natural frequency is likely to be structure specific.

Moser & Moaveni (2011) explored the environmental effects on the identified natural frequencies of the Dowling Hall Footbridge at Tufts University in Medford Massachusetts. The bridge is 44 m long and 3.7 m wide. Eight accelerometers and ten thermocouples were used on the bridge. The bridge's data was recorded for 16 weeks from January through most of April. They made three observations. First, the identified natural frequencies increase as temperatures decrease. Second, the effect of frequency and temperature is more significant when the temperatures are below the freezing point resulting in a nonlinear relationship. Third, modes one, three, and four show more clear correlation with temperature while Modes two, five, and six show more scatter. These are similar results to what Liu and De Wolfe saw in the curved post-tensioned bridge. The natural frequencies of the six identified modes varied from four to eight percent in the temperature range of -14 to 39°C.

Xia et al. investigated the Tsing Ma Suspension Bridge. The bridge is 2132 m long and has a highway on the upper deck and railway tracks on the lower deck. A structural health monitoring system was installed for the Tsing Ma Bridge in 1997. The monitoring system has 280 sensors, including 13 accelerometers and 110 temperature sensors. The frequencies generally decrease when the temperature goes up before noon, and they increase as the temperature drops in the afternoon. The minimum and the maximum temperatures do not occur at the same time. However, they do tend to occur within about 3 hours of one another. The temperature is non-uniformly distributed across the bridge; one temperature cannot represent the temperature of the entire bridge. No clear correlation between the damping ratio and the temperature can be observed.

Xia et al. (2012) also gave results from research that is being conducted on the Guanghzhou New TV Tower. The tower is 600 m tall and consists of a main tower and an

antennary mast. The tower has a structural health monitoring system as well, with more than 700 sensors. These sensors include temperature sensors, vibrating wire strain gauges, accelerometers, fiber optic strain and temperature gauges, and cameras to monitor deflection. They concluded that the frequencies generally decrease when temperature goes up and increase when temperature goes down, although variation in the frequencies is very small. Like the Tsing Ma Bridge, minimum frequencies and maximum temperatures do not occur at the same time. It is interesting that in structures the same correlation between frequencies and temperatures have been found as in many bridges.

Mosavi et al. (2012) studied how temperature effects the daily modal variability of the Chicken Road bridge, a steel concrete composite bridge with a skewed span. The bridge is a four-lane two-span bridge with span lengths of 41.28 m and 38.96 m with a total deck width of 10.99 m. The bridge has four steel girders per span that measure 1.5 m deep and are spaced every three meters. The bridge was equipped with accelerometers, string pots, and thermocouples. The bridge was excited in a similar manner as the Alamosa Canyon Bridge, using a large impact hammer, instrumented with a load cell. The analysis extracted the first five natural frequencies. An almost 1-2% change in the natural frequencies was investigated in all modes of the bridge from night to noon, but the natural frequencies showed little change from night to morning. The shifts in the natural frequencies from night to noon were coincident with an inversion of the temperature gradients in the composite cross section of the bridge from night to noon. They argue that this inversion of the temperature gradients from night to noon is the main reason for a relatively large upward deformation of the steel girders and changes in the natural frequencies during that time.

Wahab & De Roeck (1997) measured the dynamic response of a concrete bridge twice, once in the spring and once in the winter. An impact hammer was used to test the bridge. The difference in the temperatures in the spring and the winter was 15ºC. Decreasing the temperature led to an increase in the natural frequencies for almost all modes by 4 - 5%. They report that the change in natural frequencies due to damage is mode-dependent. Frequencies of modes with high curvatures in the most damaged zones tend to shift the most. The damping ratios did not exhibit uniform changes in all of the modes, they discourage the use of damping ratios for damage detection because of the relatively high level of error involved in extracting it from the experimental measurements and its dependence on the type of excitation and the amplitude of vibration.

Zolghadri et al. (2016) installed three velocity transducers and five thermocouples on a precast roadway bridge and monitored the bridge for six months. It was concluded that natural frequencies are dependent on previously measured temperatures. The conclusion was validated by using different sets of data and comparing those using statistical properties.

Statistical Models of Temperature Effects on Modal Frequencies

Regression Models

Several researchers have employed regression models. One of these regression models is the linear model. This is the simplest of the models. For example, Xia et al. (2006) used this method to model their tests of a reinforced concrete or RC slab. Sohn et al. (1999) used a trained linear regression technique. In this technique, the data was trained to new measurement data and checked if the new frequencies matched the model at the specified confidence level, which was used to determine whether frequency changes were caused by temperature changes or by stiffness deterioration. (Xia 2012)

Liu and DeWolf (2007) also developed a linear regression model with a 5% estimate error to represent the three natural frequencies of a three span curved post-tensioned box concrete bridge located in Connecticut as a function of temperature.

Moser and Moaveni (2011) employed nonlinear methods on the Dowling Hall Footbridge. They tried several models, including a bilinear model, a quadratic model, a fourth order model with cross terms and a fourth order model without cross terms. The first method is linear, but the others are nonlinear. They concluded the bridge was strongly correlated and nonlinear. They recommended a fourth-order polynomial without cross terms.

Ni et al. (2005) used the support vector machine technique to quantify the relation between temperature and modal frequencies on the bridges they studied. The basic idea of this technique is to establish a hyperplane that has the largest distance to the nearest data points of any class (Xia et al. 2006). Laory et al. (2014) compared multiple linear regression, artificial neural networks, support vector regression, regression tree, and random forest models to predict the natural frequencies of the Tamar Suspension Bridge using 3 years of continuously monitored data. They concluded that Random forest and support vector regression were the most appropriate and that traffic loading and temperature are the most influential parameters on the suspension bridge.

Autoregressive (AR) Models

The temperature distribution of bridges is associated with multiple factors including the present ambient temperature, radiance from the sun, and conditions at earlier periods (Xia 2012). Autoregressive (AR) models or autoregressive models with an exogenous input (ARX) seem to represent the relationship between frequency and temperature. This method is widely used

(Moser and Moaveni 2011, Zolghadri 2016, Peeters and De Roeck 2001). Some equations have been developed for linear regression. Xia et al. uses the following equation:

$$q = \beta_0 + \beta_t t + \epsilon_f \quad (17)$$

Where q represents the dynamic parameter such as frequency and percentage damping ratio, β_0 (intercept) and β_t slope are regression coefficients, and ϵ_f is the error. β_0/β_t indicates the percentage of the frequency change when the structural temperature increases by unit degree Celsius (Zhou and Yi 2014).

Sohn et al. (1999) created a linear adaptive filter that uses the following formula:

$$y = w_0 + \mathbf{x}^T\mathbf{w} + \epsilon \quad (18)$$

Where w_0 is a bias or offset, $\mathbf{w}$ is a column vector of coefficients that weigh each temperature input, and ϵ is the filter error. The equation is rewritten to account for the offset term w_0 by redefining the input and weight vectors to have $p\ (=r+1)$ dimensions:

$$y = \mathbf{x}^T\mathbf{w} + \epsilon \quad (19)$$

Supposing that n observations are available and $\mathbf{x}(i)$ and $y(i)$ denote the i^{th} input-output pairs, the above equation can be written in matrix notation:

$$\mathbf{y} = \mathbf{X}\mathbf{w} + \epsilon \quad (20)$$

where with n observations

$$\boldsymbol{y} = \begin{bmatrix} y(1) \\ y(2) \\ \vdots \\ y(3) \end{bmatrix}, \quad \mathbf{X} = \begin{bmatrix} 1 & x_1(1) & x_2(1) & \cdots & x_1(1) \\ 1 & x_1(2) & x_2(2) & \cdots & x_r(2) \\ \vdots & \vdots & \vdots & \cdots & \vdots \\ 1 & x_1(1) & x_2(n) & \cdots & x_r(n) \end{bmatrix}, \quad \boldsymbol{\epsilon} = \begin{bmatrix} \epsilon(1) \\ \epsilon(2) \\ \vdots \\ \epsilon(3) \end{bmatrix} \quad (21)$$

Principal Component Analysis (PCA) and Neural Networks

Principal component analysis has to do with analyzing the eigenvector with the highest eigenvalue in a set of data points. It can be used to reduce the dimensions of a data set by

stripping away its unnecessary parts. If there is a data set of 3D variables, each with an x, y, and z number to describe each point, but all of the points are on a plane, then the data can be simplified to two dimensions (Dallas 2016). PCA and the Novelty Detection Technique were used to model the "Pedro e Ines" bridge (Hu et al. 2009). Some have used neural networking to perform nonlinear PCA or NLPCA according to Sohn et al. (1999), Ni et al. (2005), and Li et al. (2010). Cury et al. (2012) also used neural networks to formulate regression models for quantifying the effect of temperature on frequencies and mode shapes. Zolghadri et al. (2016) used principle component analysis to reduce the dimensions of the data obtained for their bridge.

Chapter 3: Bridge Description

Introduction

Bridge C-846 is a steel girder flyover bridge that connects I-15 with SR 201. The bridge includes four individual structures, containing 25 spans, with a total length of 1.14 km (3741 ft). The instrumentation was confined to a single 13 span structure with two expansion joints. The reinforcing steel is epoxy coated M284. The structural steel is AASHTO M270M Grade 345. The strength of the cast in place concrete is f'_c = 28 MPa (4060 psi). The steel girders are continuous bearing on concrete filled steel pipe piles. The soils consist of deep soft sediments, silts, and clays (Hales 2002). The site description is shown in Figures 3.1-3.2. A description of the bents of the bridge is in Figure 3.3. Note that in and Figures 3.1-3.3, North is to the right.

Accelerometers

Several accelerometer channels are located on and around Bent 7, where an expansion joint is located. A tri-axial instrument is on Bent 7, and bi-axial instruments with transverse and longitudinal channels are located on either side of the expansion above it. The 78.89 m span between bents 6 & 7 contains three bi-axial instruments with vertical and transverse channels. Two of these are located at mid-span, one on each side of the deck. The other is at the quarter span measuring from Bent 7. A bi-axial instrument is on the deck above Bent 6, containing transverse and longitudinal channels. Instrumentation at Bent 9 includes a bi-axial instrument with a transverse and vertical channel on the bent, and a uni-axial instrument with a vertical channel directly above it. The locations of all of the accelerometers and their names are in Figure 3.4. In the figure, the large rectangle represents the deck and it is divided by the bents, denoted

BNT6, BNT7, etc. The smaller rectangles represent the accelerometers on the bent. The direction of the arrows indicates the positive sense of the accelerometer.

All of the accelerometers are enclosed in 12 in. x 12 in. x 6 in. NEMA 12 rated enclosures to protect the instruments as shown in Figure 3.5.

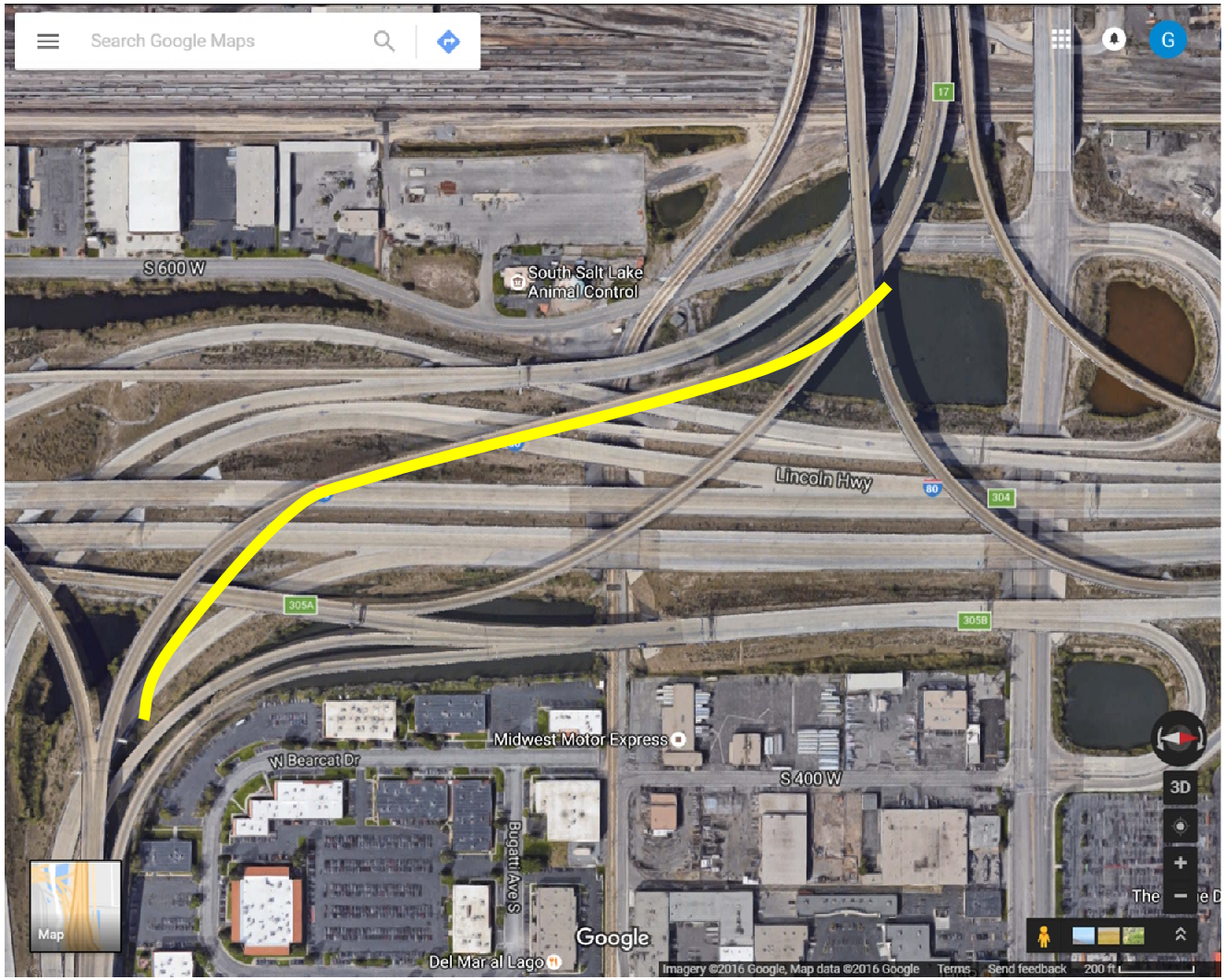

Figure 3.1 Map of the site with North to the right

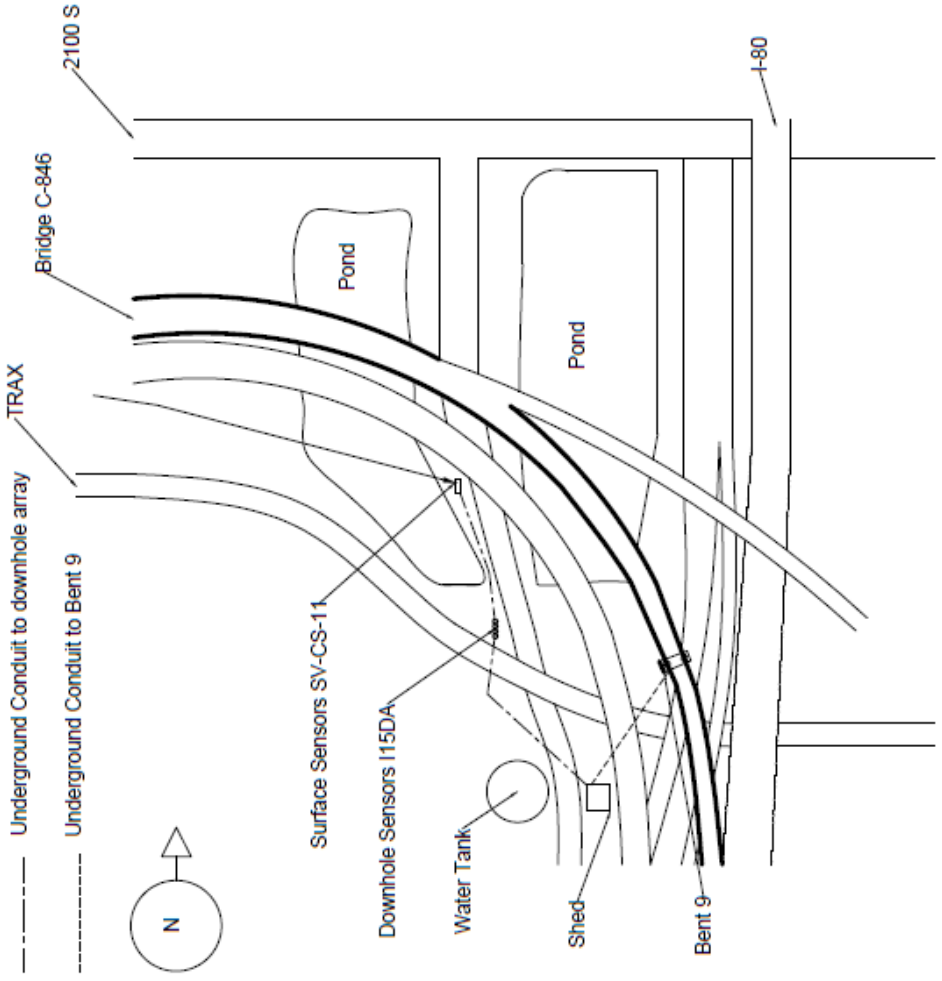

Figure 3.2 Close up of the site with North to the right

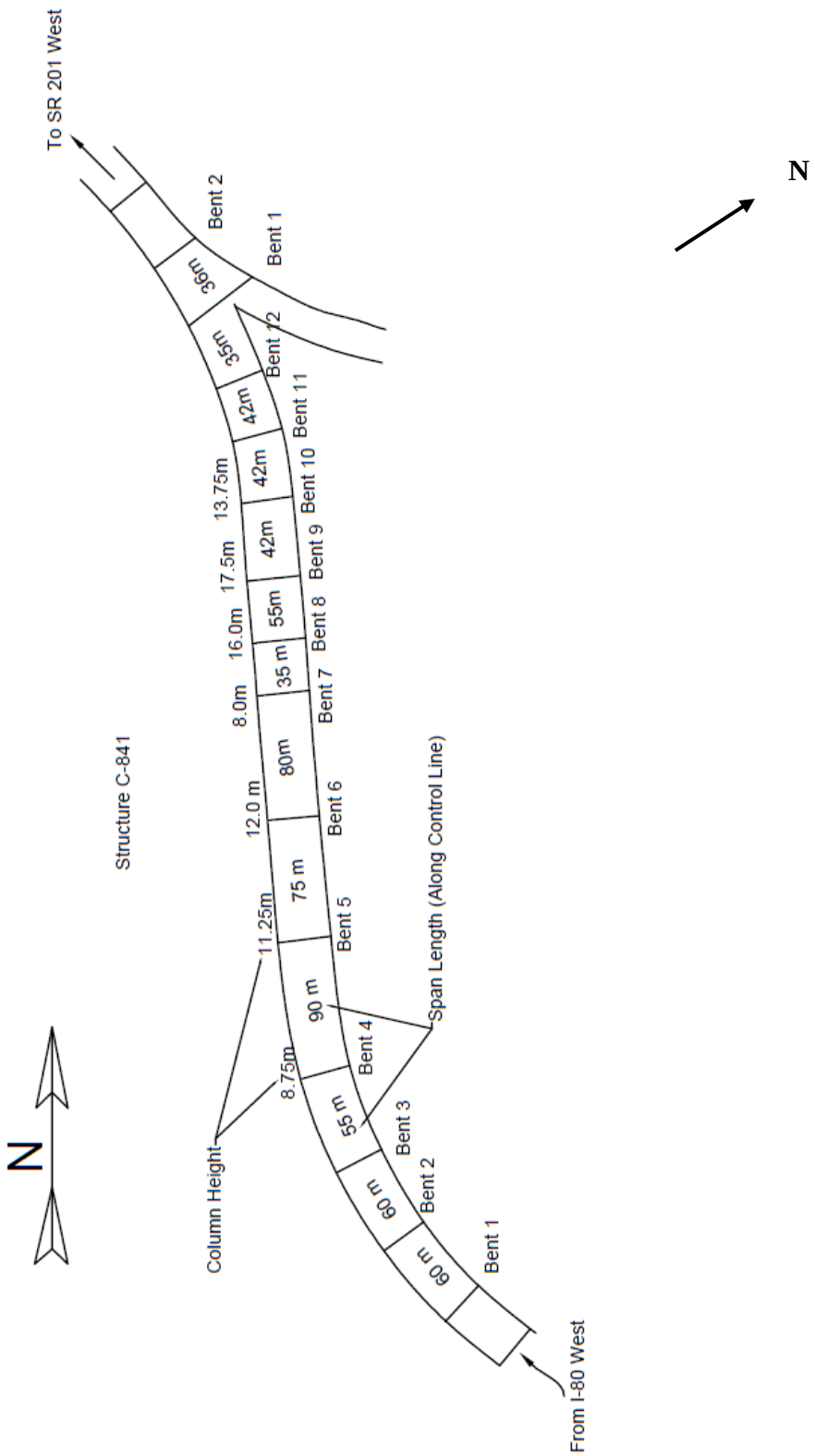

Figure 3.3 Bent locations and distances

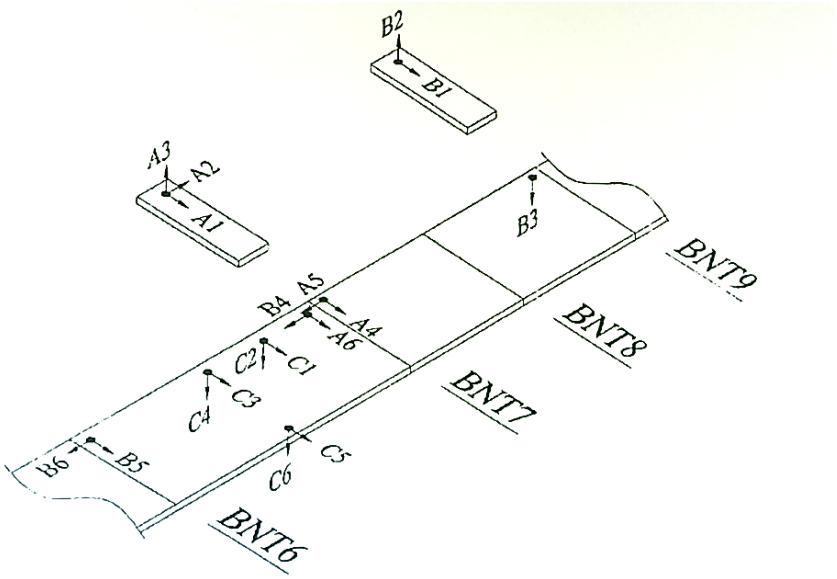

Figure 3.4 Sensor locations

Figure 3.5 NEMA 12 enclosure (UDOT)

Instruments placed on the deck are located on the underside of the deck. The locations of all of the channels and their cables are in table 3.11 . The locations of the boxes and channel locations and descriptions are also in Figure 3.6.

Table 3.1 Location and information about the boxes

	Instrument			Channel	
Box #	**Location**	**Type**	**Connection Information**	**Number**	**Orientation**
1	On Bent 9	ES-B	Cable #1 connected to screw board	B1	Transverse
				B2	Vertical
2	On Deck above Bent 9	ES-U	Junctioned at instrument 1	B3	Vertical
3	On Bent 7	ES-T	Cable #2 connected to screw board	A2	Longitudinal
				A1	Transverse
				A3	Vertical
4	On deck above Bent 7 on north side of expansion	ES-B	Junctioned at junction box*	A5	Longitudinal
				A4	Transverse
5	On deck above Bent 7 on south side of expansion	ES-B	Junctioned at junction box*	B4	Longitudinal
				A6	Transverse
6	On deck at 1/4 span from Bent 7 to Bent 6	ES-B	Junctioned at junction box*	C1	Transverse
				C2	Vertical
7	On deck at midspan between Bents 6 & 7	ES-B	Junctioned at junction box*	C3	Transverse
				C4	Vertical
8	On deck above Bent 6	ES-B	Junctioned at junction box*	B6	Longitudinal
				B5	Transverse
9	On deck at midspan between Bents 6 & 7	ES-B	Junctioned at junction box*	C5	Transverse
				C6	Vertical

* Junction Box is located on Bent 7

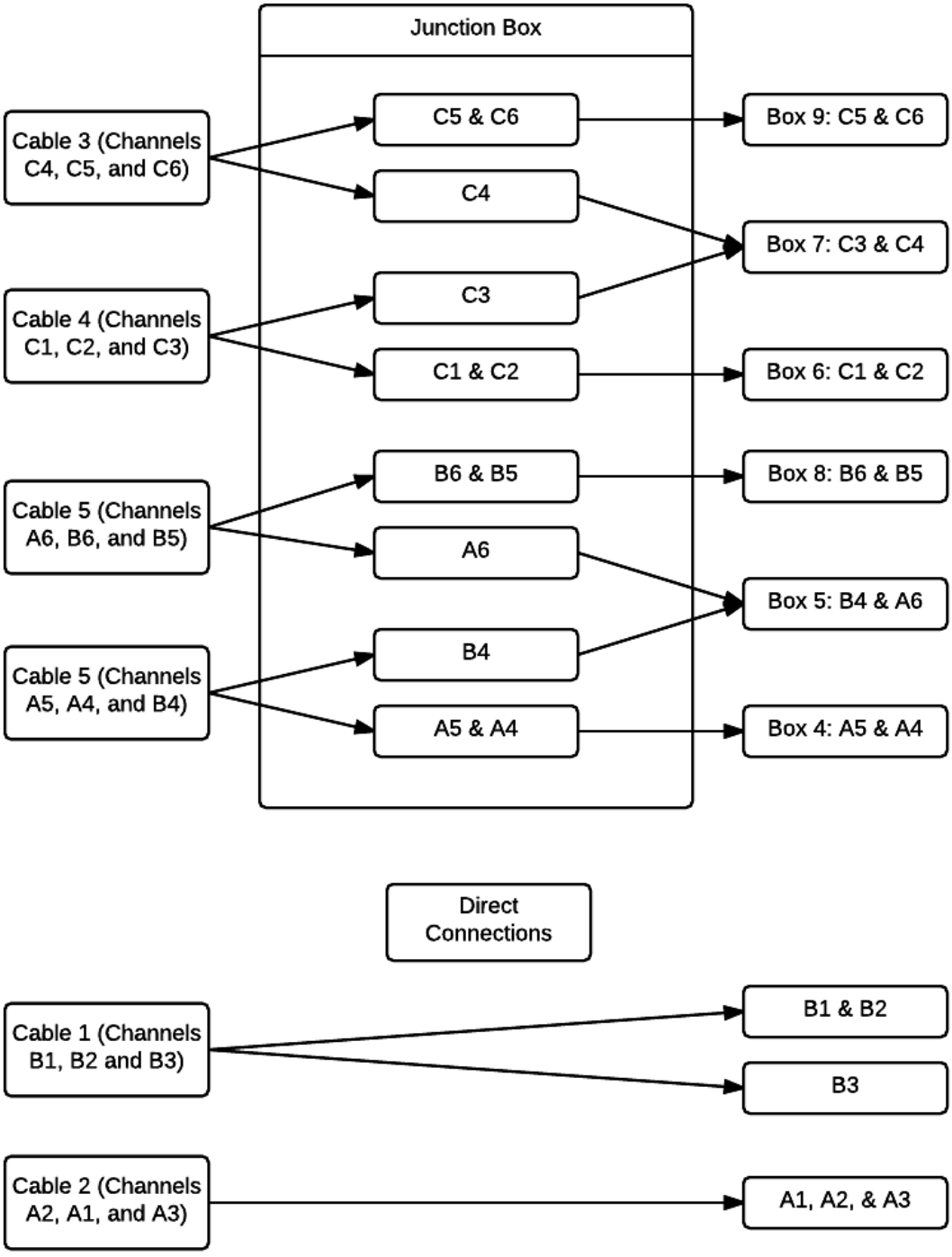

Figure 3.6 Breakout of channels and cables.

Belden 9774 cables connect the structural instrumentation. These cables are number 18 American wire gauge (AWG), 6 pair, individually shielded instrumentation cables. Cables run through two inch and one inch galvanized, rigid steel conduit (GRC) on the bottom of the deck. The casing of the EpiSensor accelerometer is isolated; therefore, the instruments are not grounded to or through the conduit or concrete. The grounding of each channel is carried to the permanent station where all instrumentation and power have been grounded into a copper rod driven into the ground. This effectively isolates the instrumentation from the bridge (Utah State University 2001).

The information for how the accelerometers were installed is not included in this report. However, more detailed information on the location and installation of the accelerometers and the history of the Salt Lake Seismic Station can be found in the UDOT report UT-01.12 *Strong Motion Instrumentation of I-15 Bridge C-846.*

Thermocouples

An array of thermocouples was installed at the bridge in June 2016. This array consists of 25 channels that are concentrated at a single longitudinal cross section on bent number nine. Each thermocouple requires one channel. Nine thermocouples are located through the deck of the left shoulder at approximately 15 inches outward toward the parapet from the girder. The through-deck thermocouples are located 10.5 inches from the underside of deck upward. The bent where the thermocouples are located is shown in Figure 3.7. There are thermocouples attached to the underside of the deck, the steel girders, and to the bent. The approximate locations of the thermocouples are outlined in figure 3.8 . All nine thermocouples embedded in the deck are in a plastic tube full of epoxy as shown in Figure 3.9. The thermocouples are evenly

spaced throughout the tube to measure the temperature gradient as shown in figure 3.10 . The thermocouples are spaced approximately every 2 cm, (0.5 in) along the plastic tube. The holes next to the tube in the picture hit rebar, so the hole had to be drilled again to achieve a sufficient depth. The other thermocouples are located on or near each of the girders. Each girder has a thermocouple that is next to the top of the girder on the underside of the deck on the concrete, one thermocouple at the top, middle, and bottom of the deck, and one thermocouple next to the bottom of the girder on the bent as shown in figure 3.8. There are 16 of these thermocouples associated with the girders. Epoxy connects each thermocouple end to the concrete or steel. The cable near the ends is attached with a magnet to the steel or with a metal clip that is attached to the concrete. These connections are shown in Figure 3.12 and Figure 3.11. The thermocouple cables go into a NEMA box closest to their girder. There is one NEMA box associated with each girder. All of the wire for the 24 thermocouples runs from the NEMA boxes through 1 in. conduit to the box on the bent at the west column and then runs through 2 in. conduit to the bottom of the west column to a box with a multiplexer. The box at the top of the west column is shown in Figure 3.13. The nine through deck sensors go through the same conduit down the column to the box with the multiplexer. The multiplexer (Figure 3.14) takes the 24 two-wire cables with 24 channels of data and sends them through one larger cable that has three twisted pairs through a large conduit in the ground, to the Campbell Scientific CRX 5000 data logger, see Figure 3.14. This data logger sends the information to the LTBP lab at Utah State University. There are 24 channels, but channel one on the multiplexer was found to give temperatures that were much higher than the others. The temperatures were assumed faulty data and the

thermocouple wire was moved in October 2016 to channel 25. This yielded more realistic results. The channels on the multiplexer that correspond to each thermocouple are depicted in Table 3.2.

Obsidian Data Logger

The Obsidian Data Logger is a 36-channel accelerograph that interprets the data from the accelerometers. The data sheet for the Obsidian is located in Appendix B. The Obsidian is capable of sampling rates up to 5000 samples per second, although not all of the channels are capable of sampling at this rate at the same time. Additionally, the Obsidian filters the data while it is still in analog, allowing for clearer results. A picture of the data logger is shown in Figure 3.16.

The orientation of the accelerometers is either transverse (across the bridge), longitudinal (along the bridge), or vertical. The channels and their orientation have been previously shown in Figure 3.4. The channel mapping, including the sensor name, channel, and location, and orientation on the bridge is shown in Table 3.3.

The other channels from 19-36 are for the downhole sensors. Their channels are outlined in Table 3.4. The borehole channels are named on the Obsidian software with the depth and the orientation, with the exception of 0 ft are F0[ENZ], 400 ft are 40[ENZ] and 160 ft are 16[ENZ]. For the bridge channels, screw terminals were used as in Figure 3.17. The bridge terminals are unlabeled, but follow the same pinout pattern as all of the other sensors that are on lightning suppression panels. The difference is in the ordering of the power supply pins, the +12V and -12V are switched. See Table 3.5. For the Obsidian connections, three channel connectors are used in series starting at channel 1. See Table 3.6.

Figure 3.7 Bent number 9, and its columns

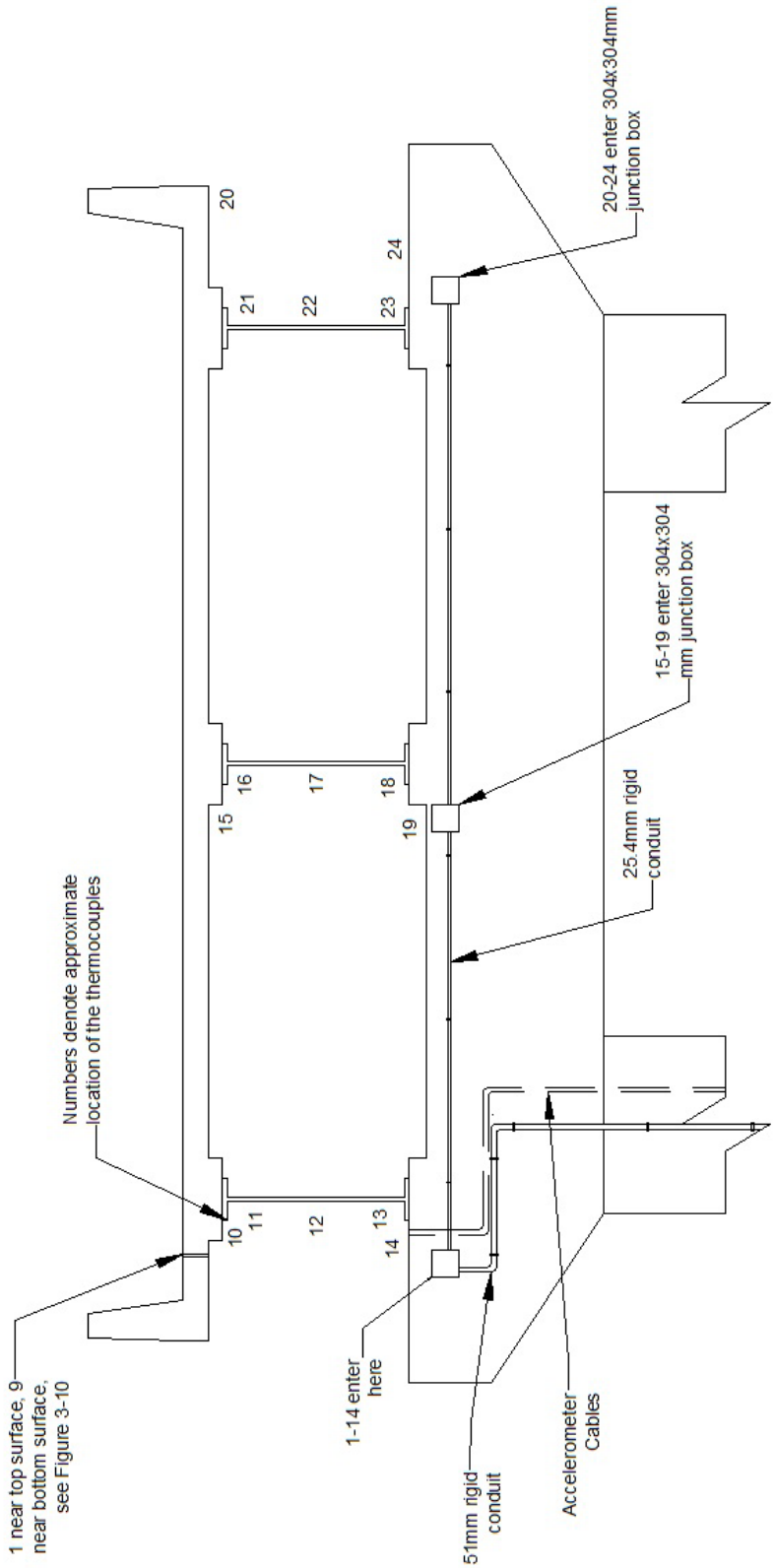

Figure 3.8 Elevation view looking north

Figure 3.9 Tube with the thermocouples inside, with the cable tips protruding

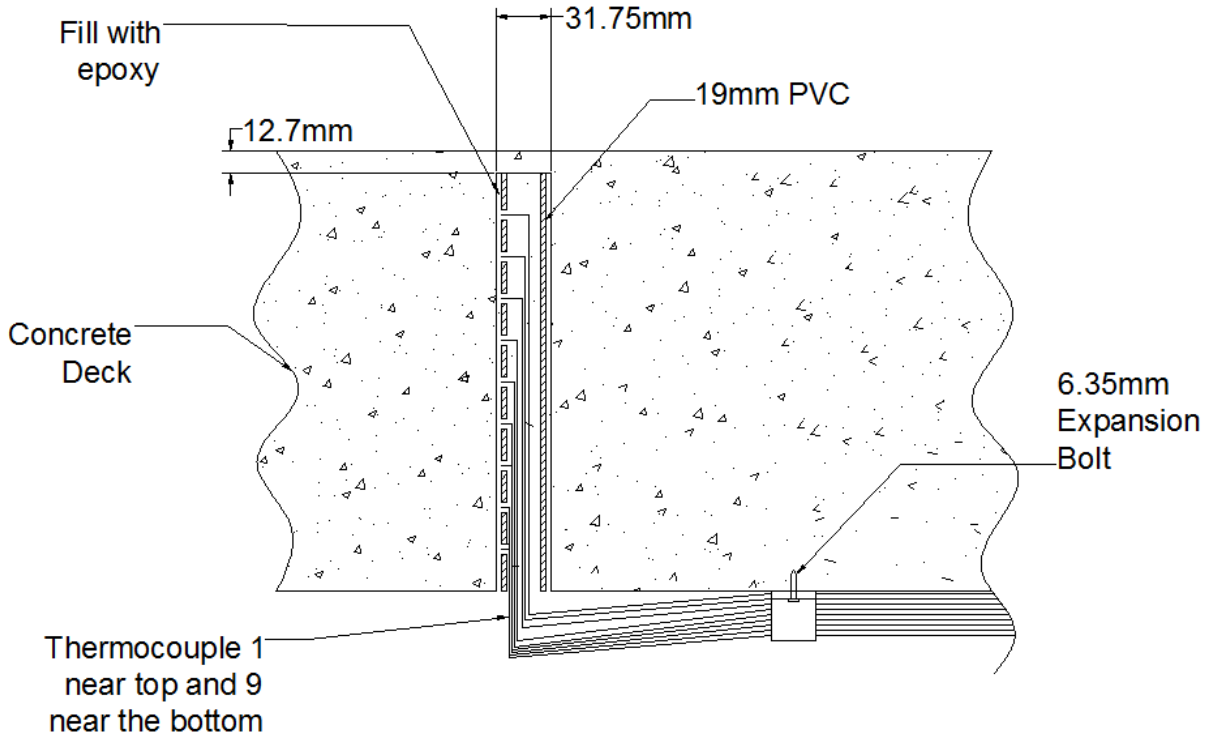

Figure 3.10 Thermocouples are at different locations around the perimeter of the tube.

Figure 3.11 Thermocouples that are attached to the girder and to the concrete with epoxy

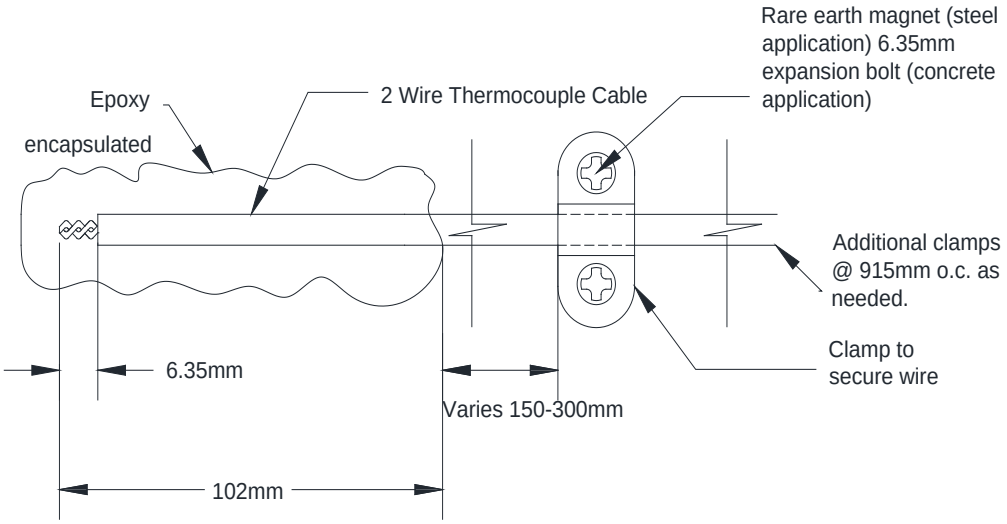

Figure 3.12 Attachment detail of the thermocouple

Figure 3.13 West column junction box

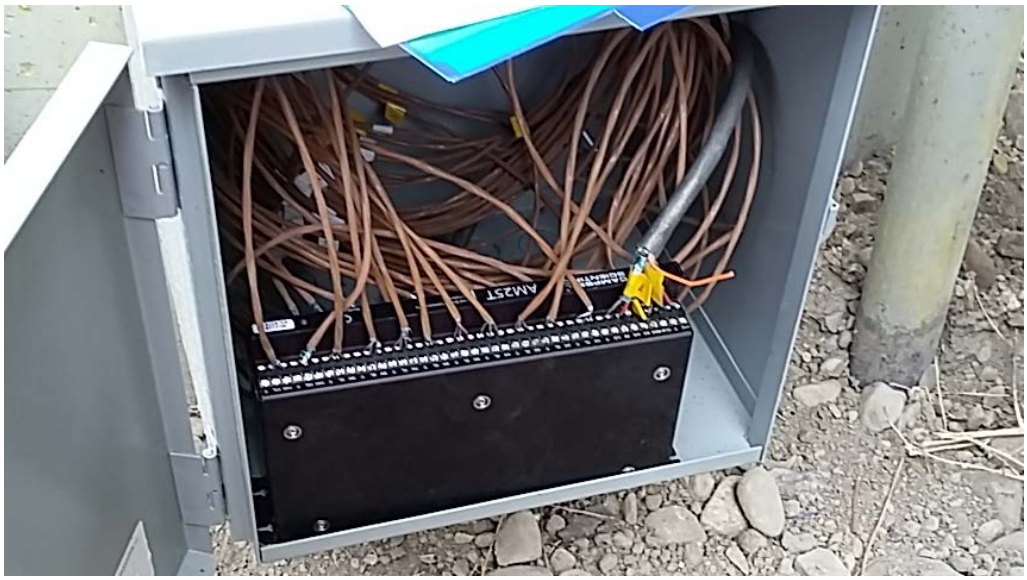

Figure 3.14 Multiplexer

Figure 3.15 CRX 5000

Table 3.2 Thermocouple locations and channels

Channel	***Thermocouple Location***
25	*Deck*
2	*Deck*
3	*Deck*
4	*Deck*
5	*Deck*
6	*Deck*
7	*Deck*
8	*Deck*
9	*Deck*
10	*West girder on concrete deck*
11	*West girder on steel top flange*
12	*West girder on steel web*
13	*West girder on steel bottom flange*
14	*West girder on concrete bent*
15	*Middle girder on concrete deck*
16	*Middle girder on steel top flange*
17	*Middle girder on steel web*
18	*Middle girder on steel bottom flange*
19	*Middle girder on concrete bent*
20	*East girder on concrete deck*
21	*East girder on steel top flange*
22	*East girder on steel web*
23	*East girder on steel bottom flange*
24	*East girder on concrete bent*

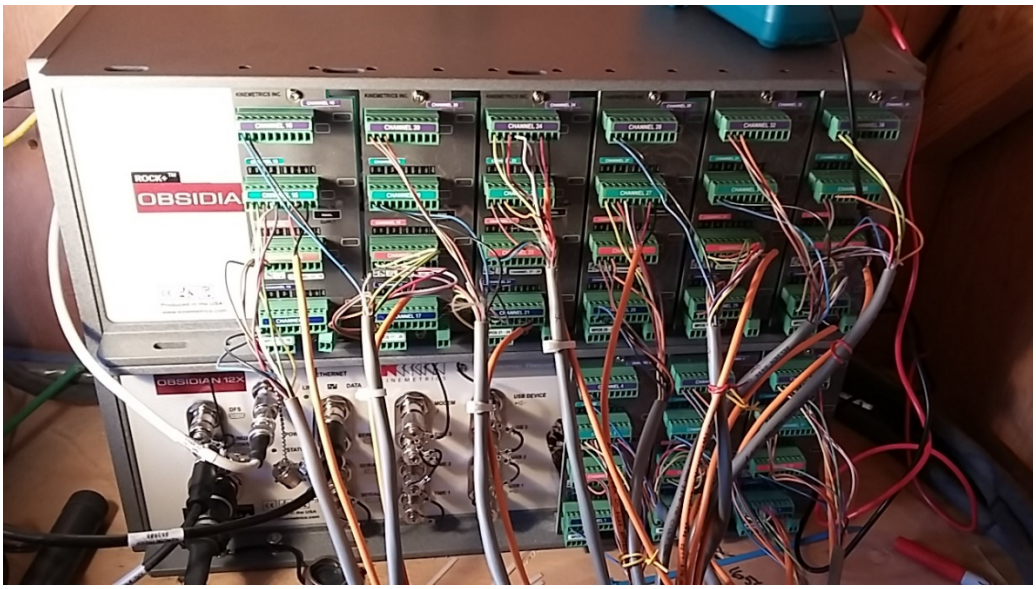

Figure 3.16 Obsidian data logger

Table 3.3 Bridge sensor channel, accelerometer, and location table

		Instrument		Channel	
Box #	**Location**	**Type**	**Connection Information**	**Number**	**Orientation**
1	On Bent 9	ES-B	Cable #1 connected to screw board	B1 B2	Transverse Vertical
2	On Deck above Bent 9	ES-U	Junctioned at instrument 1	B3	Vertical
3	On Bent 7	ES-T	Cable #2 connected to screw board	A2 A1 A3	Longitudinal Transverse Vertical
4	On deck above Bent 7 on north side of expansion	ES-B	Junctioned at junction box	A5 A4	Longitudinal Transverse
5	On deck above Bent 7 on south side of expansion	ES-B	Junctioned at junction box	B4 A6	Longitudinal Transverse
6	On deck at 1/4 span from Bent 7 to Bent 6	ES-B	Junctioned at junction box	C1 C2	Transverse Vertical
7	On deck at midspan between Bents 6 & 7	ES-B	Junctioned at junction box	C3 C4	Transverse Vertical
8	On deck above Bent 6	ES-B	Junctioned at junction box	B6 B5	Longitudinal Transverse
9	On deck at midspan between Bents 6 & 7	ES-B	Junctioned at junction box	C5 C6	Transverse Vertical

Table 3.4 Downhole sensor table

Downhole Sensors	
Channel	***Accelerometer***
19	*0ft E*
20	*0ft N*
21	*0ft Z*
22	*30ft E*
23	*30ft N*
24	*30ft Z*
25	*400ft E*
26	*400ft N*
27	*400ft Z*
28	*60ft E*
29	*60ft N*
30	*60ft Z*
31	*60ft E*
32	*25ft N*
33	*25ft Z*
34	*25ft E*
35	*160ft N*
36	*160ft Z*

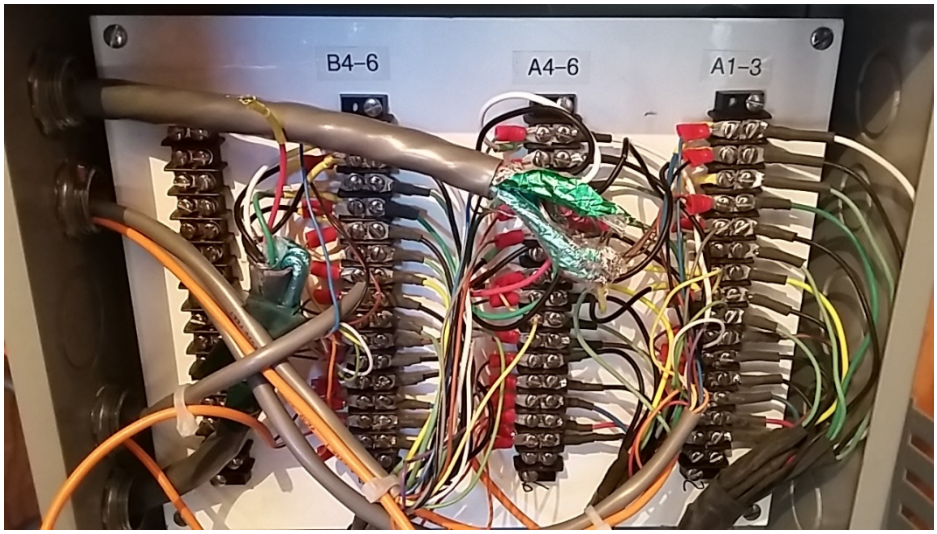

Figure 3.17 Screw terminals for B4-6, A4-6, and A1-3 channels

Table 3.5 Pinout table for the screw terminals in box in the shed.

Pinout number	Description	Color of wire
1	Channel 1+	Blue
2	Channel 1 -	Black
3	Shield (unused)	-
4	Channel 2+	Brown
5	Channel 2-	Gray
6	Shield (unused)	-
7	Channel 3+	Yellow
8	Channel 3-	Green
9	Shield (unused)	-
10	Calibration	White
11	Calibration enable	Violet
12	-12v	Black – orange power cable
13	Common	Shield – orange power cable
14	+12V	Red - orange power cable
15	Ground	Red and Orange

Table 3.6 Example of pinouts on the Obsidian side

Channel	Pinout Number	Description	Color of Wire
1	1	Channel 1+	Blue
	2	Channel 1-	Black
2	1	Channel 2+	Brown
	2	Channel 2-	Gray
	3	Ground	Orange
3	1	Channel 3+	Yellow
	2	Channel 3-	Green
	3	Ground	Red
	4	Calibration	White
	5	Calibration Enable	Violet
	6	No connection	-
	7	Common	Shield – orange power cable
	8	+12V	Red – orange power cable
	9	-12V	Black – orange power cable

Chapter 4: Data Analysis Methods

Introduction

The data from the thermocouples and the accelerometers were recorded and the natural frequencies were obtained from the accelerometers. The natural frequencies were then compared with the temperature, and the resulting daily and seasonal trends were identified.

Natural Frequency of a bridge

The natural frequency of a bridge can be determined using forced vibration methods such as a shaker or pull testing, or by using ambient excitation. In this case, the natural frequency is obtained by measuring the time history of the ambient vibration on the bridge.

Ambient Vibration Time History to Frequency

The time history of the acceleration information is taken with the accelerometers as a change in voltage. That change in voltage is then digitized into discrete amounts with the data logger. Then the data points from the data logger are transferred from the time history to frequency by using a discrete Fourier Transform. The Discrete Fourier Transform (DFT) and its inverse are respectively:

$$F_k = \frac{1}{N}\sum_{n=0}^{N-1} f_n e^{-ik\omega_0 n} \qquad \text{for } k = 0 \text{ to } N-1 \qquad (22)$$

$$f_n = \frac{1}{N}\sum_{k=0}^{N-1} F_k e^{ik\omega_0 n} \qquad \text{for } n = 0 \text{ to } N-1 \qquad (23)$$

where $\omega_0 = 2\pi/N$.

In Equation 22 the time is represented by n and the displacement of the accelerometer is denoted by f_n. Evaluating the sum yields the frequency k and the amplitude F_k. The inverse

transform would be able to convert the information back to the time history information. Since these calculations would be long and extremely arduous to perform for thousands of data points, computer algorithms have been developed to perform the Fourier transform. There are two algorithms discussed, the Fast Fourier Transform and the Welch Power Spectral Density Estimate.

Fast Fourier Transform and Welch's Power Spectral Density Method.

The Fast Fourier Transform Algorithm (FFT) is a way to evaluate the (DFT) but with fewer calculations than the N^2 number of calculations required by Equation 22. This involves computing the even values and the odd values of the sum for the Fourier Transform separately and then unscrambling the results. This yields $N \log_2 N$ calculations. For a more detailed discussion of FFT, see Chopra and Canale (2010) and Osgood (2007).

Welch's power spectral density estimate (PWELCH) uses the FFT, but also divides the data into segments and overlaps them and averages the spectra of the overlapped segments. Because of the averaging, the spectra are low passed and the peaks are not so narrow. This filters out a lot of the noise from the signal. If the signal was a perfect mix of sines and cosines then it would be easy to use the Fast Fourier transform, but because the signal from the bridge is much more complicated and erratic, the PWELCH function is warranted. A good explanation is given in Augusto (2016).

Matlab has a variety of intrinsic functions, including both FFT and PWELCH algorithms. The FFT was considered, but in the end the PWELCH method was used in the analysis of the natural frequencies because of the greater control over the output of the results. The parameters used in the PWELCH function were NFFT = 4096, which is almost twice the number of data points and gives a 50% overlap. The y-axis was initially multiplied by 20log10 in order to extend

the y-axis for better viewing and to better identify the natural frequency maximums. Later, the number 5 was multiplied by the Obsidian data logger amplitude values, and the number 10,000 was multiplied by the CR5000 data values. This seemed to give a much better view of the data. This is shown in the next chapter.

Methods of Finding Maximums

From the power spectral density estimate of the data, maximums show up at the natural frequencies. The maximum is variable from hour to hour and is affected by temperature. However, there are some hours where the data does not show a maximum, or, because the data has a low sampling rate, the maximum can shift more than it should. This shift happens because there is no data point for it to fill between the points. The data is not as fine as it should be. There were several different methods that were attempted to solve the problems with the resolution.

First, the data can be added up. This causes the static to cancel out and the frequencies to be accentuated. Second, the data can be matched with its temperature for many days at a time. Third, a cubic curve can be fit to each hour's data. The spectral density often has several maxima clustered together around the largest maximum. The curve fit takes the weighted average of these maxima and a maximum can be chosen from the curve fit. Since the curve fit resolution can be as fine as it needs to be, the maximums show up between the points. This provides a higher resolution scatter plot, and a more accurate equation to fit the data. Of the three following methods, only method three was chosen because it gave the most reliable results.

Method 1

The first method used the power spectral density data for multiple days at a specific temperature. The data were added because the noise tends to cancel out and natural frequencies are amplified. Figure 4.1 is a graph of the data for all three accelerometers for 45 days at 10°C (50°F). Similar graphs were developed for every 5.6 degrees Celsius (10 degrees Fahrenheit), from 4.44°C (40°F) through 38°C (100°F). The next step was to pick off each of the maximums of interest. This was done using the graph as shown in Figure 4.2 by highlighting the values at the peaks of interest as shown. After the peaks for each of the maximums of interest had been identified for each of the graphs, seven in this case, then the points were plotted on a scatter plot with frequency vs temperature. The results from using this method for accelerometers C2, C4, and C6, for thermocouple 16 are in Figure 4.3.

Method 2

A second method was used to find the correlation between the temperature and frequencies. In this method, the data were not added, but all of the points for every temperature were simply plotted with the frequency at the area of interest on the graph. The code takes in a set of frequency bounds and searches for a maximum in those bounds. Frequency bounds were based off previous graphs with a wider range and then focusing in on a group of highly concentrated points. For example, two clusters of points that represent different natural frequencies show up in Figure 4.4, with one group somewhere between 9.15 and 9.25 Hz, and the other group between 9.4 and 9.6 Hz.

Next, the time at which the frequency is recorded is matched with the temperature for any thermocouple at the same time. An example of the kind of results that this method yields are

shown in Figure 4.5. This data gets separated into bins, and the resolution is poor. For this reason, this method was not chosen to be used in the experiment.

Method 3

To avoid this problem, instead of only choosing the maximum from the spectral density curve, a line was fitted to the data. A comparison of how the maximums are determined is shown in Figure 4.6. The third method of finding the maximums was chosen for the experiment because it was not as tedious as method 1 and was more reliable than method 2. Given this third method of extracting the portion with the highest amplitudes, the data is improved. The bins from the previous method have disappeared, and there are many more points than in the first method. This method was chosen for the experiment because it takes the best things from all of the previous methods and combines them. An example of what this data looks like is shown in Figure 4.7.

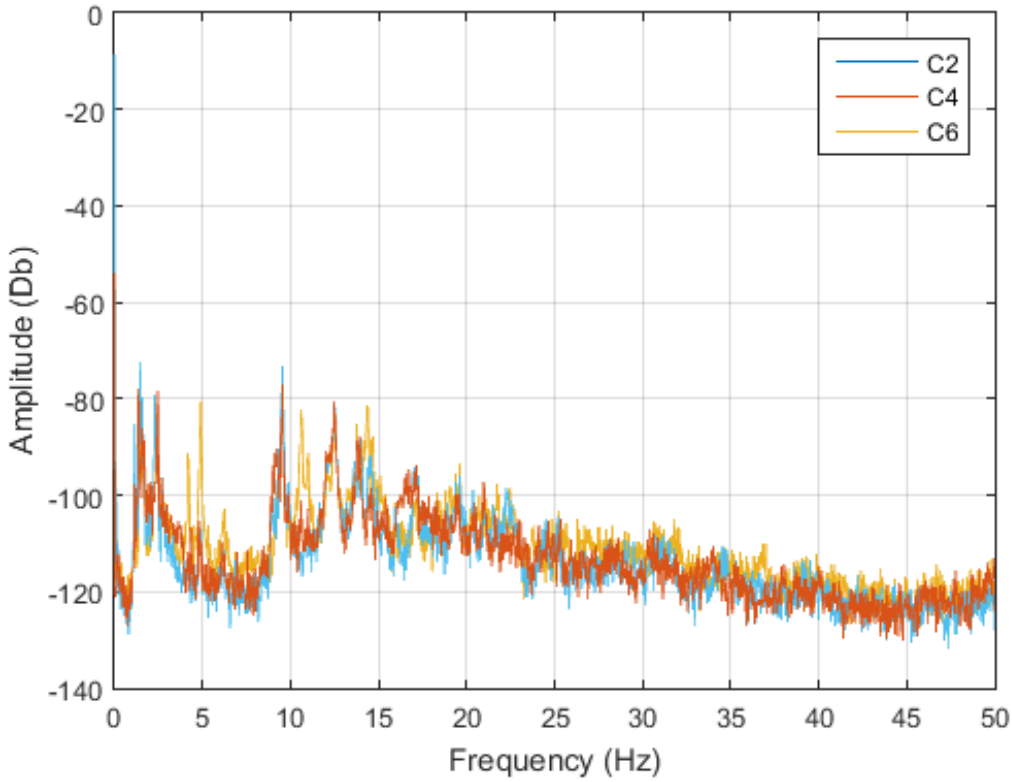

Figure 4.1 Added frequency spectra for 45 days for accelerometers C2,C4 and C6 for thermocouple 16 at 10^{o}C.

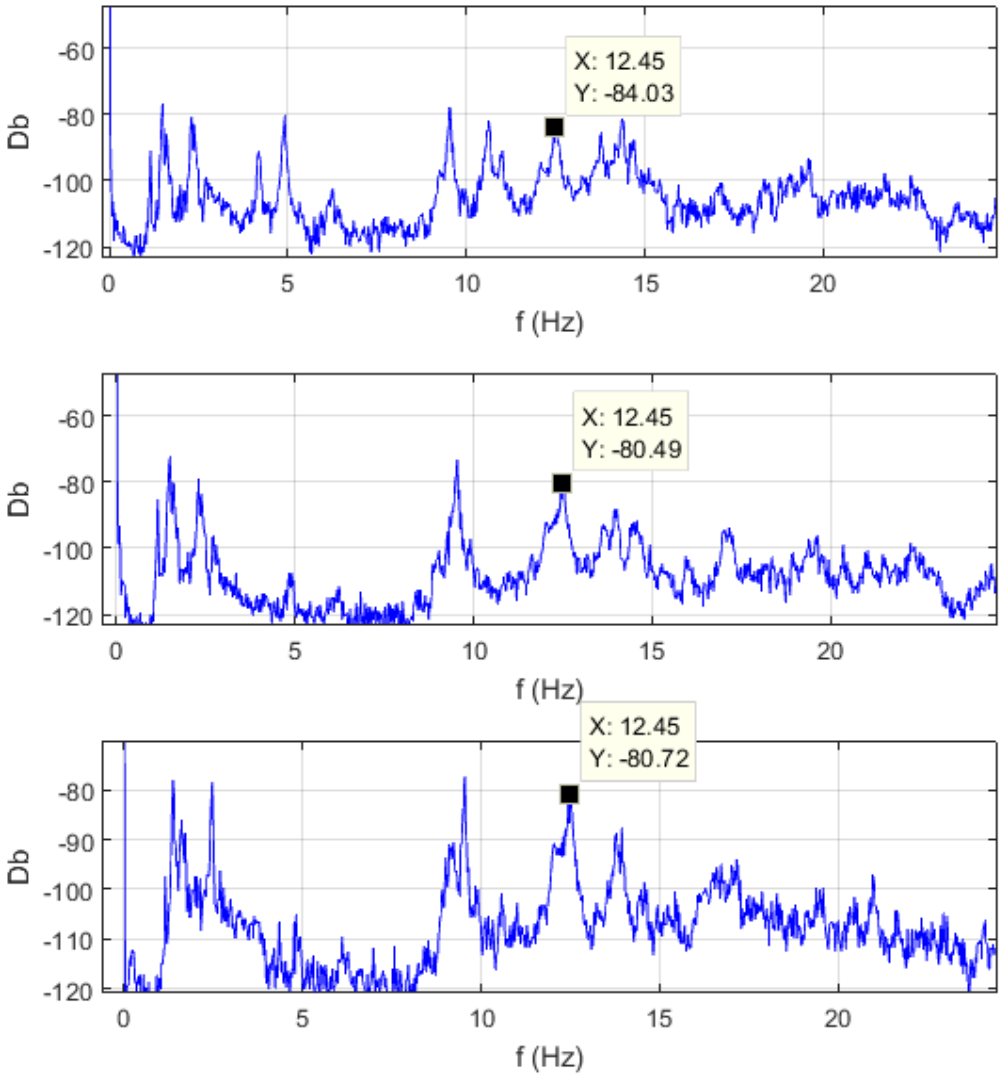

Figure 4.2 From top to bottom, accel.C2, C4,and C6 added power spectral density estimate at 10°C on thermocouple 16.

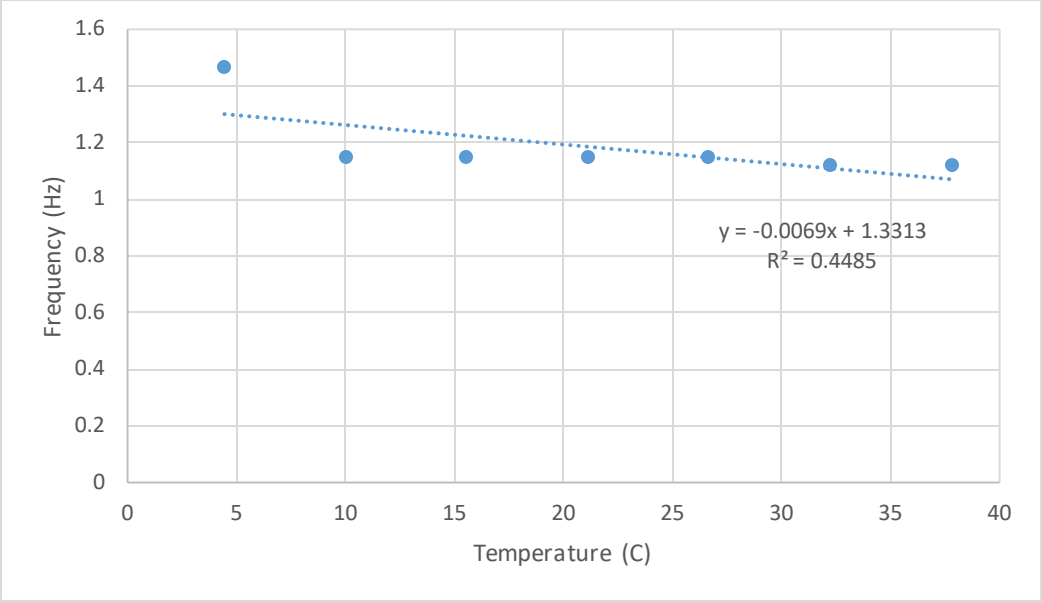

Figure 4.3 Accel. C2 against thermocouple 16 for the average frequency of 1.186 Hz.

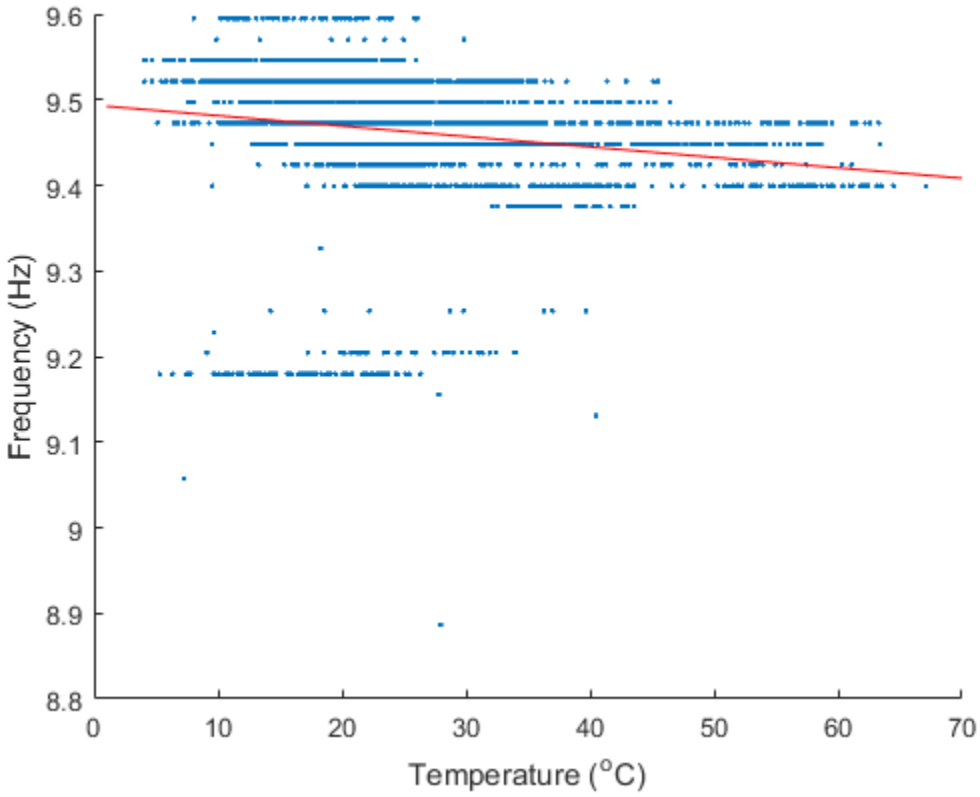

Figure 4.4 Temperature vs. Frequency plotted with a trend line for the accel. C6 and thermocouple 16 for maximums between 8.8 and 9.6.

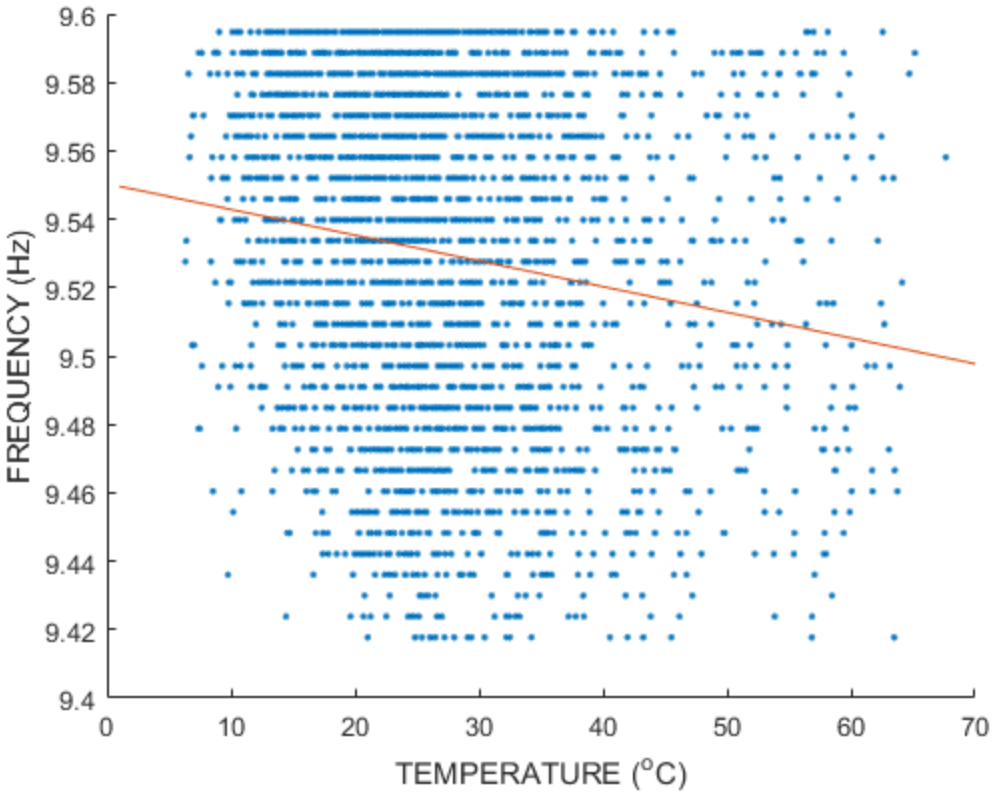

Figure 4.5 Frequency vs Temperature for accel.C2 and thermocouple 14 for the range of 9.4 to 9.6 Hz using method 2.

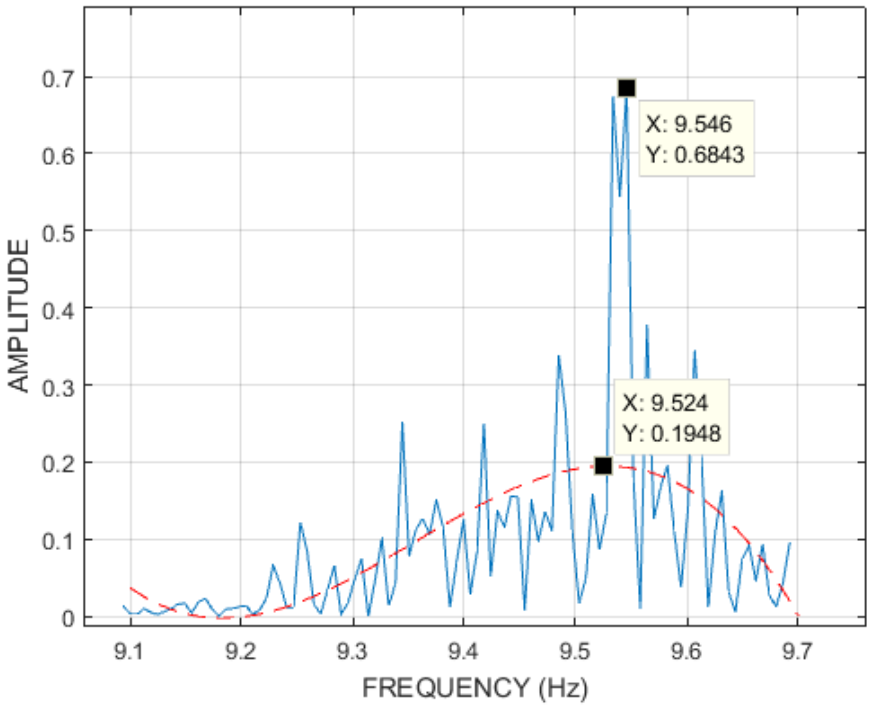

Figure 4.6 Two different methods of determining the maximum: choosing the highest amplitude, or taking a curve fit and choosing its maximum.

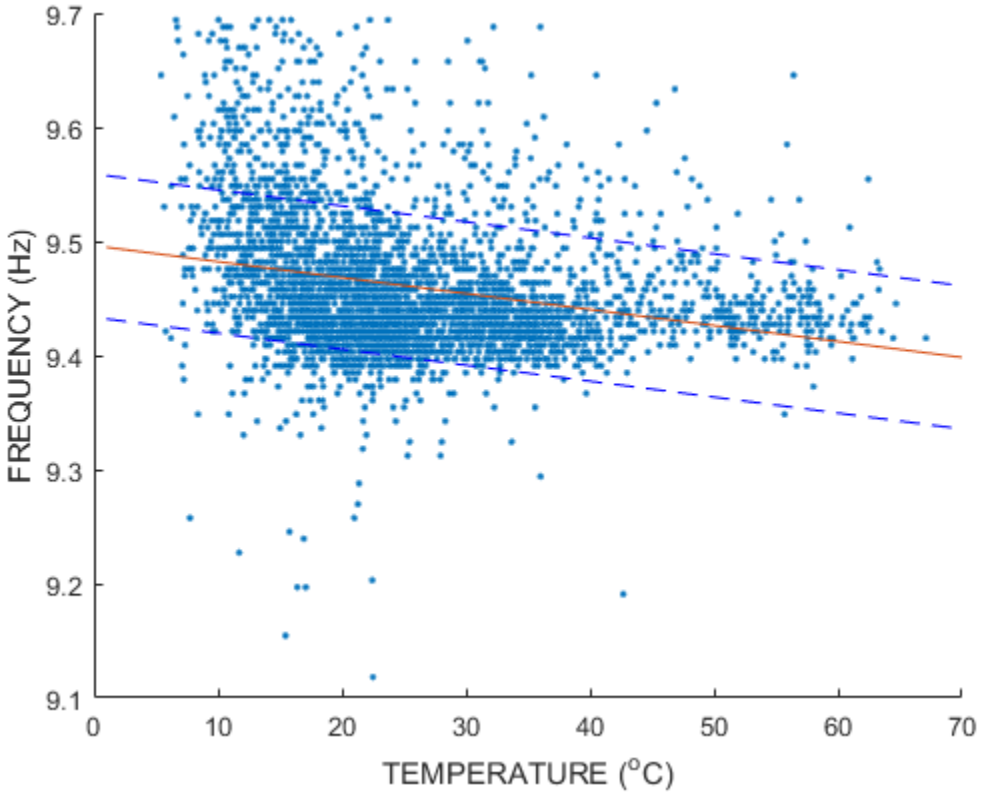

Figure 4.7 Results from using method 3.

Chapter 5: The Experiment

Questions to be Answered

Three parts are addressed in this report. First is a discussion of how the ambient temperature and the thermocouples compare. Second, is how the Kinemetrics Obsidian® data logger compares with the CR5000 data logger. Third is an explanation of the correlation between temperature and frequency.

Ambient Temperature and Thermocouple Temperature

A comparison of the ambient temperature to the bridge temperature shows that from about 10 pm to 11 am the correlation is very close, but from 11 am to 10 pm, there is a large difference in the temperatures. At first, this rapid increase in temperature was thought to be plausible, but after closer examination, the high temperatures were deemed unsuitable for correlating with the natural frequencies. In some cases, the bridge was giving temperatures in the shade during the summer in excess of 60ºC, which does not happen when the ambient temperature is barely at 40ºC. An example of the temperature throughout a typical day is shown in Figure 5.1.

The solid lines represent the temperature readings from the thermocouples, and the dashed line is the ambient temperature throughout the day. In this particular graph at 2 pm, the temperature of the thermocouples stops following the ambient temperature and forms a peak. Based on the review of many such graphs on different days, the best correlation between the ambient and the sensor temperatures seems to occur from midnight to 6 am. There are some other interesting effects of the temperature that happen during the daylight hours. First, the temperature drops below the ambient temperature in the webs on the east side during the

morning and on the west side during the evening. In the middle girder the temperature stays close to the ambient temperature during the morning and evening, see Figures 5.2-5.4. Most days exhibit this behavior, but on rainy days the behavior can change dramatically. Below in Figure 5.5 is a graph of Thermocouple 16 during three rainy days in May. During May 7 and 8 the temperature remained relatively constant compared to other days, and stayed between 10°C and 4°C (50°F and 40°F) the entire time.

One of the possible reasons for the temperature spikes and dips in the graph is the reference temperature on the AM25T multiplexer. The thermocouple compares the reference temperature on the multiplexer with the temperature on the bridge when it sends information to the CR5000. The multiplexer is outdoors inside of a NEMA box and the temperature is not controlled; this could contribute to the unreasonable temperature swings that are so far outside of the ambient temperatures.

In order to provide more consistent data, temperature information from the Salt Lake International Airport was used (Airport 2016). This data proved to give closer correlations with the natural frequencies, and usually gave a closer confidence interval for each of the graphs.

CR5000 Versus Obsidian Data Logger

The obsidian data logger varied from the CR5000 in the results it yielded. There were some similarities and differences.

Both the CR5000 and the Obsidian data logger were able to find natural frequencies of the bridge. The frequencies that were found tended to be in a similar range for each temperature.

There are several differences between the data loggers. The Obsidian data logger is capable of 500 samples per second on all of the channels, while the CR5000 has a maximum sampling rate of 100 samples per second. The Obsidian also incorporates low pass filtering in the

analog stage of the data. Both of these features make the Obsidian more accurate at sampling the data. Comparing the power spectral densities of the two data loggers, the frequencies show up in very similar locations. For example, the Obsidian power spectral density (PSD) in Figure 5.6 looks very similar to the CR5000's PSD in Figure 5.7 even though the CR5000 only took the data for 3 minutes and the Obsidian sampled the data for 7 minutes. The data were taken at different times about 15 minutes apart. The higher sampling rate of the Obsidian makes the data more accurate, because the distance between points on the PSD is smaller. Since variations in the natural frequency and temperature tend to be small, the Obsidian is able to pick up changes in the natural frequency more readily than the CR5000. For this report, the CR5000 was used for the results only because there was more data with the CR5000 than the Obsidian. In the future, the Obsidian should be used.

Correlation of Natural Frequency due to Temperature

The natural frequencies can be found in several different ways. There were three methods that were tried in this report. The third method was chosen, which takes a cubic fit of spectral density and then takes a maximum of the cubic fit. The temperature and frequency were monitored every hour starting on January 1, 2016. The temperature data was measured at the Salt Lake International Airport because the thermocouple data was thought to have errors. The accelerometer data was chosen from sensors C2, C4, and C6 because they give the vertical excitation of the bridge, which is the dominant excitation given from the traffic across the bridge. Each hour of accelerometer data was sampled for 3 minutes starting at the top of each hour. The temperature data was not as consistent, but usually was taken at seven minutes before the beginning of each hour. The temperature and accelerometer times were rounded to the nearest

hour. Figure 5.8 through Figure 5.16 show the results of using this method. The equations in the figures correspond to the center line that goes through the data.

Only three frequencies were used because they gave the best confidence intervals. The lower frequencies tended to have peaks that were close together, this caused clusters of data to form when the scatter plot was made because the maximums overlapped.

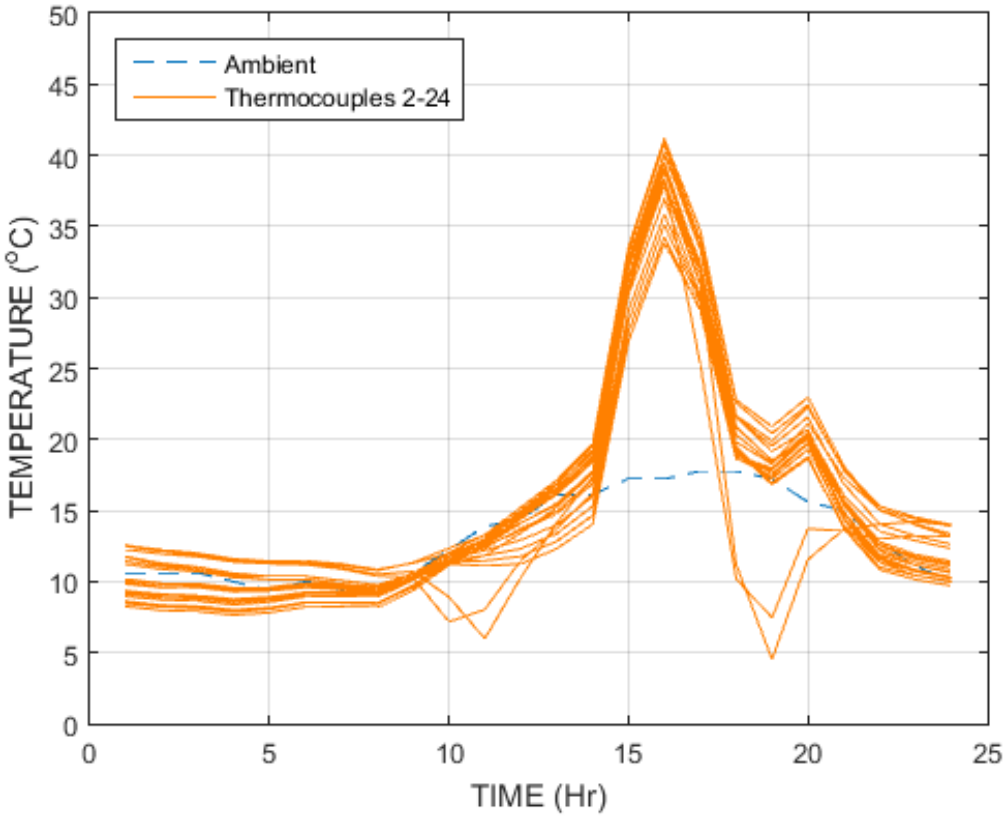

Figure 5.1 Comparison of thermocouples vs. ambient temperature

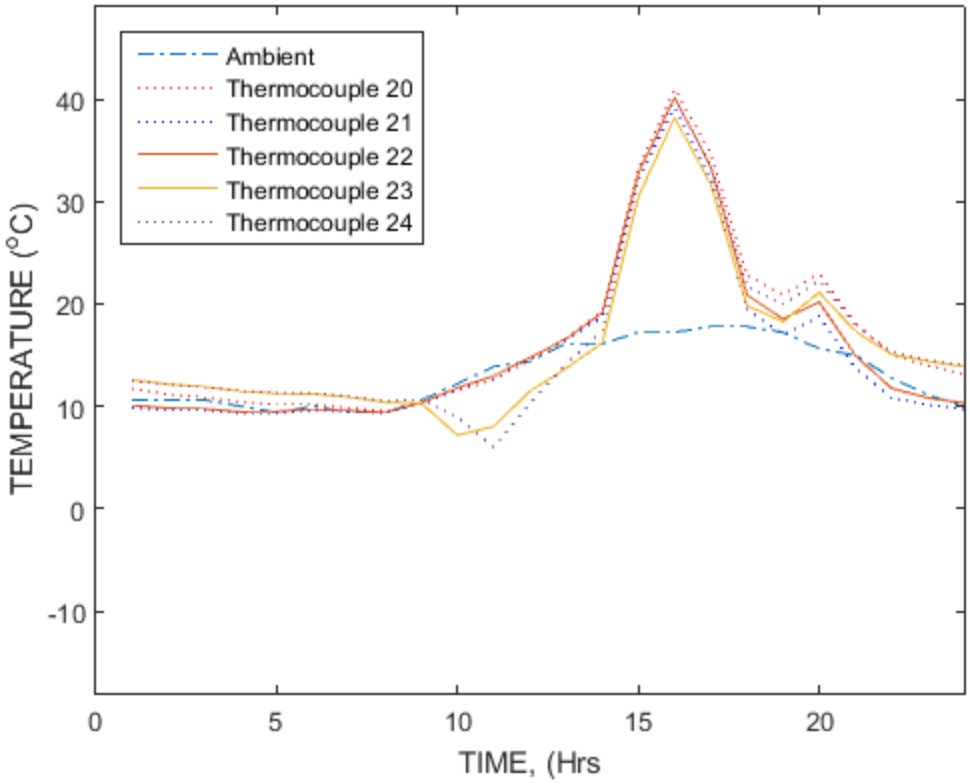

Figure 5.2 Thermocouples 22 and 23 are less than ambient in the morning

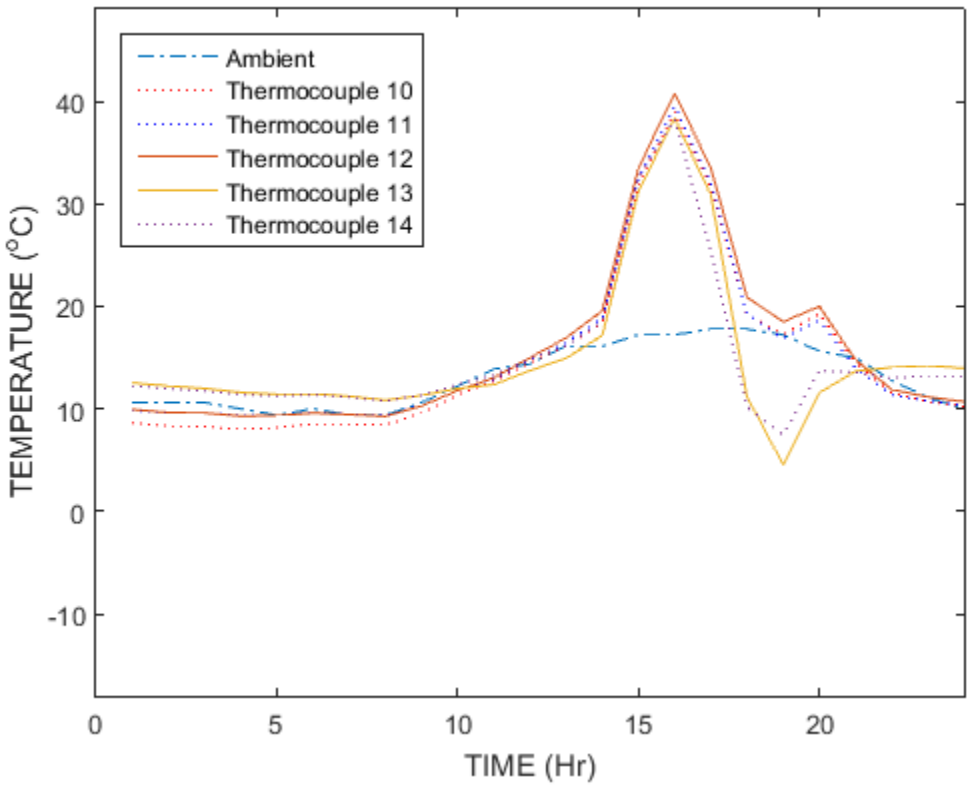

Figure 5.3 Thermocouples 12 and 13 are less than ambient in the evening

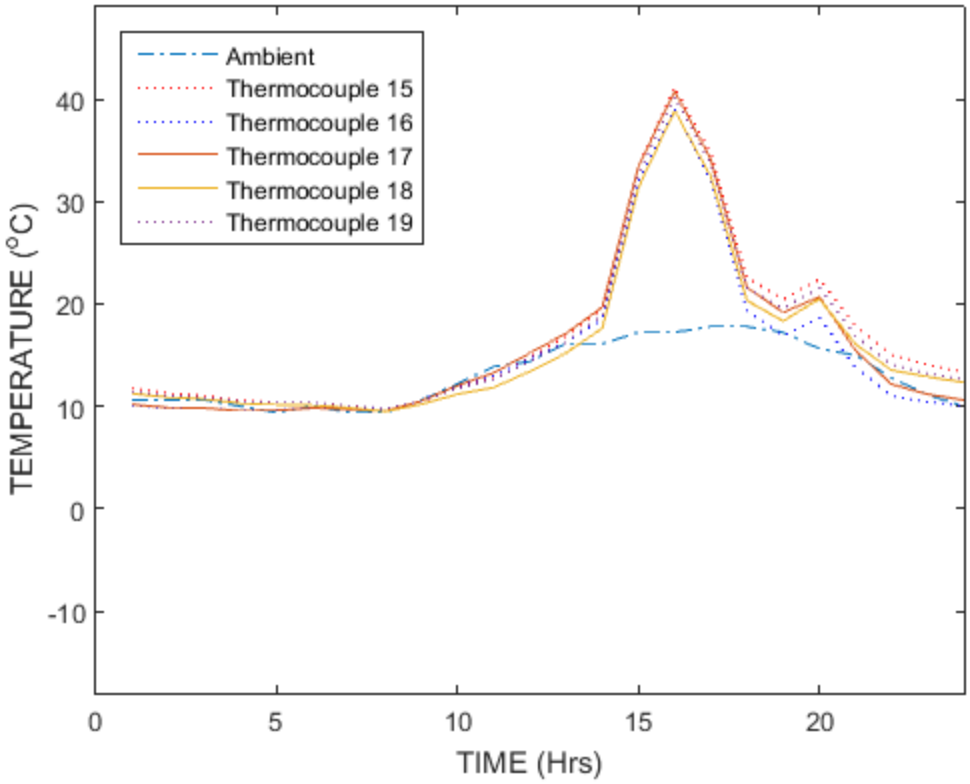

Figure 5.4 The middle steel girder temperature stays at ambient in the morning and evening

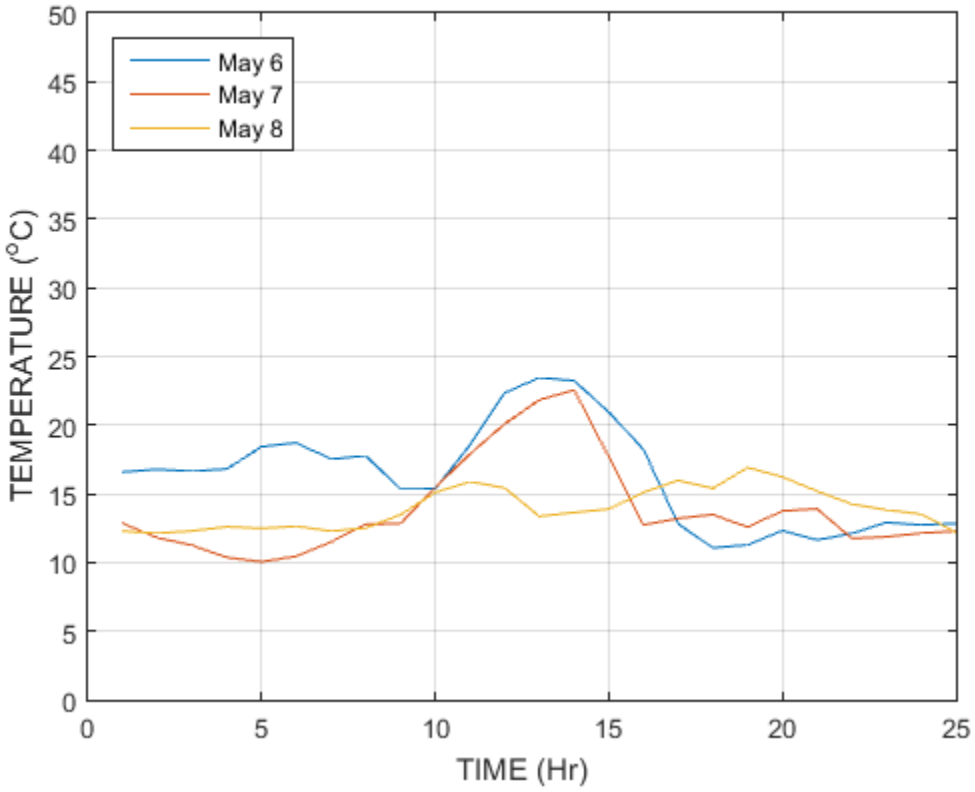

Figure 5.5 Three days in May with precipitation

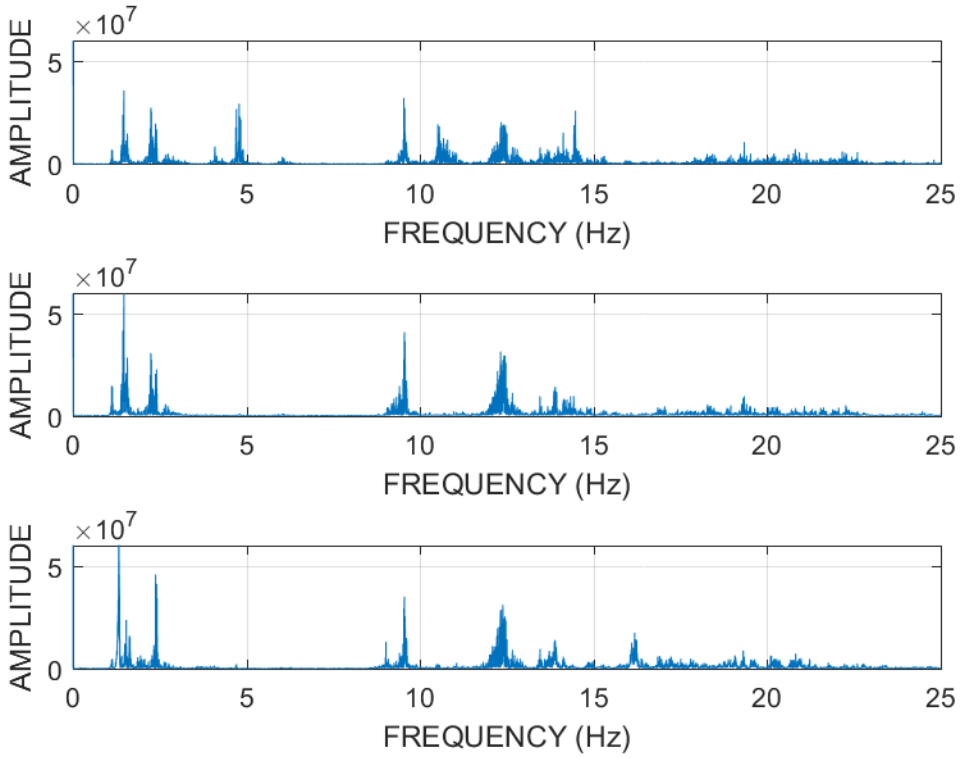

Figure 5.6 PSD from the Obsidian, from top to bottom sensors C2, C4 and C6 at 18.8 ᶜC. (66ºF).

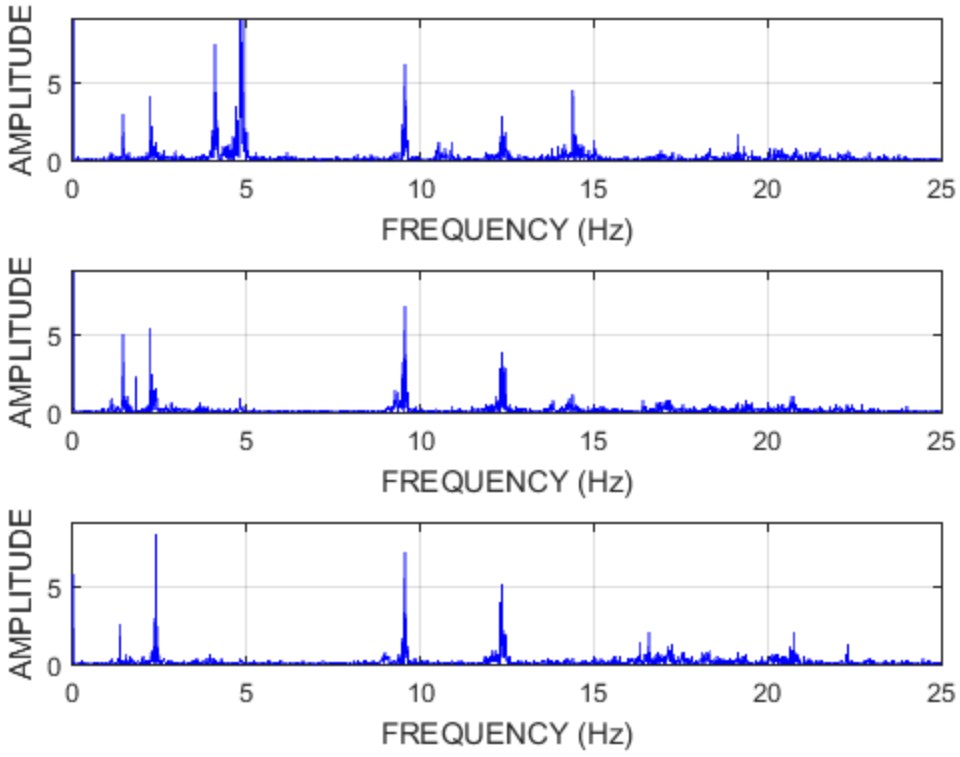

Figure 5.7 PSD from the CR5000, from top to bottom, sensors C2, C4 and C6 at 18.8 °C. (66°F).

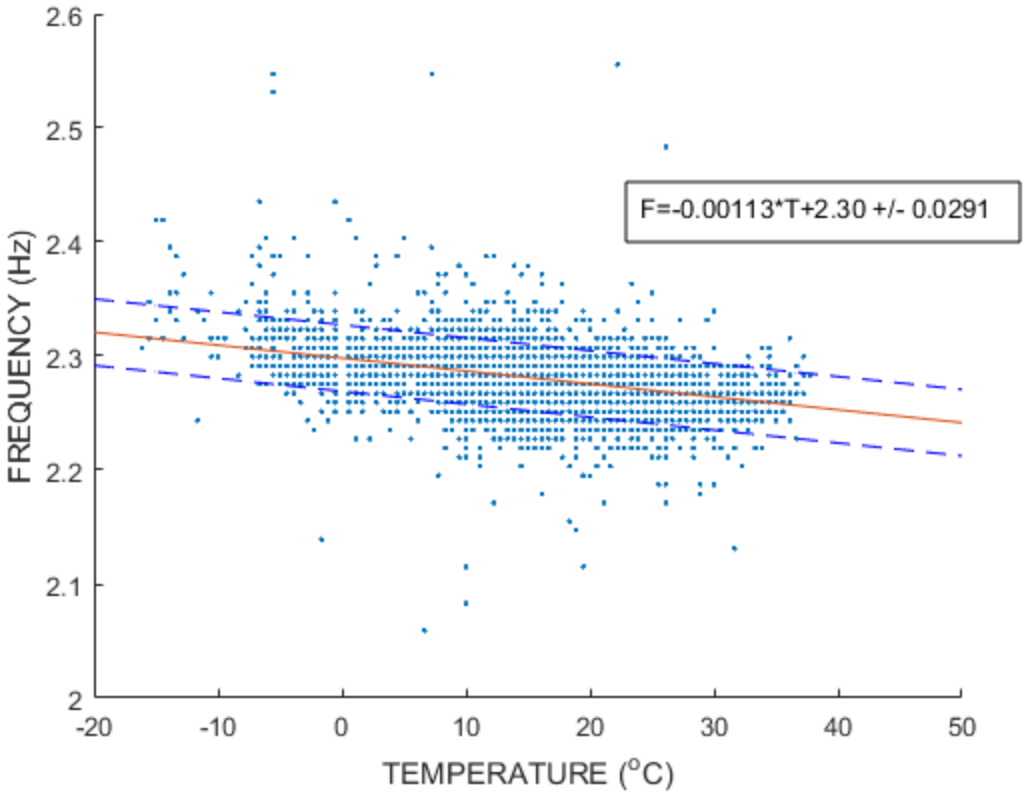

Figure 5.8 Sensor C2, Frequency 2.4 Hz

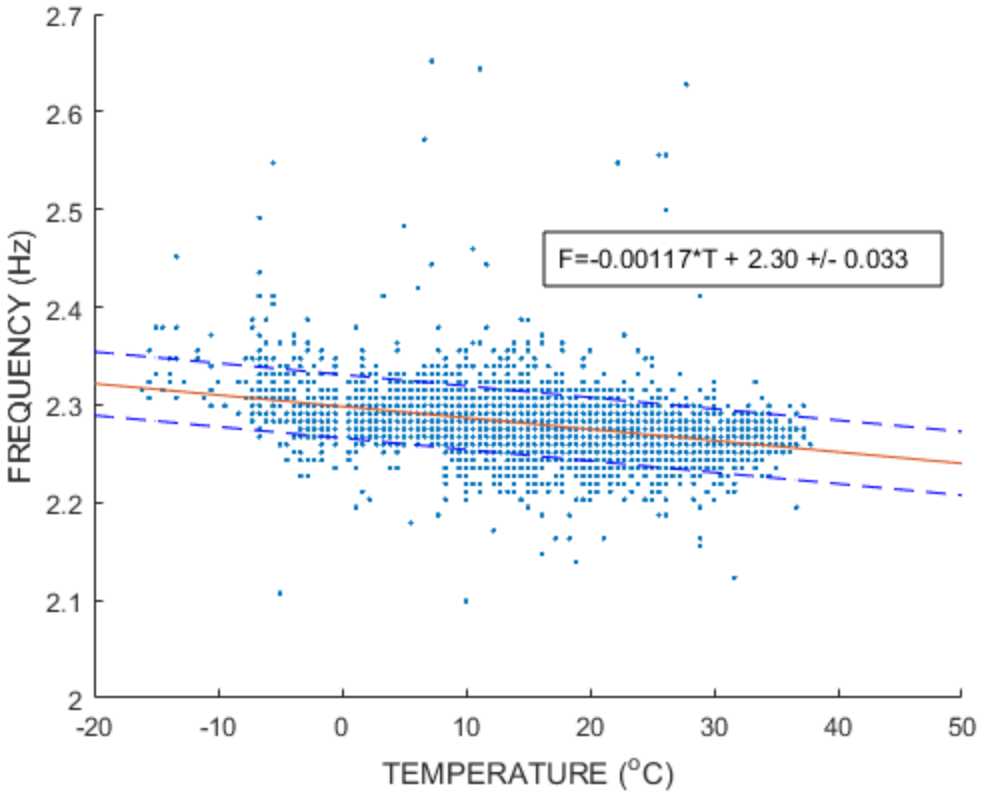

Figure 5.9 Sensor C4, Frequency 1

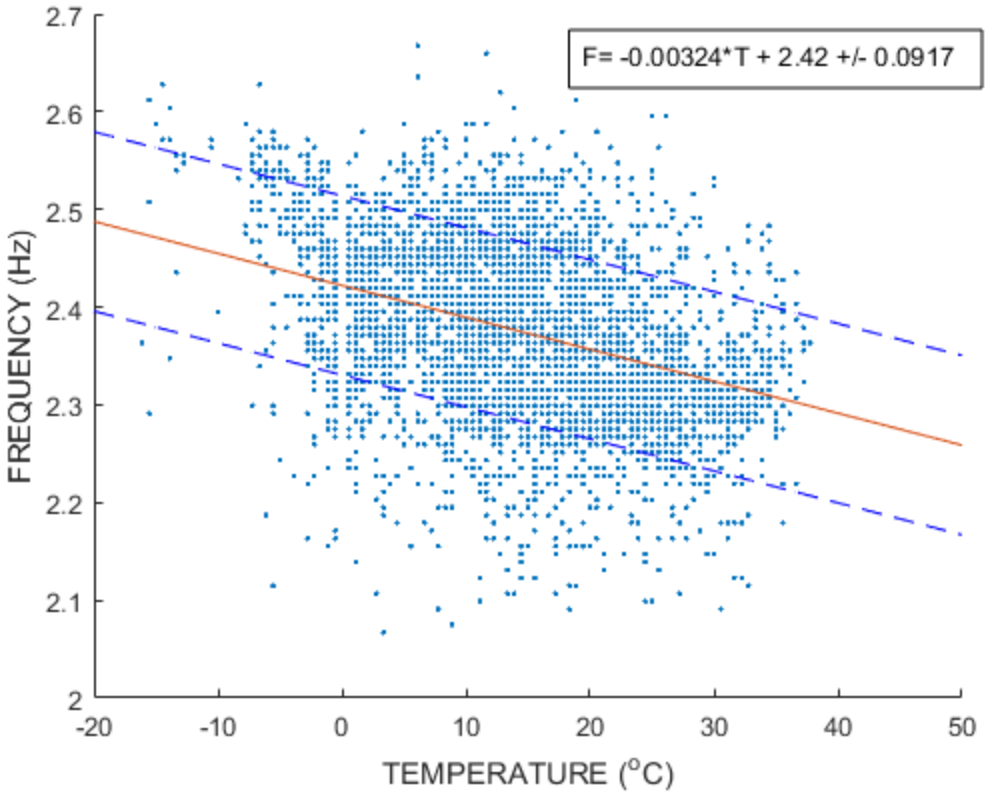

Figure 5.10 Sensor C6, Frequency 1

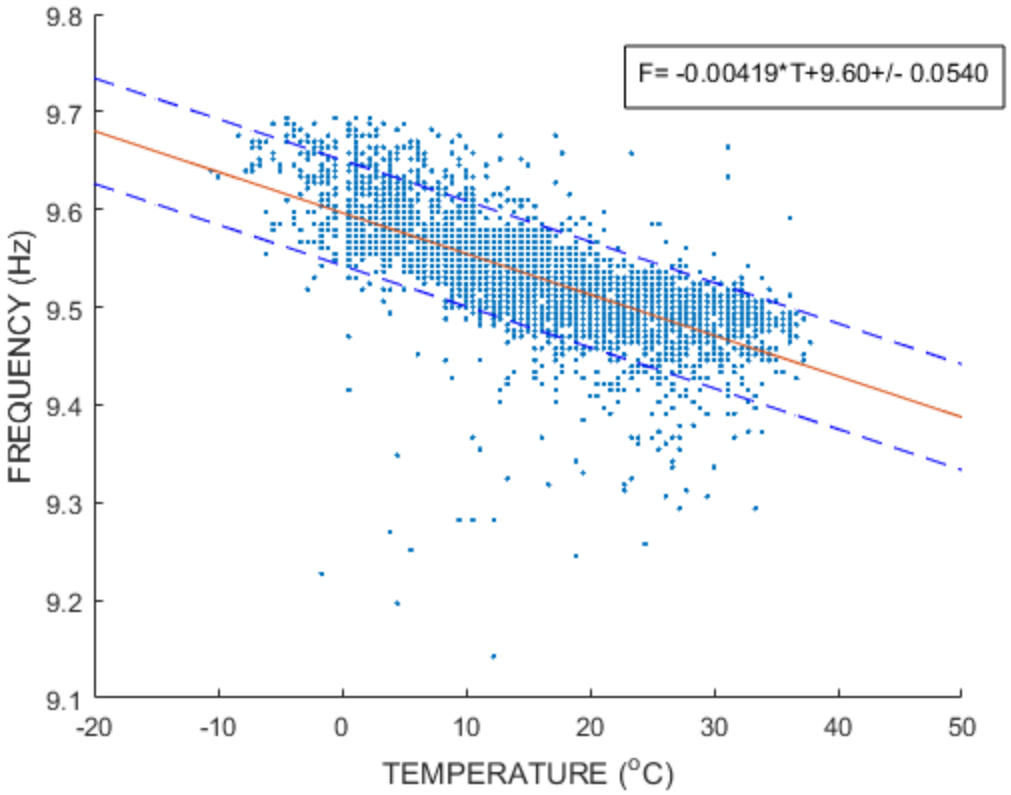

Figure 5.11 Sensor C2, Frequency 2

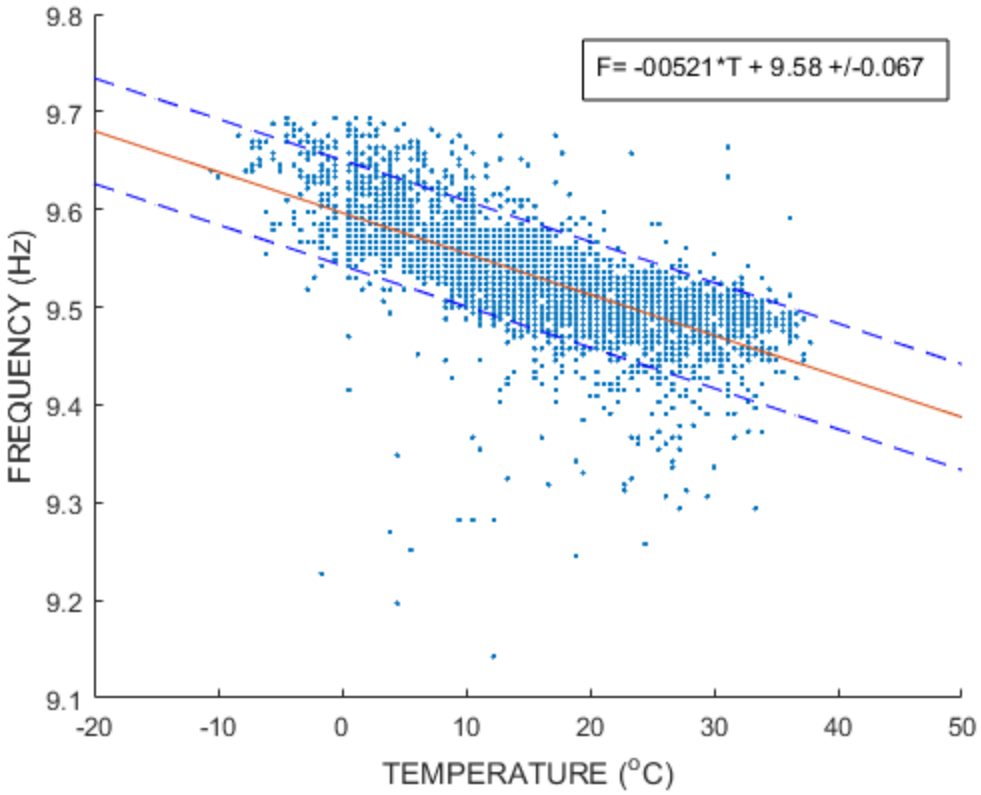

Figure 5.12 Sensor C4, frequency 2

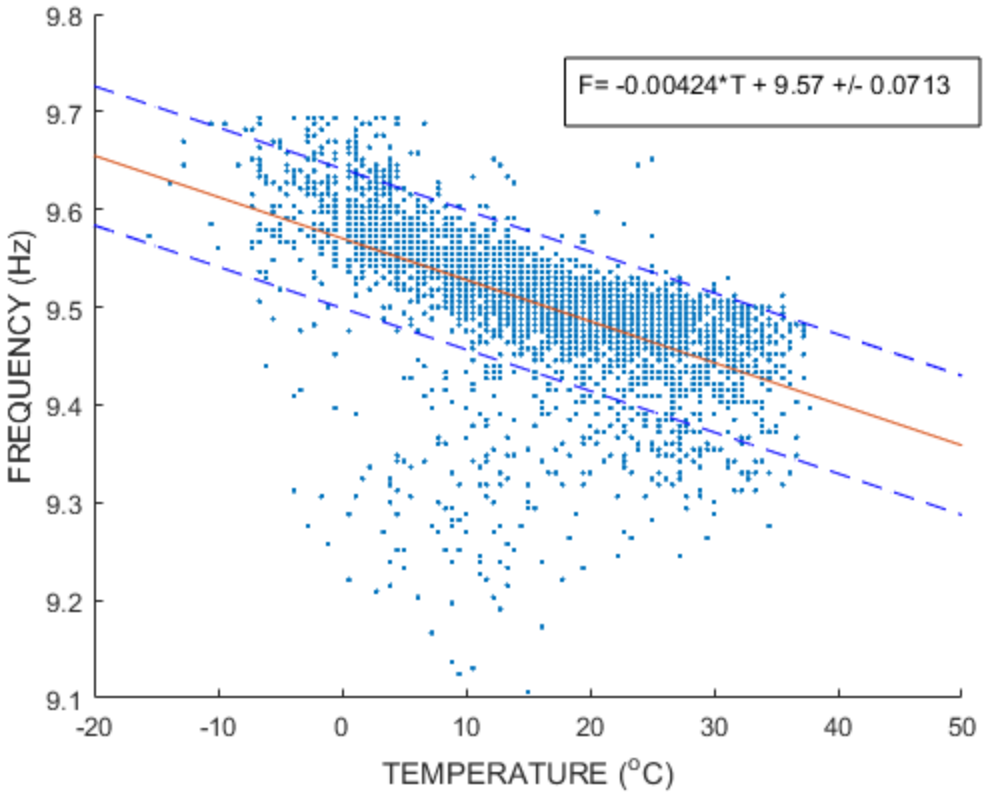

Figure 5.13 Sensor C6, frequency 2

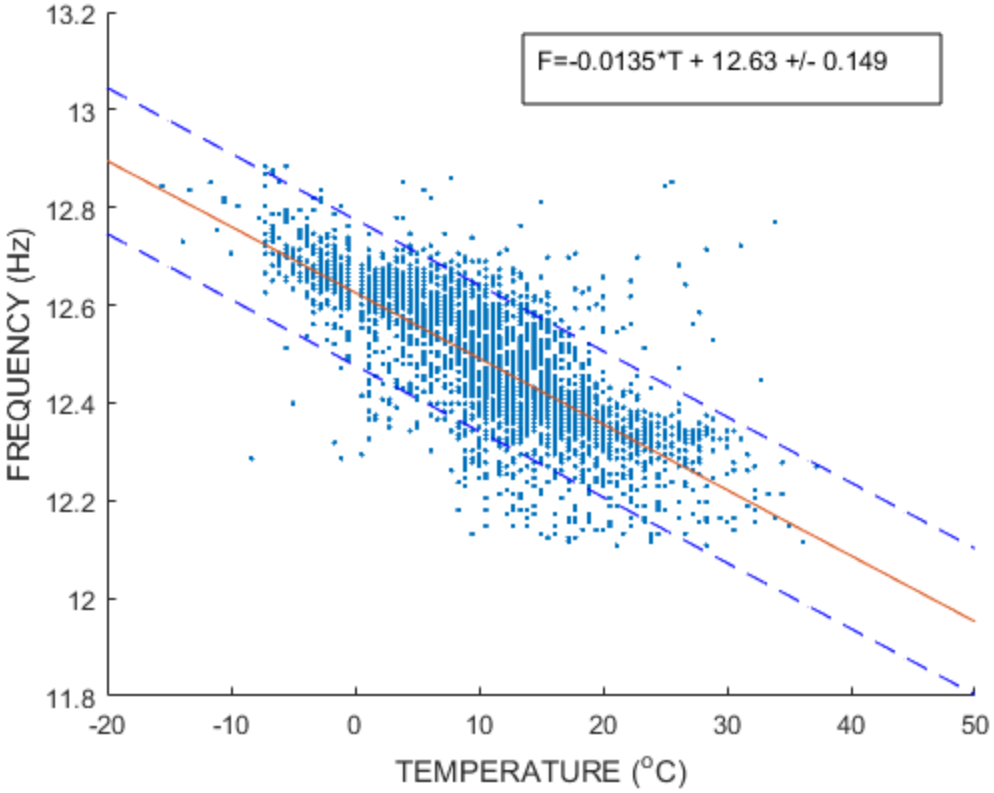

Figure 5.14 Sensor C2, frequency 3

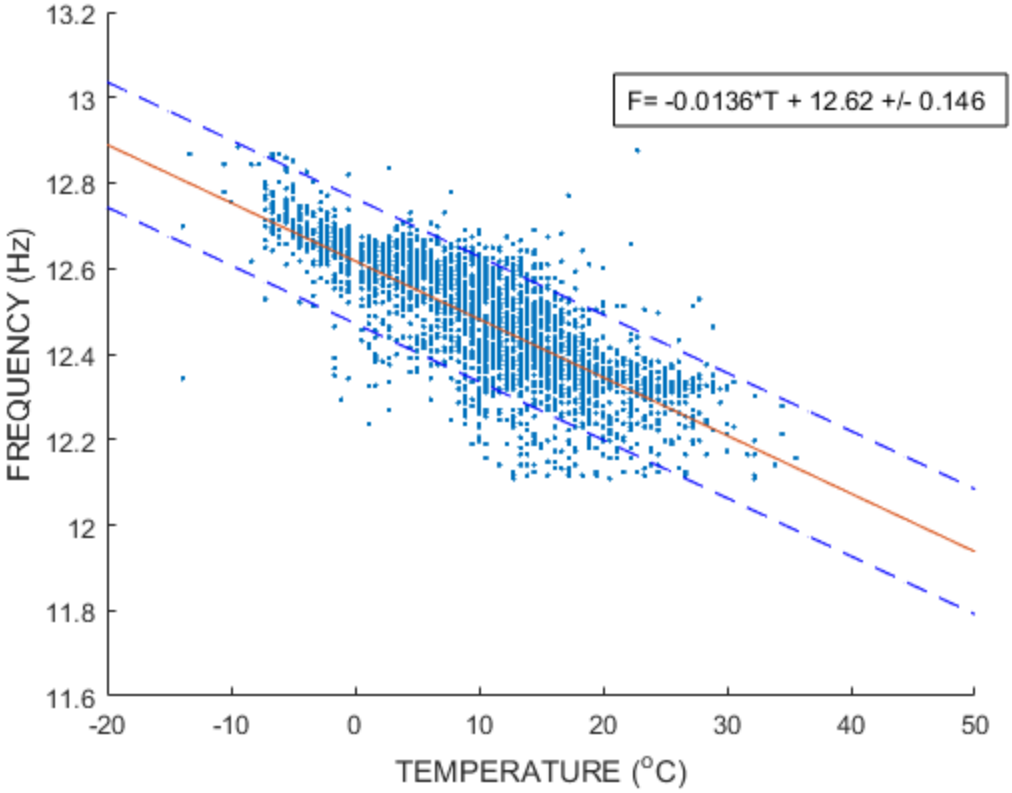

Figure 5.15 Sensor C4, frequency 3

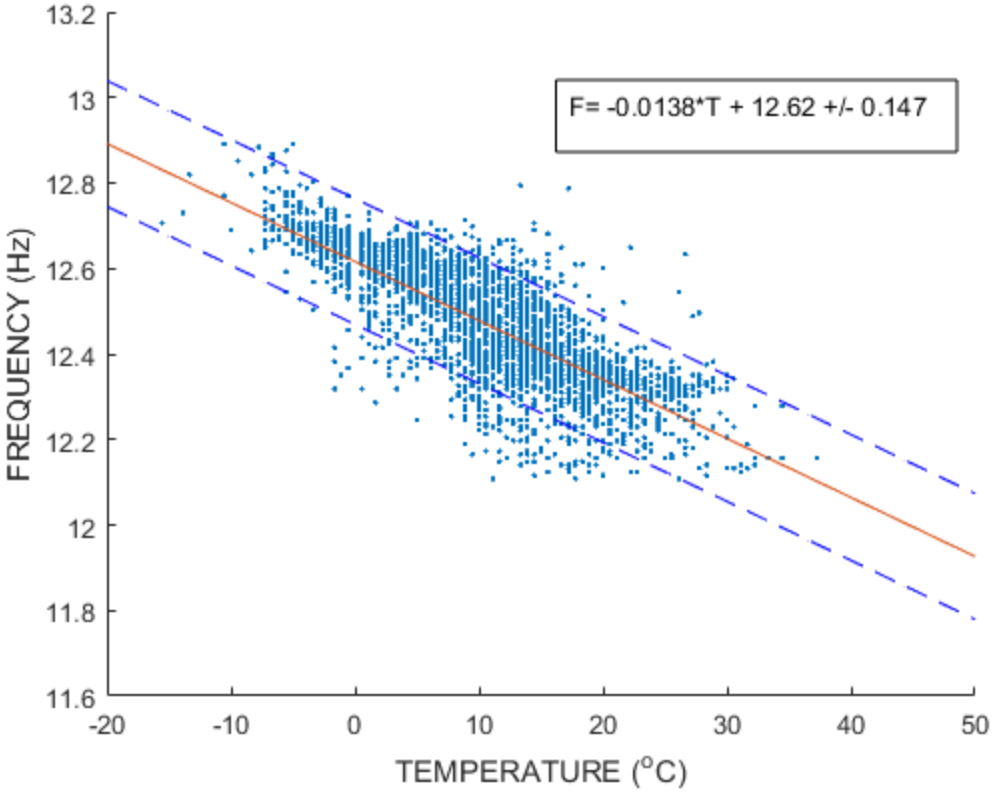

Figure 5.16 Sensor C6, frequency 3

Chapter 6: Comparisons and Discussion of Results

From the data analysis, several conclusions are drawn. First, nine natural frequencies of the bridge are shown and numbered in Table 6.1. The frequencies were taken at approximately 19°C with the Obsidian data logger.

Table 6.1 Natural frequencies of bridge C-846 at 19°C

Freq.	***C2***	***C4***	***C6***
1	*1.12*	*1.12*	*1.12*
2	*1.47*	*1.47*	*1.32*
3	*2.38*	*2.41*	*2.38*
4	*4.09*	-	-
5	*4.79*	-	-
6	*9.53*	*9.55*	*9.55*
7	*10.51*	-	-
8	*12.34*	*12.32*	*12.39*
9	*13.68*	*13.9*	*13.89*

As the temperature increases the frequency decreases. A linear regression was taken for each accelerometer paired with the temperature in Chapter 5. Then all of the points for each of the accelerometers were plotted on the same graph and the linear regression and confidence interval of the resulting equation was taken. Using these lines, the frequencies from Table 6.1 are used, and as expected fall within the confidence bounds on the graphs. The graphs and the equations of a line are shown in Figure 6.1 through Figure 6.3 and Table 6.2.

From the equation in Table 6.2, it is shown that the slope of the line tends to increase with higher frequencies. The higher frequencies are more temperature dependent than the lower frequencies. Lower frequencies less than 3 Hz start to give clusters of data because multiple frequencies are overlapping one another. This makes it difficult to write an equation of the line for the natural frequency.

To monitor the bridge, an inspector would look at the power spectral density estimate in the range of each of the graphs for the bridge on accelerometer C2, C4, and C6. Then the inspector would take the frequency and correct it for temperature using the equations in Table 6.2 or Figure 6.1, Figure 6.2, and Figure 6.3. If all three of the corresponding points are in the confidence interval for all three of the graphs or equations, then it is a green level on the bridge. This means the bridge is behaving as usual. If one or two of the three points are out of the confidence interval, this is a yellow level. In this case, the frequencies should be taken several times throughout the day. It also means that the bridge may need to be inspected for damage, or that one of the accelerometers needs to be recalibrated. If all of the points are out of their confidence intervals then the bridge probably has damage. Since softening of a structure is usually an indication of damage, a point below the confidence interval is a better indication of damage than a point above the confidence interval. A point above the confidence interval would be an indication of a loss of mass to the bridge.

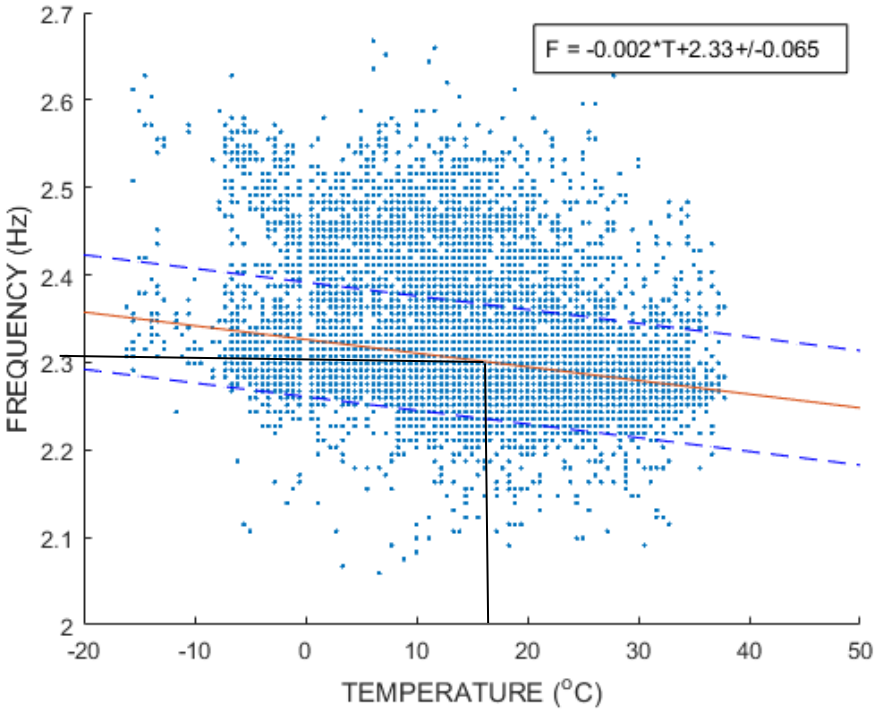

Figure 6.1 Frequency 3

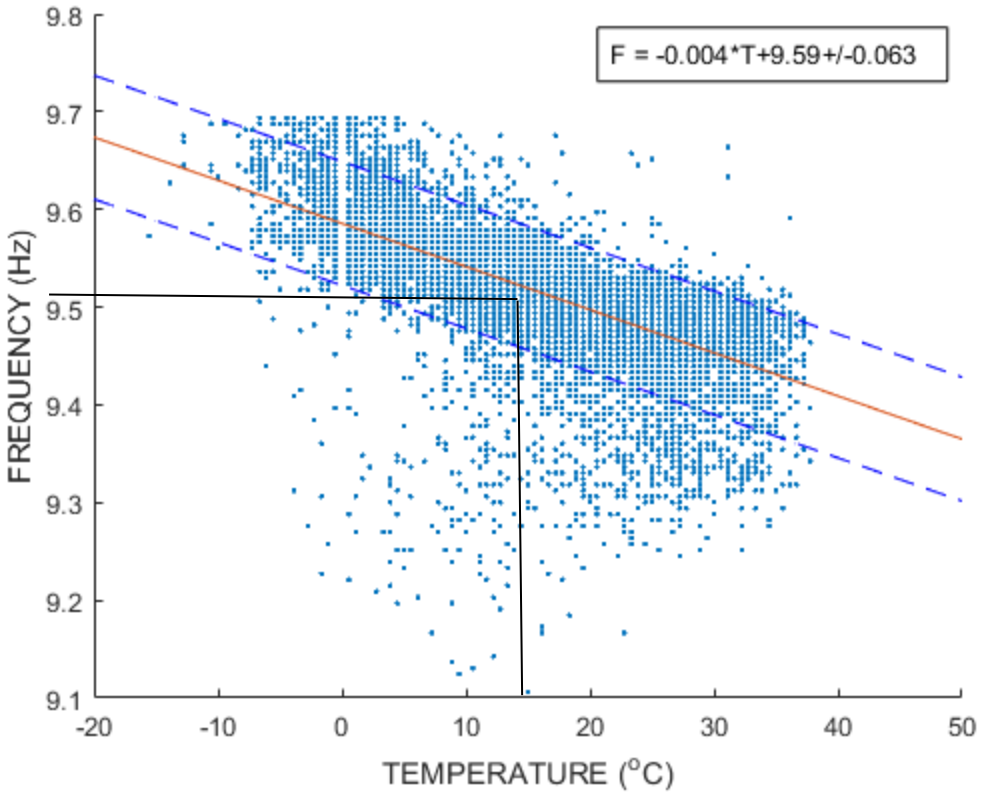

Figure 6.2 Frequency 6

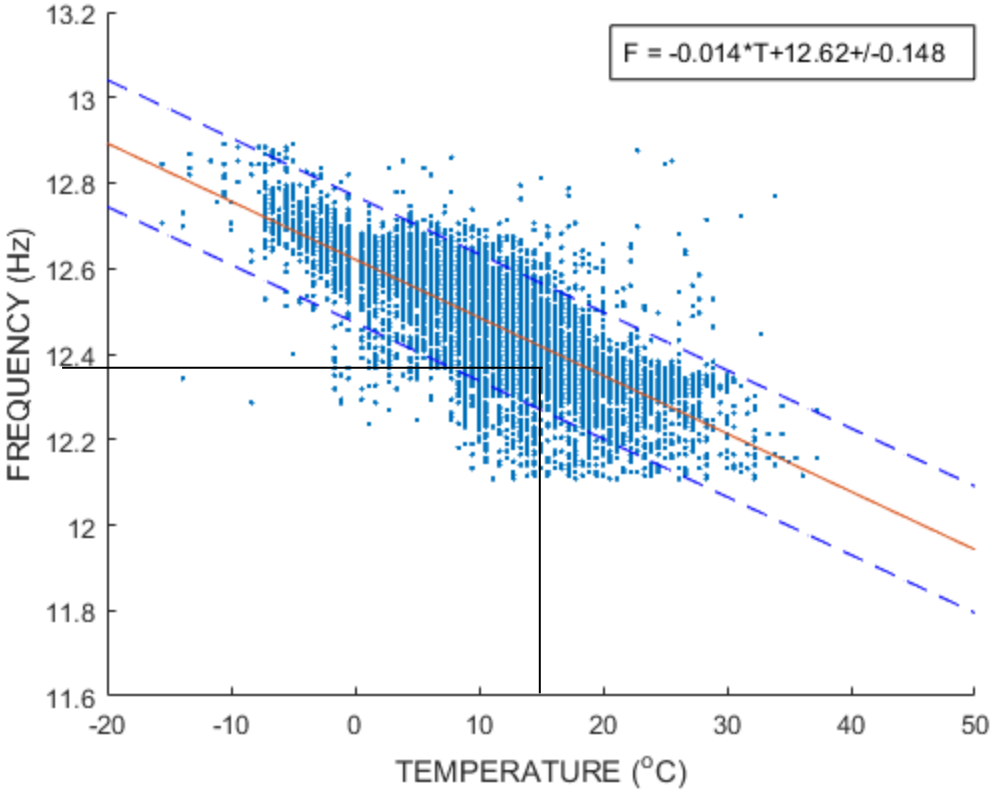

Figure 6.3 Frequency 8

Table 6.2 Equations to correct for frequency

Freq.	***Equation***
3	$F = -0.002 * T + 2.279 \pm 0.065$
6	$F = -0.004 * T + 9.59 \pm 0.063$
8	$F = -0.014 * T + 12.62 \pm 0.148$

Chapter 7: Conclusions

This report presents the results of 300 days of the correlation of frequency with temperature. Three different methods were tried. The method of taking the maximum of the cubic fit of the power spectral density estimate in the considered range for each frequency was used. The natural frequencies of the bridge were also found. Scatter plots were made and a linear regression was made with a confidence interval. A method of correcting the frequencies based on a linear regression was developed. If the natural frequency and temperature pair are out of the confidence interval for their particular range, then the bridge may have damage.

The natural frequencies were found to be temperature dependent. Distinct, higher frequencies have a stronger relationship with the temperature than the lower frequencies. The temperature and frequency show an inverse relationship. As the temperature increases, the natural frequencies of the bridge decrease. CR5000 natural frequencies proved to be reasonable when compared with the data from the Obsidian data logger. The maximums were in similar locations. The thermocouples are showing temperatures inconsistent with the ambient temperatures, and should be further investigated before being used to correlate with the natural frequency.

References

Airport, Salt Lake International. 2016. "Quality Controlled Local Climatology Data." *National Centers for Environmental Information*. 12 7. https://www.ncdc.noaa.gov/qclcd/QCLCD.

Augusto, Jose Soares. 2016. *When is Welch's method preferred over using the fast Fourier transform on a signal when computing the power spectral density?* August 18. https://www.quora.com/When-is-Welchs-method-preferred-over-using-the-fast-Fourier-transform-on-a-signal-when-computing-the-power-spectral-density.

Bálmes, É, M Bassevile, Mevel L, and H Nasser. 2008. "Handling the temperature effect in vibration monitoring of civil structures: a combined subspace-based and nuisance rejection approach." *Control Engineering Practice* 80-87.

Bálmes, Étienne, Michéle Bassevill, Laurent Mevel, Nasser Houssein, and Frédéric Bourquin. 2008. "Merging sensor data from multiple temperature scenarios for vibration montioring of civil structures." *Structural Health Monitoring* 129-142.

Breccolotti, M, G Fraceschini, and A L Materazzi. 2004. "Sensitivity of dynamic methods for damage detection in structural concrete bridges." *Shock and Vibration* 383-394.

Changqing, Miao, Chen Liang, and Feng Zhaoxiang. 2011. "Study on effects of environmetnal temperature on dynamic characteristics of Taizhou Yangtze River Bridge." *Engineering Sciences* 78-82.

Chopra, Steven C., and Raymond P. Canale. 2010. *Numerical Methods for Engineers*. New York: McGraw Hill.

Cury, Alexandre, Christian Cremona, and John Dumoulin. 2012. "Long-term monitoring of a PSC box girder bridge: Operational modal analysis, data normalization and structural modification assessment." *Mechanical Systems and Signal Processing* 13-37.

Dallas, George. 2016. *Principal Component Analysis 4 Dummies: Eigenvectors, Eigenvalues and Dimension Reduction*. 5 13. https://georgemdallas.wordpress.com/2013/10/30/principal-component-analysis-4-dummies-eigenvectors-eigenvalues-and-dimension-reduction/.

Duffie, J A, and Beckman W A. 2013. *Solar Engineering of Thermal Processes*. Hoboken, NJ: Wiley & Sons.

Farrar, Charles, and David Jauregui. 1996. *Damage Detection Algorithms Applied to Experimental modal Data from the I-40 Bridge*. NM.

Fu, Yongda, and DeWolf John T. 2001. "Monitoring and Analysis of a Bridge with Partially Restrained Bearings." *Journal of Bridge Engineering* 23-29.

Gonzales, Ignacio, and Mahir, Karoumi, Raid Ülker-Kaustell. 2013. "Seasonal effects on the stiffness properties of a ballasted railway bridge." *Engineering Structures 57* 63-72.

Google. n.d. *Map data*. Google, Salt Lake City.

Hales, Michael Bill. 2002. *Long-Term Bridge Vibration Monitoring of a Full-Scale Bridge Using a Permanent Accelerometer Array*. Logan: Utah State University.

Housner, G, L Bergman, T Caughey, A Chassiakos, R Claus, S Masri, R Skelton, T Soong, B Spencer, and J Yao. 1997. "Structural Control: Past Present, and Future." *Journal of Engineering Mechanics* 897-971.

Hu, Wei-Hua, Carlos Moutinho, Filipe Magalhães, Elsa Caetano, and Álvaro Cunha. 2009. "Analysis and Extraction of Temperature Effects on Natural Frequencies of a Footbridge based on Continuous Dynamic Monitoring." *Proceedings of the 3rd International Operational Modal Analysis Conference*. Portnovo, Italy. 55-62.

2007. "Kim, Jeong-Tae; Park, Jae-Hyung; Lee, Byung-Jun." *Vibration-based damage monitoring in model plate-girder bridges under uncertain temperature conditions* 1354-1365.

Laory, Irwanda, Thanh N Trinh, Ian F C Smith, and James M W Brownjohn. 2014. "Methodologies for predicting natural frequency variation of a suspension bridge." *Engineering Structures* 211-221.

Li, Hui, Shunlong Li, Jinpin Ou, and Hongwei Li. 2010. "Modal identification of bridges under varying environmental conditions: Tempearture and wind effects." *Structural Control and Health Monitoring* 495-512.

Liu, Chengyin, and John T DeWolf. 2007. "Effect of Temeparture on Modal Variability of a Curved Concrete Bridge under Ambient Loads." *Journal of Structural Engineering* 1742-1751.

Macdonald, John H G, and Wendy E Daniell. 2005. "Variation of modal parameters of a cable-stayed bridge identified from ambient vibration measurements and FE modelling." *Engineering Structures* 1916-1930.

Maeck, Johan, Bart Peeters, and Guido De Roeck. 2001. "Damage identification on the Z24 bridge using vibration monitoring." *Smart Materials and Structures* 512-517.

McClure, Richard M, Harry H West, and P C Hoffman. 1983. "Observation from Tests on a Segmental Bridge." *PCI* 60-67.

Moser, Peter, and Babak Moaveni. 2011. "Environmental effects on the idetified natrual frequencies of the Dowling Hall Footbridge." *Mechanical Systems and Signal Processing* 2336-2357.

Nandan, Harsh, and Mahendra P Singh. 2014. "Effects of thermal environment on structural frequencies: Part I A simulation study." *Engineering Structures* 480-490.

Nandan, Harsh, and Mahendra P. Singh. 2014. "Effects of thermal enivronment on structural frequencies: Part I- A simulation study." *Engineering Structures* 480-490.

Ni, Y Q, X G Hua, K Q Fan, and J M Ko. 2005. "Correlating modal properties with temperature using long-term." *Engineering Structures* 1762-1773.

Oh, B H, S C Choi, and S W Cha. 2006. "Temperature and Relative Humidity Analysis in Early-Age Concrete Decks of Composite Bridges." (Springer) 305-316.

Orgill, J F, and K G T Hollands. 1977. "Correlation equation for houly diffuse radiation on a horizontal surface." *Solar Energy* 357-359.

Osgood, Brad. 2007. *EE 261 The Fourier Transform and its Applications.* Stanford: Stanford University.

Peeters, Bart, and Guido De Roeck. 2001. "One-year monitoring of the Z24-Bridge: environmental effects versus damage events." *Earthquake Engineering and Structural Dynamics* 149-171.

Peeters, Bart, Johan Maeck, and Guido De Roeck. 2001. "Vibration-based damage detection in civil engineering: excitation sources and temperature effects." *Smart Materials and Structures* 518-527.

Sohn, Hoon, Mark Dzwonczk, Erik G Straser, Anne S Keremidjian, Kincho H Law, and Teresa Meng. 1999. "An Experimetnal Study of Temperature Effect on Modal Parameters of the Alamosa Canyon Bridge." *Earthquake Engineering and Structural Dynamics* 879-897.

Utah State University. 2001. *Strong Motion Instrumentation of I-15 Bridge C-846.* Salt Lake City: UDOT.

Wahab, Magd Abdel, and Guido De Roeck. 1997. "Effect of Temperature on Dynamic System Parameters of a Highway Bridge." *Structural Engineering National* 266-270.

Xia, Yong. 2012. "Temperature effect on vibration properties of civil structures: a literature reviw and case studies." *Journal of Civil Structural Health Monitoring* 29-45.

Xia, Yong, Hong Hao, Giovanna Zanardo, and Andrew, et al. Deeks. 2006. "Long term vibration monitoring of an RC slab: Temperature and humidity effect." *Engineering Structures* 441-452.

Xia, Yong, You-Lin Xu, Ze-Long Wei, Hong-Ping Zhu, and Xiao-Qing Zhou. 2011. "Variation of structural vibration characterisitcs versus non-uniform temperature distribution." *Engineering Structures* 146-153.

Xu, Zhao-Dong, and Zhishen Wu. 2007. "Simultaion of the Effect of Temperature Variation on Damage Detection in a Long-Span Cable-stayed Bridge." *Structural Health Monitoring* 177-189.

Zhou, Guang-Dong. 2013. "Thermal Load in Large-Scale bridges: A State-of-the-Art Review." *International Journal of Distributed Sensor Networks* 1-18.

Zhou, Guang-Dong, and Ting-Hua Yi. 2014. "A summary review of correlations between temperatures and vibration properties of long-span bridges." *Mathematical Problems in Engineering, 2014* 1-20.

Zolghadri, Navid, Marvin Halling, and Paul J. Barr. 2016. "Effects of temperature variations on structural vibration properties." *Geotechnical and Structural Engineering Congress.*

Appendix A: Table Of Data

Table A.1 Data from method 3

Freq.	*Accel.*	*slope*	*y-intercept*	*standard deviation*	*ρ*	R^2
1	*C2*	*-0.00113*	*2.30*	*0.0291*	*-0.39*	*0.15*
2	*C2*	*-0.00419*	*9.60*	*0.0540*	*-0.68*	*0.46*
3	*C2*	*-0.01347*	*12.63*	*0.149*	*-0.78*	*0.61*
1	*C4*	*-0.00117*	*2.30*	*0.033*	*-0.36*	*0.13*
2	*C4*	*-0.00521*	*9.58*	*0.067*	*-0.72*	*0.52*
3	*C4*	*-0.01361*	*12.62*	*0.146*	*-0.80*	*0.64*
1	*C6*	*-0.00327*	*2.42*	*0.0917*	*-0.35*	*0.12*
2	*C6*	*-0.00424*	*9.57*	*0.0713*	*-0.55*	*0.30*
3	*C6*	*-0.01380*	*12.62*	*0.147*	*-0.81*	*0.65*

Appendix B: Data Sheets of the Equipment Used

KINEMETRICS

Obsidian

Next Generation of Web Based, High Dynamic Range, GPS/PTP Ready Accelerographs

Ready for the *right tool* for the job?

The **Obsidian** accelerograph is Kinemetrics' NEW product matched to Kinemetrics' exemplary EpiSensor accelerometer performance. It represents a new paradigm in open-architecture seismic data acquisition systems defining the *World's Next Generation* of seismic products.

It is designed to give you the flexibility required by the earthquake monitoring solutions of tomorrow capturing very-small to very-large earthquake sequences with a single sensor while being the *most versatile* accelerograph of today. No more and no less than you need.

You expect outstanding data fidelity and spectral purity. High accuracy data timing is of course required. But it goes beyond that. There are several standard recorded data formats to select from, or you can add your own. On the fly processing of parametric data using your algorithms. Interface to major data center software packages using *their* protocols. For timing use GPS where it makes sense and/or PTP when several units are connected via Ethernet along with DC power.

And when you're ready to get into Earthquake Early Warning Systems (EEWS), the **Obsidian** is ready too. Balance communications bandwidth and data latency with not one but two mechanisms to deliver *ultra-low* latency data.

Why struggle with limited keypads and hard to read displays when you're usually not there anyway? Access the system using your favorite web browser remotely or locally and wirelessly. Where it makes sense to retrieve data locally, do it with a simple thumb drive without commands or buttons.

And for those whose job it is to maintain the station we developed Streamlined Station Maintenance (SSM) that allows you to use your browser to log maintenance activities such as software updates, site inspections, or battery replacements right on the unit. These logs can be automatically uploaded to your data center for archiving, reducing paper work in the field.

Choose from a suite of built-in Kinemetrics features, add-on packages from trusted providers or expand the capabilities of the system yourself. It's the *open-architecture* seismic data acquisition system!

Quanterra and Kinemetrics data acquisition products provide *data availability* of over 99% in several large networks year after year. Our users will tell you so.

FEATURES

- 3 +1 sensor channels w/internal EpiSensor triaxial deck
- 24-bit Delta Sigma converter, one per channel
- Matched to Kinemetrics outstanding EpiSensor accelerometer performance
- Built-in GPS, built-in PTP
- Record and communicate multiple sample rates
- Multiple data formats and telemetry protocols
- Ultra-Low latency data for Earthquake Early Warning Systems
  - * 0.1sec data packet
  - * 0.01sec DFS at 100sps
- Streamlined Station Maintenance (SSM)
- Data offloaded automatically to removable thumb drives connected to a USB host port. Parallel recording (mirroring) data on an external USB thumb drive.
- Wireless communications via USB based Wi-Fi
- Extensive state-of-health monitoring, including input and system voltages, internal temperature, humidity, communication link diagnostics
- Application Programming Interface (API) to develop your own add-on software modules. You can customize real-time data processing, file formats, stream data using your own protocol, shape data with a custom filter, and so on.
- IP Security through SSH and SSL
- Transient and EMI/RFI protection on all connections
- System Status LEDs
- Rugged aluminum extruded case designed for 1m drop and 1m temporary immersion (IP67)
- Designed for RoHS Compliance and easy re-cycling
- Designed for the lowest Total Cost of Ownership (TCO)

Continued

KINEMETRICS

SPECIFICATIONS

Channels

Obsidian:	3 +1 sensor channels w/internal sensor
Sensor type:	Triaxial EpiSensor force balance accelerometer, Orthogonally oriented, Internal
Full scale range:	User selectable at ±2g or ±4g
Bandwidth:	DC to 200 Hz
Dynamic range:	155 dB+
Calibration & test:	Calibr. Coil Functional Test; Calibr. Coil Response Test
Input level:	5Vpp, 10Vpp, 40Vpp Differential Input

Data Acquisition

Type:	Individual 24-bit Delta Sigma converter per channel
Anti-alias filter:	Double Precision FIR Filter Causal/Acausal; >140 dB attenuation at output Nyquist
Dynamic range:	200 sps ~127 dB (RMS noise to RMS clip - Typical) 100 sps ~130 dB (RMS noise to RMS clip - Typical)
Frequency response:	DC to 80 Hz @ 200 sps
Sampling rates:	1, 10, 20, 50, 100, 200, 250, 500, 1000, 2000, 5000 sps
Channel skew:	None – simultaneous sampling of all channels
Acquisition modes:	Continuous, triggered, time windows
Output data format:	24 bit signed (3 bytes) in user selectable format
Parameter calculations:	Calculations of key parameters in real- time, including JMA intensity
Real time digital output:	Ethernet or RS-232 output of digital stream

Trigger

Type:	IIR bandpass filter (three types available)
Trigger selection:	Independently selected for each channel
Threshold trigger:	Selectable from 0.01% to 100% of full scale
Trigger voting:	Internal, external and network trigger votes with arithmetic combination
Additional trigger:	STA/LTA, Time Window

Timing

Type:	Oscillator digitally locked to GPS or PTP: Integrates completely with system, providing timing, internal oscillator correction and position information.
Shared timing:	3 Ports for shared timing for multiple local units
Timing: accuracy:	<1 microseconds of UTC with GPS or PTP

Storage

Data slot:	Internal SDHC Card Slot, standard 32 GB
System slot:	Internal SDHC Card Slot, 4 GB
Recording capacity:	Approximately 42 kB per channel per minute on Memory Card of 24-bit data @ 200 sps. (33 days of 4x200sps recording on 8GB Data card)
SDHC Format:	Linux EXT4
Data:	Offloaded automatically to removable thumb drives connected to a USB host port. Parallel recording (mirroring) data on an external USB thumb drive. USB drives format: FAT32

Communications

Ethernet interface:	Real Time Telemetry (Multiple destinations TCP/IP Protocol), Parameter set up, and event retrieval (FTP/ SFTP) RS-232 interface: Real Time Telemetry (over modem, radio, etc.), Parameter set up, and event retrieval
Modem:	Built in modem, Remote access, initiated by user or by the Obsidian
Telemetry:	Real-time data via DFS, SEEDLink, Earthworm, Antelope compatible ORB server, or Altus SDS protocols.

Instrument Software

Type:	Multi-tasking operating system supports simultaneous acquisition and interrogation; allows remote and automatic firmware upgrades
Security:	Supports SSH and SSL
System control:	Configure sample rate, filter type, trigger type and voting, maintains communications and event storage
File formats:	Kinemetrics EVT, MiniSEED, SAC, COSMOS, MATLAB, SUDS, SEISAN, ASCII, others
Intelligent alerting:	Initiate communications when an event is detected or if an auto-diagnostic failure occurs
Auto-diagnostics:	Continuously check system voltages, temperature, humidity, and timing system integrity
Rapid setup:	Can be configured from a parameter file
System timing:	Supports PTP Slave and PTP Master timing (Using Internal GPS as Master clock), NTP and External 1PPS

I/O and Display

Power input:	Mil-style connector for DC power input, external battery connection, Power over Ethernet (Option)
Interfaces:	10/100 BaseT Ethernet Port
(M12 connectors)	3 x USB 2.0 Host Ports USB 2.0 Device 3 x RS-232 DFS Port (RS232) Linux Console (RS232) POTS Modem 3 x Time/Power Ports (1PPS In/Out, Switched Power) GPS Antenna (TNC)
EMI/RFI protection:	All I/O lines EMI/RFI and transient protected
LED:	System, power and event status, Ethernet Link & Data

Continued

KINEMETRICS

SPECIFICATIONS

Power Supply

Type:	Internal high efficiency switched power supply and battery charger system with extensive SOH outputs
DC input:	9-28 VDC (>15.5VDC for Battery Charger Operation)
External AC/DC:	Universal Input 100-250 VAC 50/60 Hz
Power module:	Output 15.5 VDC
Internal battery charger:	Digitally temperature compensated output for External Valve Regulated Lead Acid (VRLA) batteries with reverse protection and deep discharge recovery.
Fuses:	None. Uses resettable Polyswitch protection
Current drain:	Current drain: 215ma @12V (w/o 4th channel sensor)

Environment

Operating temp: -20° to 70°C Operation
Humidity: 0-100% RH (Non-condensing)

Physical

Size: 13.25" (L) x 7.25"(D) x 6.8"(H)
Enclosure rating: IP67 Equivalent
Environmental: RoHS Compliant Unit

Support Software

Altus File Viewer:	Multiplatform program for rapid review of waveforms and event information.
Antelope:	Comprehensive commercial network operational and management system for medium and large networks
Earthworm:	Comprehensive public domain network operational and management system for medium and large networks
NMS:	Commercial PC-based network management system for small to medium sized networks via modem or real-time data
RockTalk:	Multiplatform program for command and control
Rockhound:	Commercial open architecture user-extensible real-time data collection and processing software that runs on a variety of computers
PSD:	Commercial Pseudo Spectral Density software for earthquake data analysis
SMA:	Commercial Strong Motion Analyst software for earthquake data analysis and processing
K2COSMOS:	Conversion software from Altus EVT file format to COSMOS v1.20 format (COSMOS format can also be produced natively from the Obsidian)
Miscellaneous:	Format converters to ASCII and other formats. Web Server for command and control, Optional Software Development Kit and Compilers. Contact Kinemetrics for other options.

Specifications subject to change without notice

USA - 222 Vista Ave., Pasadena, CA 91107
Tel (626)795-2220 I Fax (626)795-0868

Switzerland - Z.I. Le Tresi 6B, 1028 Preverenges
Tel +41 (21) 803-2829 I www.kinemetrics.com

10-20-15

AM25T

Solid State Multiplexer for Thermocouples

CAMPBELL SCIENTIFIC
WHEN MEASUREMENTS MATTER

The AM25T sequentially connects up to 25 thermocouples[1] to a differential analog input on a CR800, CR850, CR10X, CR1000, CR3000, CR5000, CR7, or CR9000X datalogger. A PRT attached to the multiplexer's grounding bar provides a temperature reference for the thermocouple measurements. The heat capacity of the grounding bar and an insulated aluminum cover reduce thermal gradients along the length of the multiplexer. Reducing the thermal gradients allow more accurate measurements.

AM25T cover not shown.

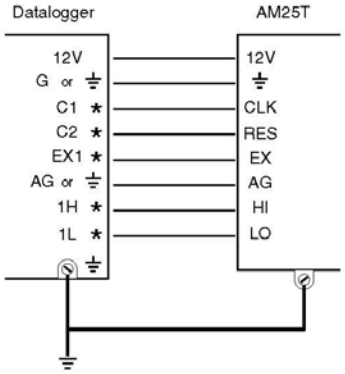

Channel numbers shown are for example only and may vary depending on the application.

Features

- Operates at -40° to +85°C
- Provides spark gaps on all inputs
- Measures the panel (reference) temperature using a built-in PRT that has an accuracy of ±0.2°C over -25° to +50°C range, ±0.4°C over -40° to +85°C range
- Contains multi-layered circuit boards (uses a metallic, internal ground plane to reduce thermal gradients)
- Allows one datalogger to control several AM25Ts
- Provides a vertical package for a smaller "footprint" in enclosure
- Supports a maximum cable length of 500 feet when lightning protection is used

Connections

Up to 25 thermocouples are wired into paired terminal sets on the AM25T. The 4-wire reference PRT is measured by the datalogger via the EXcitation, Analog Ground, HI, and LO terminals. Subsequent pulses switch each pair of AM25T terminals into continuity from the thermocouple junction, through the input and HI/LO terminals of the multiplexer, to a differential analog input on the datalogger.

Two CABLE4CBL-L cables carry control, power, and measurement signals between the AM25T and the datalogger. A separate 10 to 12 AWG single-conductor wire connects AM25T ground to datalogger ground.

Scanning Multiple AM25Ts

Multiple AM25T's can be connected to the datalogger. The dataloggers are then programmed to measure sensors from each multiplexer sequentially.

Environmental Enclosures

The AM25T operates in most field conditions but requires a non-condensing environment. Outdoor applications require a weather-resistant enclosure augmented by desiccant; a Campbell Scientific enclosure is recommended.

Our ENC12/14 enclosure can house up to two AM25Ts, a CR800, CR850, CR10X, CR1000, or CR3000, and a power supply. The ENC16/18 houses several AM25Ts, a CR800, CR850, CR10X, CR1000, CR3000, or CR5000, and a power supply.

These white fiberglass-reinforced polyester enclosures can attach either to a wall with lag bolts or to a 1.25-in. IPS pipe (1.66-in. O.D.) with U-bolts. Please note that the ENC10/12 is not deep enough to house the AM25T. Consult the factory for CR7 and CR9000X enclosure options.

[1]*Other low-level voltage output sensors that do not exceed the common mode range of the datalogger can also be measured. The AM25T should NOT be used to measure resistive bridges or configured with a voltage divider between the AM25T and the datalogger; ask about our AM16/32B multiplexer for these applications.*

Ordering Information

Multiplexer	
AM25T	25-Channel Solid State Multiplexer (-40° to +85°C)
Calibration Certificate	
-CC	If specified, the multiplexer is shipped with a two-page calibration certificate.
Cable	
CABLE4CBL-L	4-conductor, 22-AWG cable with drain wire and Santoprene jacket. Enter cable length, in feet, after the -L. A 2-ft cable length should be sufficient if the datalogger and AM25T are housed in the same ENC16/18 Enclosure. Must choose a cable termination option (see below).
Cable Termination Options (choose one)	
-PT	Cable terminates in stripped and tinned leads for direct connection to a datalogger's terminals.
-PW	Cable terminates in connector for attachment to a prewired enclosure.

Specifications

Expandability[1]:
2 AM25Ts per CR800 or CR850
4 AM25Ts per CR1000, CR3000, or CR10(X)
6 AM25Ts per CR23X or 21X
7 AM25Ts per CR725 card for the CR7s

Electrical

Power:	9.6 to 16 Vdc (under load), unregulated
Current Drain (typical)	
Quiescent:	0.5 mA
Active:	1.0 mA
Enable Levels	
Inactive:	<0.9 V
Active:	3.5 to 5 V
Clock	
Levels:	Scan advance occurs on the falling edge of the clock pulse (from above 3.5 V to below 1.5 V).
Minimum ON Time:	50 µs
Minimum OFF Time:	60 µs
Typical Relay Resistance:	500 ohms
Maximum Switching Current[2]:	25 mA

Footprint for Mounting

Physical

Operating Temperature:	-40° to +85°C
Operating Humidity:	0 to 95%, non-condensing
Dimensions:	9.3-in L x 5.2-in H x 2-inW (23.6 cm x 13.2 cm x 5.1 cm)
Weight:	2.0 lbs (0.9 kg)

[1] *Assumes sequential activation of multiplexers and that each datalogger channel is uniquely dedicated.*

[2] *Switching currents greater than 25 mA will damage the relays and render them unusable.*

Campbell Scientific, Inc. | 815 W 1800 N | Logan, Utah 84321-1784 | (435) 753-2342 | www.campbellsci.com
USA | AUSTRALIA | BRAZIL | CANADA | COSTA RICA | ENGLAND | FRANCE | GERMANY | SOUTH AFRICA | SPAIN

CAMPBELL SCIENTIFIC
WHEN MEASUREMENTS MATTER

CR5000

Measurement & Control System

A rugged,

high-performance

data acquisition

system

CR5000 Measurement and Control System

The CR5000 Measurement and Control System is a self-contained, low power, rugged datalogger that is capable of a maximum throughput of 5 kHz. Standard operating range is -25° to +50°C; an optional extended range of -40° to +85°C is available.

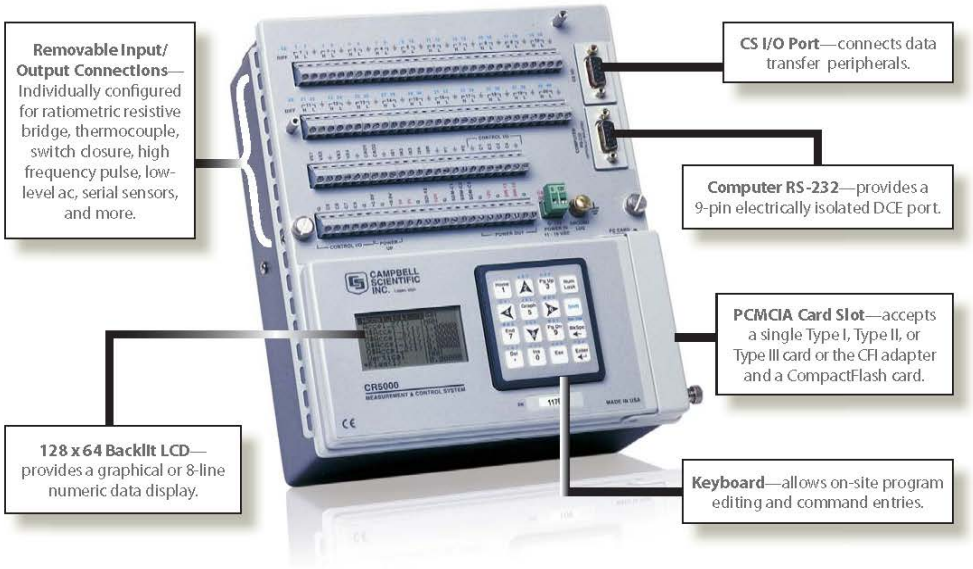

Design Features

- Stand-alone unit offering high performance and an environmentally rugged design
- Maximum throughput of 2k to 5k measurements per second (configuration dependant)
- Powerful instruction set that supports measurement of most sensor types, on-board processing, data reduction, and intelligent control
- Backlit display allowing numerical or graphical display of stored data
- PCMCIA card slot for extended data storage and transporting data to a PC
- Battery-backed SRAM memory and clock ensuring data, programs, and accurate time are maintained while the CR5000 is disconnected from its main power source
- Robust ESD protection
- Low power, 12 Vdc operation
- Data values stored in tables with a time stamp and record number

Operating System/Logic Control

The on-board operating system includes measurement, processing, and output instructions for programming the datalogger. The programming language, CRBasic, uses a BASIC-like syntax. Measurement instructions specific to bridge configurations, voltage outputs, thermocouples, and pulse/frequency signals are included. Processing instructions support algebraic, statistical, and transcendental functions for on-site processing. Output instructions process data over time and control external devices. These instructions include averages, maximums, minimums, standard deviations, histograms, rainflow histograms, level crossings, and Fast Fourier Transfers (FFTs).

Data Storage Capacity

Data and multiple programs are stored on-board in battery-backed SRAM. Data is stored in a table format. Up to 900,000 low-resolution data points can be stored in its CPU memory. Storage capacity can be increased by using a PC or CompactFlash card.

Input Output Terminals

Analog Inputs
Twenty differential (40 single-ended) input channels support five full-scale ranges (±20 mV to ±5000 mV) at 16-bit measurement resolution. Larger signal voltages are accommodated with precision 2:1 and 10:1 input voltage divider modules.

Pulse Counters
Two 16-bit pulse channels count switch closures, low level ac pulses, and high frequency square waves.

Switched Excitation Outputs
Four switched voltage and four switched current outputs provide precision excitation for ratiometric sensor/bridge measurements.

Digital I/O Ports
Eight ports have multiple functions including digital control output, interrupt, pulse counting, switch closure, frequency/period measurements, and edge timing communication. One other port is dedicated for SDI-12 measurements, and three additional ports are dedicated for measuring SDM devices.

Continuous Analog Outputs
Two continuous analog outputs provide voltage levels to displays or proportional controllers.

RS-232 Port
The RS-232 port is for connecting a PC, serial sensor, or RS-232 modem. The PC attaches to the CR5000 via an RS-232 cable—no interface required. This port isolates the PC's electrical system from the datalogger, thereby protecting against ground loops, normal static discharge, and noise.

CS I/O Port
Many communication devices connect with the CR5000 via this port. A PC may also connect with this port, but an SC32B or SC-USB interface is required.

Power Connections
The continuous 5 V and 12 V terminals are for connecting sensors and non-Campbell Scientific peripherals. Two switched 12 V terminals are program controlled.

Transient Protection

Rugged gas tubes protect all terminal block inputs and outputs from electrical transients. The CR5000 is CE compliant under the European Union's EMC Directive.

PCMCIA Card Slot

The PCMCIA card slot supports one Type I, Type II, or Type III PC Card or the CF1 adapter and one CompactFlash (CF) card. The card can be used to expand the CR5000's storage capacity or transport data or programs to a PC.

The storage capacity of Type II cards exceeds 1 GB. Type III cards provide data storage capacities exceeding 1 GB but may not be suitable for all environments. Campbell Scientific offers CF cards that store up to 2 GB of data.

Enclosures

The CR5000 can be housed in an ENC14/16 and ENC16/18 enclosure. A CR5000 housed in a weather-resistant enclosure can collect data under extremely harsh conditions. The enclosure protects the CR5000 from dust, water, sunlight, or pollutants. An internal mounting plate is prepunched for easy system configuration and exchange of equipment in the field.

Operating Temperature Ranges

Standard operating range is -25° to +50°C; an extended range of -40° to +85°C is available. The rechargeable battery base has a different temperature range (see below).

Battery Base Options

Rechargeable Base
The rechargeable base includes an internal 7-Ah sealed rechargeable battery that can be charged from vehicle power, solar panels, or ac power. Operating temperature range is -40° to +60°C.

When using vehicle power, our DCDC18R Boost Regulator is used to increase the vehicle's supply voltage to charging levels required by the CR5000.

Low-Profile Base (no battery)
The low-profile base requires a user-supplied dc source. It is preferred when the system's power consumption needs a larger capacity battery or when it's advantageous to have a thinner, lighter datalogger.

Data Storage and Retrieval Options

To determine the best option for an application, consider the accessibility of the site, availability of services (e.g., cellular phone or satellite coverage), quantity of data to collect, and desired time between data-collection sessions. Some communication options can be combined—increasing the flexibility, convenience, and reliability of the communications.

Keyboard Display
The CR5000's integrated keyboard display is used to program the datalogger, manually initiate data transfer, and display data. It displays 8 lines x 21 characters (64 x 128 pixels) and has a 16-character keyboard. Custom menus are supported allowing customers to set up choices within the datalogger program that can be initiated by a simple "toggle" or "pick list".

Direct Links
A PC or laptop can be connected directly to the datalogger's RS-232 port (no interface required). This port provides optical isolation. Alternatively, the PC or laptop can be connected to the CR5000's CS I/O port via an SC32B or SC-USB interface.

PC Cards or CF Cards
The CR5000 can store data and programs on a PC card or CF card. The card can then be carried to a computer. The computer directly reads PC cards via its PCMCIA card slot. CF cards are read using either a CF1 adapter or the 17752 Reader/Writer. Please note that the CF card should be industrial-grade with a storage capacity of 2 GB or less.

Ethernet
The NL100 interface enables a CR5000 datalogger to communicate over a local network or a dedicated Internet connection via TCP/IP.

Short Haul Modems
The SRM-5A RAD Short Haul Modem supports communications between the datalogger and a PC via a four-wire unconditioned line (two twisted pairs).

Multidrop Interface
The MD485 intelligent RS-485 interface allows a PC to address and communicate with one or more dataloggers over a single two-twisted-pair cable. Distances up to 4000 feet are supported.

Spread Spectrum Radios
Spread spectrum radios provide communications between a base station computer and several field sites over short distances. Line-of-sight is required.

Telephone Networks
The CR5000 can communicate with a PC using landlines, cellular CDMA, or cellular GPRS transceivers. Telephone networks can be combined with spread spectrum radios, multidrop modems, and Ethernet interfaces, which extends the distance between datalogger and PC.

Satellite Transmitters
Our NESDIS-certified GOES satellite transmitter supports one-way communications from a Data Collection Platform (DCP) to a receiving station.

A GOES satellite system transmits data from a remote weather station in Nevado Sajama, Bolivia, to climate researchers in the United States.

Channel Expansion

Multiplexers

Multiplexers increase the number of sensors that can be measured by a datalogger by sequentially connecting each sensor to the datalogger. Several multiplexers can be controlled by a single datalogger. The CR5000 is compatible with the AM16/32B and AM25T multiplexers.

Synchronous Devices for Measurement (SDMs)

SDMs are addressable peripherals that expand the datalogger's measurement and control capabilities. For example, SDMs are available to add control ports, analog outputs, pulse count channels, interval timers, or even a CANbus interface to the system. Multiple SDMs, in any combination, can be connected to one datalogger.

The SDM-CAN (left of CR5000) allows a vehicle's on-board diagnostic system to output standardized data streams that are synchronized with other measurements and stored in the CR5000.

Software

Starter Software

Our easy-to-use starter software is intended for first time users or applications that don't require sophisticated communications or datalogger program editing. SCWin Short Cut generates straight-forward CR5000 programs in four easy steps. PC200W allows customers to transfer a program to, or retrieve data from a CR5000 via a direct communications link.

At www.campbellsci.com/downloads, you can download starter software at no charge. Our Resource CD also provides this software as well as PDF versions of our brochures and manuals.

Datalogger Support Software

Our datalogger support software packages provide more capabilities than our starter software. These software packages contains program editing, communications, and display tools that can support an entire datalogger network.

Short Cut is available from our website (at no charge) and Resource CD. It is also bundled with PC200W, PC400, LoggerNet, and RTDAQ Software.

PC400, our mid-level software, supports a variety of telemetry options, manual data collection, and data display. For programming, it includes both Short Cut and the CRBasic program editor. PC400 does not support combined communication options (e.g., phone-to-RF) or scheduled data collection.

RTDAQ is an ideal solution for industrial and real-time users desiring to use reliable data collection software over a single telecommunications medium, and who do not rely on scheduled data collection. RTDAQ's strength lies in its ability to handle the display of high speed data.

LoggerNet is Campbell Scientific's full-featured datalogger support software. It is referred to as "full-featured" because it provides a way to accomplish almost all the tasks you'll need to complete when using a datalogger. LoggerNet supports combined communication options (e.g., phone-to-RF) and scheduled data collection.

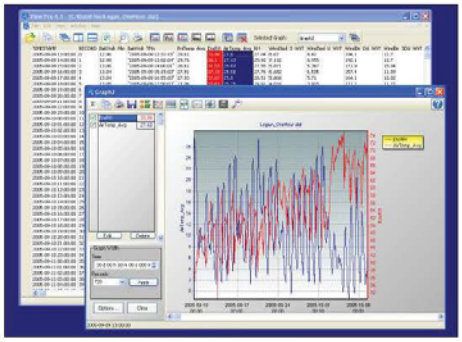

Both LoggerNet and RTDAQ use View Pro to display historical data in a tabular or graphical format.

Applications

Open Path Eddy Covariance Systems

These systems use eddy covariance techniques to calculate water vapor, carbon dioxide, and heat flux.

For eddy covariance applications, the CR5000 can measure the EC150 Open-Path CO_2 Analyzer, CSAT3A Sonic Anemometer, and KH20 Krypton Hygrometer then compute fluxes on-line.

Below are the sensors used and their measurements:

- CSAT3A Sonic Anemometer—absolute wind and sonic temperature fluctuations
- KH20 Hygrometer—fluctuations of atmospheric water vapor
- EC150 Open Path Gas Analyzer—both absolute CO_2 and water vapor
- FW05 Fine Wire Thermocouple—absolute temperature

The CR5000 measures the above sensors and computes fluxes on-line. The raw time-series data can be saved to a PC-card, along with processed data for later analysis. A PC at the site is not required. The CR5000's storage capacity can be increased using PC cards.

Structural and Seismic Monitoring

The CR5000 can be used in applications ranging from simple beam fatigue analysis, to structural mechanics research, to continuous monitoring of large, complex structures. The on-board instruction set supports many algorithms and math functions that are useful for structural and seismic monitoring.

The datalogger can store data as rainflow or level crossing histograms. The rainflow and level crossing algorithms can be processed for extended periods of time, not just a finite number of cycles.

The datalogger's control functions allow it to activate alarms, actuate electrical devices, or shut down equipment based on time or measured conditions.

Typical sensors used for structural and seismic monitoring include:

- Carlson strain meters
- Foil strain gages (set up in quarter, half, or full bridge strain configurations)
- Inclinometers
- Crack and joint sensors
- Tilt sensors
- Piezoresistive accelerometers
- Piezoelectric accelerometers
- Capacitive accelerometers
- Borehole accelerometers
- Servo force balance accelerometers

Cracks in the walls of Castillo de San Marcos, Florida were instrumented to determine their genesis and the best course for corrective action.

Vehicle Monitoring and Testing

The versatile, rugged design and low power requirements of the CR5000 datalogger make it well suited for vehicle monitoring. It excels in cold and hot temperature, high altitude, off-highway, and cross-country performance testing. The CR5000 is compatible with our SDM-CAN interface.

Compatible sensors often used for vehicle monitoring and testing include thermocouples, pressure transducers, GPS receivers, pulse pick-ups, flow transducers, potentiometers, strain gages, load cells, digital switches, accelerometers, LVDTs, and tilt sensors. Most sensors connect directly to the datalogger, eliminating costly external signal conditioning.

Photo courtesy Case Corporation

Vehicle monitoring includes not only passenger cars but locomotives, airplanes, helicopters, tractors, buses, heavy trucks, drilling rigs, race cars, ATVs, and motorcycles.

Common measurements include:

- Suspension—strut pressure, spring force, travel, mounting point stress, deflection, ride
- Fuel system—line and tank pressure, flow, temperature, injection timing
- Comfort control—ambient and supply air temperature, solar radiation, fan speed, blower currents, ac on/off, refrigerant pressures, time-to-comfort
- Brakes—line pressure, pedal pressure and travel, ABS, fluid and pad temperature
- Engine—pressure, temperature, crank position, RPM, time-to-start, oil pump cavitation
- General vehicle—chassis monitoring, road noise, traction, payload, vehicle position/speed, steering, air bag, hot/cold soaks, wind tunnels, CANbus, wiper speed/current, vehicle electrical loads

Other Applications

- HVAC Systems—measures inside and outside temperatures, flow rates, differential pressures, motor temperatures, and relative humidity.
- Mining—monitors mine ventilation, slope stability, convergence, and equipment performance.
- Process monitoring and control—provides on-line quality control while minimizing production downtime.

The CR5000 can monitor and control pumps, fans, and starter motors in an HVAC system.

- Laboratory—can serve as a monitoring device to record parameters over time and can also be used to regulate and control test conditions.
- Aerospace/aviation—can endure the rigors of space travel and provide acceleration, structural, and equipment performance measurements.
- Utilities and energy—monitors conditions at power generation plants (hydroelectric, solar, and wind), terminals, substations, oil and gas pumping facilities, commercial and residential consumer sites, and along transmission lines.

Wide operating temperature ranges, solar-, AC- or battery-powered operation, wireless communications, and reliable performance make our systems ideal for unattended monitoring.

CR5000 Specifications

Electrical specifications are valid over a -25° to +50°C range unless otherwise specified; non-condensing environment required. To maintain electrical specifications, Campbell Scientific recommends recalibrating dataloggers every two years. We recommend that you confirm system configuration and critical specifications with Campbell Scientific before purchase.

PROGRAM EXECUTION RATE

The CR5000 can measure one channel and store the result in 500 µs; all 40 single-ended (SE) channels can be measured in 8 ms (5 kHz aggregate rate).

ANALOG INPUTS

20 differential (DF) or 40 single-ended (SE) individually configured. Channel expansion provided by AM16/32B and AM25T multiplexers.

RANGES, RESOLUTION, AND TYPICAL INPUT NOISE: Basic Resolution (Basic Res) is the A/D resolution of a single conversion. Resolution of DF with input reversal is half the Basic Res. Noise values are for DF with input reversal; noise is greater with SE.

Input Rng (mV)	Basic Res (µV)	0 Int. (µV RMS)	250 µs Int. (µV RMS)	20/16.7 ms Int. (µV RMS)
±5000	167	70	60	30
±1000	33.3	30	12	6
±200	6.67	8	2.4	1.2
±50	1.67	3.0	0.8	0.3
±20	0.67	1.8	0.5	0.2

ACCURACY[1]:
±(0.05% of reading + offset), 0° to 40°C
±(0.075% of reading + offset), -25° to 50°C
±(0.10% of reading + offset), -40° to 85°C (-XT only)

[1]The sensor and measurement noise is not included and the offsets are the following:
Offset for DF w/input reversal = Basic Res + 1.0 µV
Offset for DF w/o input reversal = 2Basic Res + 2.0 µV
Offset for SE = 2Basic Res + 10 µV

MINIMUM TIME BETWEEN VOLTAGE MEASUREMENTS:

Zero Integration:	125 µs
250 µs Integration:	475 µs
16.7 ms Integration:	19.9 ms
20 ms Integration:	23.2 ms

INPUT LIMITS: ±5 V

DC COMMON MODE REJECTION: >100 dB with input reversal (>80 dB without input reversal)

NORMAL MODE REJECTION: 70 dB @ 60 Hz when using 60 Hz rejection

SUSTAINED INPUT VOLTAGE W/O DAMAGE: ±16 Vdc

INPUT CURRENT: ±2 nA typ., ±10 nA max. @ 50°C

INPUT RESISTANCE: 20 Gohms typical

ACCURACY OF BUILT-IN REFERENCE JUNCTION THERMISTOR (for thermocouple measurements):
±0.25°C, 0° to 40°C
±0.5°C, -25° to 50°C
±0.7°C, -40° to 85°C (-XT only)

ANALOG OUTPUTS

4 switched voltage; 4 switched current; 2 continuous voltage; switched outputs active only during measurements, one at a time.

RANGE: Voltage outputs programmable between ±5 V; current outputs programmable between ±2.5 mA

RESOLUTION: 1.2 mV for voltage outputs; 0.6 µA for current outputs

ACCURACY: ±10 mV for voltage outputs; ±10 µA for current outputs

CURRENT SOURCING: 50 mA for switched voltage; 15 mA for continuous

CURRENT SINKING: 50 mA for switched voltage; 5 mA for continuous (15 mA w/selectable option)

COMPLIANCE VOLTAGE: ±5 V for switched current excitation

RESISTANCE MEASUREMENTS

Provides voltage ratio measurements of 4- and 6-wire full bridges, and 2-, 3-, 4-wire half bridges. Direct resistance measurements available with current excitation. Dual-polarity excitation is recommended.

VOLTAGE RATIO ACCURACY[2]: Assumes input and excitation reversal and an excitation voltage of at least 2000 mV.
±(0.04% Reading + Basic Res/4) 0° to 40°C
±(0.05% Reading + Basic Res/4) -25° to 50°C
±(0.06% Reading + Basic Res/4) -40° to 85°C (-XT)

ACCURACY[2] WITH CURRENT EXCITATION: Assumes input and excitation reversal, and an excitation current, I_x, of at least 1 mA.
±(0.075% Reading + Basic Res/2I_x) 0° to 40°C
±(0.10% Reading + Basic Res/2I_x) -25° to 50°C
±(0.12% Reading + Basic Res/2I_x) -40° to 85°C (-XT)

[2]The sensor and measurement noise is not included.

PERIOD AVERAGING MEASUREMENTS

The average period for a single cycle is determined by measuring the duration of a specified number of cycles. Any of the 40 SE analog inputs can be used; signal attenuation and ac coupling may be required.

INPUT FREQUENCY RANGE:

Input Range	Signal (peak to peak) Min.	Max.[3]	Min. Pulse W.	Max Freq.
±5000	600 mV	10 V	2.5 µs	200 kHz
±1000	100 mV	2.0 V	5.0 µs	100 kHz
±200	4 mV	2.0 V	25 µs	20 kHz

[3]Maximum signals must be centered around datalogger ground.

RESOLUTION: 70 ns/number of cycles measured

ACCURACY: ±(0.03% of Reading + Resolution)

PULSE COUNTERS

Two 16-bit inputs selectable for switch closure, high frequency pulse, or low-level ac.

MAXIMUM COUNT: 4×10^9

SWITCH CLOSURE MODE:
Minimum Switch Closed Time: 5 ms
Minimum Switch Open Time: 6 ms
Max. Bounce Time: 1 ms open w/o being counted

HIGH-FREQUENCY PULSE MODE:
Maximum Input Frequency: 400 kHz
Maximum Input Voltage: ±20 V
Voltage Thresholds: Count upon transition from below 1.5 V to above 3.5 V at low frequencies. Larger input transitions are required at high frequencies because of 1.2 µs time constant filter.

LOW-LEVEL AC MODE: Internal ac coupling removes dc offsets up to ±0.5 V.
Input Hysteresis: 15 mV
Maximum ac Input Voltage: ±20 V
Minimum ac Input Voltage:

Sine wave (mV RMS)	Range (Hz)
20	1.0 to 1000
200	0.5 to 10,000
1000	0.3 to 16,000

DIGITAL I/O PORTS

8 ports selectable as binary inputs or control outputs.

OUTPUT VOLTAGES (no load): high 5.0 V ±0.1 V; low < 0.1 V

OUTPUT RESISTANCE: 330 ohms

INPUT STATE: high 3.0 to 5.3 V; low -0.3 to 0.8 V

INPUT RESISTANCE: 100 kohms

SWITCHED 12 V

Two independent 12 V unregulated sources switched on and off under program control. Thermal fuse hold current = 900 mA @ 20°C, 650 mA @ 50°C, 360 mA @ 85°C.

EMI and ESD PROTECTION

The CR5000 is encased in metal and incorporates EMI filtering on all inputs and outputs. Gas discharge tubes provide robust ESD protection on all terminalblock inputs and outputs. The following European CE standards apply.

EMC tested and conforms to BS EN61326:1998.

Details of performance criteria applied are available upon request.

Warning: This is a Class A product. In a domestic environment this product may cause radio interference in which case the user may be required to correct the interference at the user's own expense.

CPU AND INTERFACE

PROCESSOR: Hitachi SH7034

MEMORY: Battery-backed SRAM provides 2 Mbytes for data and operating system use with 128 kbytes reserved for program storage. Expanded data storage with PCMCIA type I, type II, or type III card, or CF card (requires an adapter).

DISPLAY: 8-line-by-21 character alphanumeric or 128 x 64 pixel graphic LCD display w/backlight.

SERIAL INTERFACES: Optically isolated RS-232 9-pin DCE port for computer or non-CSI modem connection. CS I/O 9-pin port for Campbell Scientific peripherals.

BAUD RATES: Selectable from 1,200 to 115,200 bps. ASCII protocol is eight data bits, one start bit, one stop bit, no parity.

CLOCK ACCURACY: ±1 minute per month, -25° to +50°C; ±2 minute per month, -40° to +85°C

SYSTEM POWER REQUIREMENTS

VOLTAGE: 11 to 18 Vdc

TYPICAL CURRENT DRAIN: 400 µA software power off; 1.5 mA sleep mode; 4.5 mA at 1 Hz (200 mA at 5 kHz) sample rate.

INTERNAL BATTERIES: 7 Ah rechargeable base (optional); 1650 mAh lithium battery for clock and SRAM backup, 10 years of service typical, less at high temperatures.

EXTERNAL BATTERIES: 11 to 16 Vdc; reverse polarity protected.

PHYSICAL SPECIFICATIONS

SIZE: 9.8" x 8.3" x 4.5" (24.7 cm x 21.0 cm x 11.4 cm) Terminal strips extend 0.4" (1.0 cm).

WEIGHT: 4.5 lbs (2.0 kg) with low-profile base; 12.2 lbs (5.5 kg) with rechargeable base

WARRANTY

3 years against defects in materials and workmanship.

Printed February 2012

KINEMETRICS

EpiSensor ES-T

Force Balance Accelerometer

The EpiSensor ES-T: A Flexible, Versatile Value

Kinemetrics announces its latest line of earthquake sensors – EpiSensor force balance accelerometers. Model FBA ES-T is a triaxial surface package useful for many types of earthquake recording applications. The unit consists of three EpiSensor force balance accelerometer modules mounted orthogonally in one small convenient package. With fullscale recording ranges of ± 0.25 to ± 4g (user selectable) the EpiSensor provides on-scale recording of earthquake motions even at nearfault locations and in a wide variety of structure types.

The significantly improved bandwidth of DC to 200 Hz allows engineers and scientists to study motions at higher frequencies while maintaining the very important DC response that allows simple field calibration and reduces post-processing confusion.

Output circuitry is also significantly enhanced. Several types of outputs can be field-selected by the user: ± 2.5V single-ended output for use with traditional Kinemetrics earthquake recording instruments: ± 10V single-ended or ± 20V differential output for use with Kinemetrics digital recorders and other 24-bit digital recorders currently on the market.

EpiSensor force balance accelerometers are also available in uniaxial (the FBA ES-U) and borehole (the FBA ES-SB shallow and FBA ES-DH deep) packages.

FEATURES

- Low noise
- Extended bandwidth - DC to 200Hz
- User-selectable full-scale range
- Calibration coil (standard)
- Single-end or differential output (user selectable)
- Double-stage transient protection

SPECIFICATIONS

Dynamic range:	155 dB+
Bandwidth:	DC to 200Hz
Calibration coil:	Standard
Full-scale range:	User selectable at ± 0.25g, ± 0.5g, ± 1g, ± 2g or ± 4g
Outputs:	User selectable at: ± 2.5V single-ended ± 10V single-ended ± 5V differential ± 20V differential
Zero adjust:	Three user-friendly access holes for simple, safe, efficient adjustment

Linearity:	< 1000 µg/g2
Hysteresis:	< 0.1% of full scale
Cross-axis sensitivity:	< 1% (including misalignment)
Zero point thermal drift:	< 500 µg/°C (1g sensor)
ESD, RF, EMI protection:	Double stage transient protection with gas arrester elements
Power consumption:	12mA from +/- 12V (Standard Amp) 35mA from +/- 12V (Low Noise Amp) Single supply option available
Physical size:	13.3 cm diameter (cylinder), 6.2 cm high
Mounting:	Single bolt mounting, three adjustable leveling feet and bubble level
Connection:	Single military-style metal connector
Operating Temperature:	-20° to 70°C (0° to 160°F)
Housing:	Watertight enclosure

USA - 222 Vista Ave., Pasadena, CA 91107
Tel (626)795-2220 | Fax (626)795-0868

Switzerland - Z.I. Le Tresi 6B, 1028 Preverenges
Tel +41 (21) 803-2829 | www.kinemetrics.com

10-23-13

Appendix C: Matlab Scripts

```
%GILBERT A NICHOLS
%LAST EDITED 11/22/2015
%PURPOSE: CALCULATES THE WELCHS POWER SPECTRAL DENSITY ESTIMATE
OF THE TIME
%HISTORY DATA FROM THE BRIDGE.  THE IT FITS A CUBIC FIT TO THE
DATA AND
%TAKES THE MAXIMUMS OF THE CURVE FIT AND MAKES A SCATTER PLOT.

%The folder you copy the .mat files from
MatlabDestinationFolder='C:\Users\graduate\OneDrive\Masters
Project\Data\Matlab Files';

%THESE ARE THE DIFFERENT BOUNDS THAT I TRIED.

% low=1.06;      %Lower bound in hertz   freq 2
% high=1.19;     %Upper bound in hertz

low=2.051;       %Lower bound in hertz   freq 3
high=2.844;      %Upper bound in hertz   freq 1

% low=4.5;       %Lower bound in hertz   freq 5
% high=5.11;     %Upper bound in hertz   freq 5

% low=2.228;     %Lower bound in hertz   freq 2
% high=2.251;    %Upper bound in hertz

% low=9.1;       %Lower bound in hertz   freq 3
% high=9.7;      %Upper bound in hertz

% low=12.1;      %Lower bound in hertz   freq 4
% high=12.9;     %Upper bound in hertz

%conversion factor distance between points of B LINE 93
d=0.006103515625000;
%round to the nearest integer
a=round(low/d);
b=round(high/d);


%"Year_Month_Day" format. This is the first day of the data
%Chosen by the user.
StartTime='2016_05_1';
```

```
%Thermocouple number that you want to use plus 1.
%Chosen by the user
thermocouple=17;

% Number of days you want to retrieve
%Chosen by user
DateCounter=167;

%Convert the starting time to a number the computer recognizes
DateNumStart=datenum(StartTime);
% Counter conversion from date to number
DateNumCounter=datenum(datestr(DateNumStart,'yyyy_mm_dd'));
%counter
j=0;
%Loop through the days
for i=1:DateCounter
    %Time zero is the current date
    CurrentDate=datestr(DateNumCounter+i-1,'yyyy_mm_dd');
    %see line 8 for current directory
    cd(MatlabDestinationFolder);
    %If there is a file with d at the beginning and then the
current date
    %and it ends with mat then use the exist function 2nd
condition, which
    %is true.
    if exist(['D',CurrentDate,'.mat'],'file')==2
        %so load the file
        load(['D',CurrentDate]);
    else %if the file doesn't exist, tell me so.
        fprintf('\nData from this Date does not exit.')
    end
    %Asking the question how many hours were recorded in the set
for the
    %current day.
    [hours,var] = size(DailyData{1,8});
    if (DateCounter~=168)
        if (DateCounter~=169)
            if (DateCounter~=170)
                %Looping through the hours
                for k=1:hours
                 %for k=5:6 %optional small loop to check things
                    j=j+1;
                    %If it didn't get 18000 data points I don't
want to
                    %read it.
                    if(DailyData{1,8}{k,5})==18000
```

```
                    % Returns the index of the row of the
                    temperature
                        Ttimeloc=DailyData{2,8}{k,6};
                        %Returns the serial number of the
temperature
                        timenom= DailyData{2,4}(Ttimeloc,1);
                        %Sampling rate for the CR5000, if this
is the
                        %Obsidian it will need to be changed.
                        Hz=100;
                        %Number of seconds per 3 minute sample.
                        sec=180;
                        %Starting sample point for the hour
                        timestart=DailyData{1,8}{k,6};
                        %Ending sample point for the hour
                        timeend=DailyData{1,8}{k,7};
                    %Column 14 is C2, Column 16 is C4 and Column
                    18 is
                        %C6                                    \
                        C2=DailyData{1,7}(timestart:timeend,18);
                        %How big is it?
                        [rows, columns]=size(C2);
                        %Almost twice the number of FFT points
                        NFFT=16384;
                        %Sampling Frequency
                        Fs=Hz;
                        %Sampling Period is 1/(sampling
frequency)
                        Period = 1/Fs;
                        %Length of signal
                        L = rows;
                        %time vector
                        t = (0:L-1)*Period;
                        %pwelch function doesn't like column
vectors
                        X = transpose(C2);
                        %assign x and y values to the pwelch
output.
                        [pxx,f] = pwelch(X,L,[],NFFT,Fs);
                    %Experiment with differet scalars on pxx. I
                    like
                        %one million.
                        B=[f, 1000000*(pxx)];
                        %Plot B if desired. Not recommended for
a high
                        %number of days.
                        %plot(B(:,1),B(:,2))
```

```
                        %How big is it?
                        [rowsB, columnsB]=size(B);
                        fit=polyfit(B(a:b,1),B(a:b,2),3);
                        x1=linspace(low,high);
                        f1=polyval(fit,x1);
                        %If desired plot the curve fit to see if
it is
                        %doing its job. Will crash for a high
number of
                        %days.
                    %figure
                    %plot(B(a:b,1),B(a:b,2));
                    %xlabel('FREQUENCY (Hz)')
                    %ylabel('AMPLITUDE')
                    %hold on
                    %grid on
                    %plot(x1,f1,'r--')
                    %hold off
                    %Transpose back, because column vectors make
                    more
                        %sense than rows.
                        CF1=transpose(x1);
                        CF2=transpose (f1);
                    %Concatenate the matrices so there is one
                    matrix
                        %with two rows.
                        CF=horzcat(CF1, CF2);
                        %Find the maximum of the matrix
                        [M,I]=max(CF(:,2));
                    %If the maximum is at the ends of the curve
                    fit,
                        %throw it out.
                        if (CF(I,1)~=low)&& (CF(I,1)~=high)
                            freqfit(j,1)=timenom;
                            freqfit(j,2)=CF(I,1);
                            freqfit(j,3)=CF(I,2);
                        end
                    end
                end
            end
        end
    end
end

%counter
qq=0;
```

```
%load a temperature matrix with
load('T.mat')
%how big is the frequency matrix
[rowsfit, colsfit]=size(freqfit);
%how big is the temperature matrix
[rowsT, colsT]=size(T);
%convert the temperature from Fahrenheit to Celsius
T(:,2:25)=(T(:,2:25)-32)*(5/9);


%Loop through the rows of the frequency and the rows of
temperature and if
%there is a time that the temperature was recorded that matches
when the
%acceleration data was taken, then match them up.
for k=1:rowsfit
    for j=1:rowsT
        if (freqfit(k,1)==T(j,1))&& (T(j,2)~=0)
            qq=qq+1;
            %time
            Afit(qq,1)=freqfit(k,1);
            %temperature x
            Afit(qq,2:25)=T(j,thermocouple);
            %frequency y
            Afit(qq,26)=freqfit(k,2);
        end
    end
end


%Number of the thermocouple minus 1
tnom=17;
%Number for the accelerometer, usually 26
anom=26;
%Find a coefficient of determination for the temp vs frequency.
R2fit=corr(Afit(:,tnom),Afit(:,anom))^2;
%Find a correlation coefficient (rho).
rhofit = corr(Afit(:,tnom),Afit(:,anom));
%Create a figure
figure
%Create a scatter plot
scatter(Afit(:,tnom),Afit(:,anom),('.'));
%Name of the y-axis label
ylabel('FREQUENCY (Hz)')
%Name of the x-axis label
xlabel('TEMPERATURE (^{o}C)')
%Hold on, we need to put the regression line in.
```

```
hold on
%Returns a matrix with two values if (1) option is chosen, the
slope and
%y-intercept.
p = polyfit(Afit(:,tnom),Afit(:,anom),1);
%creates a matrix with the numbers from 1 to 70 with 100 points.
x2=linspace(1,70);
%polyval takes the polyfit data and uses it to create a y value
f2=polyval(p,x2);
%plot the linear regression line.
plot(x2,f2);
%create another matrix of ascending numbers
x3=linspace(1,70);
%returns the standard deviation of the temperature
St=std(Afit(:,tnom));
%returns the standard deviation of the frequency
Sa=std(Afit(:,anom));
%use that y-intercept from polyfit in the matrix it returns
m=p(1,1);
%shift the linear regression line up one standard deviation and
down one
%standard deviation to determine the confidence intervals.
y3=m*x3+(p(1,2)+Sa);
plot(x3,y3,'--b')
y4=m*x3+(p(1,2)-Sa);
plot(x3,y4,'--b');
hold off
```

```
%GILBERT NICHOLS
%TEMPERATURE RECORD 2
%LAST EDITED 11/22/2016
%PURPOSE: TO CREATE A T.mat MATRIX SO THAT IT CAN BE USED IN THE
PWELCH 9
%CODE ABOVE.

%clear the command window
clc
%clear the workspace
clear
%This code will help you retrieve the temperature matrix T.mat
%The folder you copy the .mat files
MatlabDestinationFolder='C:\Users\graduate\OneDrive\Masters
Project\Data\Matlab Files';
```

```
%"Year_Month_Day"
StartTime='2016_05_1';
% Number of days you want to retrieve data from
DateCounter=167;
%Convert the start date to a number that the computer recognizes
DateNumStart=datenum(StartTime);
%Convert the date counter into a number that the computer can
understand.
DateNumCounter=datenum(datestr(DateNumStart,'yyyy_mm_dd'));

%number of hours in a day, used for preallocation purposes.
It's 23 so
%that the code won't show an error if there is a day with only
23 hours.
nomhours=23*DateCounter;
%preallocate a variable T
T=zeros(nomhours,25);
%Counter
j=0;

%Looping through the number of days.
for i=1:DateCounter
    CurrentDate=datestr(DateNumCounter+i-1,'yyyy_mm_dd');
    cd(MatlabDestinationFolder);
    %%If there is a file with "d" at the beginning and then the
"date"
    %and it ends with ".mat" then use the exist function 2nd
condition, which
    %means true.
    if exist(['D',CurrentDate,'.mat'],'file')==2
        load(['D',CurrentDate]);
    else
        fprintf('\nData from this Date does not exit.')
    end
    [hours,var] = size(DailyData{2,8}); %Asking the question how
many hours
    %were recorded in the set for the current day for
temperature.
    for k=1:hours %Looping through the hours
            %Accessing a location of the first temperature in
the cell
            %array.
            begintemp= DailyData{2,8}{k,6};
            %Accessing a location of the last temperature in the
cell
            %array.
            endtemp=DailyData{2,8}{k,7};
```

```
            %Accessing the time serial numbers for each
temperature.
            timenom= DailyData{2,4}(begintemp,1);
            %Take the average temperature for the hour.
            Tave= mean(DailyData{2,7}(begintemp:endtemp,:));
            %Count
            j=j+1;
            %Fill the array t in the first column with the
serial numbers
            %and in the rest of the columns with temperature
data from the
            %thermocouples.
            T(j,1)=timenom;
            T(j,2:25)=Tave;
    end
end

%     Plots what is going on.
%     [x, y]=size(HourlyTemp);
%     figure
%     plot(HourlyTemp(:,2))
%     % plot(Day(1:168,2))
%     %title('Hourly temperatures for ', int2str(DateCounter),
'days beginning on May 1.')
%     xlabel('hours')
%     ylabel('Hz')
%     xlim([0 x])
%     ylim([0, 160])
```